

DE DUB
N NA
W MO: CALIFORNIA 34-3

NAVAL POSTGRADUATE SCHOOL

Monterey, California



THESIS

USE OF THE WAVENUMBER TECHNIQUE
WITH THE LLOYDS MIRROR
FOR AN ACOUSTIC DOUBLET

by

Portia Baird King

March 1985

Thesis Advisors:

A. B. Coppens
C. R. Dunlap

Approved for public release; distribution unlimited

T222199

REPORT DOCUMENTATION PAGE		READ INSTRUCTIONS BEFORE COMPLETING FORM
1. REPORT NUMBER	2. GOVT ACCESSION NO.	3. RECIPIENT'S CATALOG NUMBER
4. TITLE (and Subtitle) Use of the Wavenumber Technique With the Lloyds Mirror For an Acoustic Doublet		5. TYPE OF REPORT & PERIOD COVERED Master's Thesis March 1985
		6. PERFORMING ORG. REPORT NUMBER
7. AUTHOR(s) Portia Baird King		8. CONTRACT OR GRANT NUMBER(s)
9. PERFORMING ORGANIZATION NAME AND ADDRESS Naval Postgraduate School Monterey, California 93943		10. PROGRAM ELEMENT, PROJECT, TASK AREA & WORK UNIT NUMBERS
11. CONTROLLING OFFICE NAME AND ADDRESS Naval Postgraduate School Monterey, California 93943		12. REPORT DATE March 1985
		13. NUMBER OF PAGES 112
14. MONITORING AGENCY NAME & ADDRESS (if different from Controlling Office)		15. SECURITY CLASS. (of this report)
		15a. DECLASSIFICATION/DOWNGRADING SCHEDULE
16. DISTRIBUTION STATEMENT (of this Report) Approved for Public Release; Distribution is Unlimited.		
17. DISTRIBUTION STATEMENT (of the abstract entered in Block 20, if different from Report)		
18. SUPPLEMENTARY NOTES		
19. KEY WORDS (Continue on reverse side if necessary and identify by block number) Lloyds Mirror, Underwater Acoustics, Fast Fourier Transform, Wavenumber Technique, Pressure Spectrum, Source Depth Determination, Acoustic Propagation, ASW, Isospeed Environment		
20. ABSTRACT (Continue on reverse side if necessary and identify by block number) This thesis examines a method to determine the depth of a point source in an isospeed ocean environment. Using the Fourier Trans- form on the acoustic pressure field in the range domain results in the attainment of the acoustic pressure spectrum in the wave- number domain and a characteristic nodal spacing unique to the source-receiver depths. Quantitative examination of a magnitude plot of the spectrum and use of simple mathematical formulae yield the source depth. The debilitating effects of narrowband		

noise and surface roughness on the pressure spectrum are also examined. The pressure spectrum is recognizable in noise after the pressure field in the range domain has been lost in the noise field. The effect of surface gravity waves on the pressure spectrum is similar to that on the pressure field in the range domain: the characteristic nodal spacing is suppressed as the height of the surface waves increases.

Approved for public release; distribution is unlimited.

Use of the Wavenumber Technique
With the Lloyds Mirror
For an Acoustic Doublet

by

Portia B. King
Lieutenant Commander, United States Navy
B.S., Louisiana State University in New Orleans, 1971

Submitted in partial fulfillment of the
requirements for the degree of

MASTER OF SCIENCE IN SYSTEMS TECHNOLOGY
(Antisubmarine Warfare)

from the

NAVAL POSTGRADUATE SCHOOL
March 1985

ABSTRACT

This thesis examines a method to determine the depth of a point source in an isospeed ocean environment. Using the Fourier Transform on the acoustic pressure field in the range domain results in the attainment of the acoustic pressure spectrum in the wavenumber domain and a characteristic nodal spacing unique to the source-receiver depths. Quantitative examination of a magnitude plot of the spectrum and use of simple mathematical formulae yield the source depth. The debilitating effects of narrowband noise and surface roughness on the pressure spectrum are also examined. The pressure spectrum is recognizable in noise after the pressure field in the range domain has been lost in the noise field. The effect of surface gravity waves on the pressure spectrum is similar to that on the pressure field in the range domain: the characteristic nodal spacing is suppressed as the height of the surface waves increases.

TABLE OF CONTENTS

I.	HISTORY AND INTRODUCTION	14
II.	THEORY	18
	A. THE LLOYDS MIRROR PHENOMENON	18
	B. THE RELATIONSHIP BETWEEN K , γ , AND β	20
	C. THE WAVENUMBER TECHNIQUE AND THE LLOYDS MIRROR	20
	D. THE EFFECTS OF SURFACE ROUGHNESS	27
	E. THE EFFECT OF ADDING NOISE	28
III.	RESULTS AND CONCLUSIONS.	33
	A. THE FFT ALGORITHM	33
	B. SOURCE DEPTH DETERMINATION	38
	C. THE EFFECT OF SURFACE ROUGHNESS	42
	D. THE EFFECT OF NOISE	43
	E. SUMMATION	44
	APPENDIX A: LLOYDS MIRROR PRESSURE FIELD SOURCE CODE . .	93
	LIST OF REFERENCES	109
	BIBLIOGRAPHY	110
	INITIAL DISTRIBUTION LIST	111

LIST OF TABLES

I	Critical Values Used in the Research	34
II	Results of Source Depth Determination Runs	39

LIST OF FIGURES

2.1	The Geometry of the Lloyds Mirror Effect	30
2.2	A Classic $ P(F) $ vs. R Curve	31
2.3	The Relationship Between K, γ and β	32
3.1	Pressure Spectrum Using FFT2C	46
3.2	Pressure Spectrum Using FFTCC	47
3.3	Pressure Spectrum Using Cooley-Tukey FFT	48
3.4	Non-smoothed Pressure Field	49
3.5	Pressure Spectrum Showing Gibbs Phenomenon	50
3.6	Pressure Field Combined With a Hanning Window	51
3.7	Pressure Spectrum Combined With a Hanning Window	52
3.8	Theoretical Source Depth Determination Curve	53
3.9	Graph of Pressure Spectrum, Source at 22.0 Meters	54
3.10	Graph of Pressure Spectrum, Source at 31.4 Meters	55
3.11	Graph of Pressure Spectrum, Source at 15.7 Meters	56
3.12	Graph of Pressure Spectrum, Receiver at 22.0 Meters	57
3.13	Graph of Pressure Spectrum, Receiver at 31.4 Meters	58
3.14	Graph of Pressure Spectrum, Receiver at 15.7 Meters	59
3.15	Pressure Spectrum, Range Window Set at 47.1 Meters	60
3.16	Pressure Spectrum, Range Window Set at 50.3 Meters	61

3.17	Pressure Spectrum, Range Window Set at 62.8 Meters	62
3.18	Pressure Spectrum, Sea State 0	63
3.19	Pressure Spectrum, Sea State 2	64
3.20	Pressure Spectrum, Sea State 3	65
3.21	Pressure Spectrum, Sea State 5	66
3.22	Pressure Spectrum, Sea State 0, $K = 1.0$	67
3.23	Pressure Spectrum, Sea State 3, $K = 1.0$	68
3.24	Pressure Spectrum, Sea State 0, $K = 2.0$	69
3.25	Pressure Spectrum, Sea State 3, $K = 2.0$	70
3.26	Pressure Spectrum, SS 2, Range Window Set at 50 Meters	71
3.27	Pressure Spectrum, SS 2, Range Window Set at 100 Meters	72
3.28	Pressure Spectrum, SS 2, Range Window Set at 200 Meters	73
3.29	Pressure Spectrum, SS 2, Range Window Set at 300 Meters	74
3.30	Pressure Field, $K = 1.0$, $\mu = 0.005$	75
3.31	Pressure Spectrum vs. Gamma	76
3.32	Pressure Spectrum vs. Beta	77
3.33	Pressure Field, $K = 1.0$, $\mu = 0.01$	78
3.34	Pressure Spectrum vs. Gamma	79
3.35	Pressure Spectrum vs. Beta	80
3.36	Pressure Field, $K = 2.0$, $\mu = 0.0001$	81
3.37	Pressure Spectrum vs. Gamma	82
3.38	Pressure Spectrum vs. Beta	83
3.39	Pressure Field, $K = 2.0$, $\mu = 0.001$	84
3.40	Pressure Spectrum vs. Gamma	85
3.41	Pressure Spectrum vs. Beta	86
3.42	Pressure Field, $K = 2.0$, $\mu = 0.005$	87
3.43	Pressure Spectrum vs. Gamma	88
3.44	Pressure Spectrum vs. Beta	89

3.45	Pressure Field, $K = 2.0$, $\mu = 0.01$	90
3.46	Pressure Spectrum vs. Gamma	91
3.47	Pressure Spectrum vs. Beta	92

LIST OF SYMBOLS

A	Amplitude
c	Sound Speed
e	2.718281828...
FFT	Fast Fourier Transform
FFT ⁻¹	Inverse Fast Fourier Transform
f	Frequency
$\underline{f}(r)$	Generic Function of Range
$\underline{g}(\gamma)$	Spectral Density of $\underline{f}(r)$
H ₀	Hankel Function
i	Square Root of -1
J ₀	Bessel Function of the First Kind
k	Wavenumber
M	Surface Roughness Factor
m	Index of Calculations or Null Number in the Range Dcmain
N	Number of Points in the Wavenumber Spectrum

n	Index of Calculations or Null Number in the Wavenumber Spectrum
\tilde{n}	Complex Narrowband Noise Field
\tilde{p}	Time Independent Factor of Complex Pressure
\tilde{p}_s	Complex Pressure of the Source
\tilde{p}_i	Complex Pressure of the Reflection
\tilde{p}_N	Complex Pressure in the Presence of Noise
$\tilde{p}(k)$	Pressure Field in the Wavenumber Spectrum
p	Time Dependent Factor of Complex Pressure
R_1	Distance of the Direct Wave Path
R_2	Distance to the Image (Reflected Path)
RCVR	Receiver
r	Range Between Source and Receiver
SRC	Source
t	time factor
\tilde{w}	Hanning Window
Y_0	Bessel Function of the Second Kind
z_s	Source Depth

z_r	Receiver Depth
Δr	Range Increment
β	Vertical Component of the Wavenumber
$\Delta\beta$	Vertical Wavenumber Increment
γ	Horizontal Component of the Wavenumber
$\Delta\gamma$	Horizontal Wavenumber Increment
θ	Angle of Grazing Incidence at the Surface
λ	Wavelength
π	3.14159265...
φ	Phase Angle
ψ_R	Surface Reflection Coefficient
ω	Angular Frequency
$\sqrt{\quad}$	Square Root Operator
\int	Integration Operator

ACKNOWLEDGEMENTS

Contrary to popular opinion, this part of the thesis was the hardest to write because, for several reasons, it is the most important part of this entire undertaking. I encountered many difficulties during the course of this research; solutions to all the myriad problems were found eventually. Let me express heartfelt gratitude for the help and guidance of three experts in the field of acoustics: Dr. A. B. Coppins, Dr. T. Gabrielson, and Dr. Suk Wang Yoon, for the support of Professor C. R. Dunlap, for the help of Dr. DeWayne White of N.O.R.D.A in understanding the FFT, and the relatively minor but ever-so-important helpful hints and good wishes of my peers and fellow officers in the class of IX-33. Most of the mathematics and much of the direction for the research came from Professors Coppins and Gabrielson. Indeed, this thesis would not have been written without Professor Coppins' patience and leadership. Each person played a role, whether major or minor, in getting this thesis done. Without them, this paper would remain just another unfulfilled wish.

And, last but not least, I wish to thank a very special person for his support, cajolery, laughter, faith and other expressions of his love for me - my husband, Dr. David Benton King. Whenever I look back at what went into the writing of this paper, I shall always remember that I met him for the first time at the start of all the research that has gone into it. I shall also remember that, if I had never come to the Naval Postgraduate School, I would never have met him. And for that, I shall always be grateful to the United States Navy.

I. HISTORY AND INTRODUCTION

This thesis is the third in a series of investigations into a proposal put forth by R. Lauer of Naval Underwater Systems Center, New London, CT, in 1979. In his memorandum [Ref. 1], Lauer describes a "new" way to analyze sound propagation in the ocean and two applications of the method, which he named the "Wavenumber Technique," or W.T. In his proposal, Lauer stated that a source of sound in the ocean could be pinpointed in both depth and range by a single omnidirectional hydrophone provided the source is generating a continuous wave tone.

The W.T. was initially described by F. DiNapoli [Ref. 2] as an intermediary step in his development of a speedier computer algorithm used in analyzing sound propagation as a function of range. DiNapoli and Lauer proposed converting the pressure as a function of range $p(r)$ to the pressure spectrum as a function of the wavenumber $p(k)$. The conversion is accomplished by taking a weighted Fourier transform of the pressure field $p(r)$. Once the pressure spectrum is obtained, analysis of the pressure field can be accomplished in a manner analogous to that presently used in signal processing.

Lauer proposed two uses for his "Wavenumber Technique:"

1. determination of the depth of the acoustic source, an ability which has obvious tactical applications;
2. use of the W.T. to evaluate the accuracy of existing, and future, acoustic models such as P.E. and F.A.C.T., by breaking the generated pressure field down into ray path "families," such as bottom-bounce, refracted-surface-reflected, and surface-ducted families, thus giving a quantitative read-out of what

proportion of the total acoustic energy is being channelled through the various ray paths.

For both uses, a knowledge of the acoustic environment is necessary.

It is the intended purpose of this thesis to investigate the validity of the first application of Lauer's wavenumber technique by using it in conjunction with an acoustic phenomenon that is well-known and for which accurate results can be calculated with precision; this phenomenon is the Lloyds Mirror for an Acoustic Doublet. Using several source/receiver combinations, this investigator intends to compare actual source depth with that predicted by the W.T. If Lauer's technique is cogent, the source depths calculated via the two methods should be equal, or very close within a statistically acceptable degree.

As mentioned in the beginning of this thesis, two prior investigators, B. Stamey and J. Blanchard, looked into applying the W.T. to determining source depth. Stamey's investigation [Ref. 3] utilized a parabolic equation computer model developed by H.K. Brock, the Split Step Fast Fourier Transform, or SSFFT, to generate the pressure fields. He qualitatively compared the model to a Normal Mode model and a P. E. Finite Difference model, both range dependent, and to DiNapoli's Fast Field Program model, a range independent model. Stamey concluded that the W.T. showed promise as an analysis tool and that further investigations were warranted.

J. Blanchard carried Stamey's researches one step further [Ref. 4]. Using two Parabolic Equation computer algorithms, Brock's Split Step Fast Fourier Transform and Jaeger's Implicit Finite Difference, as his pressure field generators, he examined the use of the spacing between nulls of the pressure spectrum to determine source depth. His results are interesting and support the need for further investigation.

The author was not satisfied with Stamey's and Blanchard's findings. Both individuals acknowledged shortcomings in their respective studies, especially with regard to the mutual presence of the "U-shaped phenomenon" encountered in the pressure spectrum. One should remember, however, that their theses were preliminary studies only and were produced within a highly restricted time frame. Also, they used existing computer algorithms specifically designed to approximate acoustic propagation in a velocity-variant medium. However, the environmental settings used by both gentlemen were that of the Lloyds Mirror for an Acoustic Doublet which requires a constant sound speed throughout the water column; thus, the approximations, assumptions and "fudge factors" used by these models make their results for an isospeed medium highly artificial and somewhat suspect. Fortunately, however, there exists for the Lloyds Mirror a simple, geometric solution specifically designed for an isospeed environment [Ref. 5]. Since the pressure fields for varying source and receiver depths and, therefore, the corresponding pressure spectra, can be precisely calculated, it was thought this model would be a good check on the operational applicability of Lauer's proposed technique.

Secondary considerations of this study were to examine what effect, if any, the introductions of, firstly, surface waves and, secondly, noise would have on the pressure spectrum. The first objective was simulated by use of mathematical formulae given in reference 5; for the second objective, it was thought that complex noise, random in both amplitude and phase and similar to a Rician distribution [Ref. 6: p. 189], would provide a simple but reasonable approximation of an ocean noise field. This investigator intends to gradually intensify the surface waves and the noise field, separately, until the original pressure spectrum is no longer recognizable. In this manner, it should

be possible to make a qualitative assessment of their respective debilitating effects under the carefully controlled conditions found in the Lloyds Mirror phenomenon.

Section II sets forth in more detail the theoretical development of each point described in this introduction. Section III summarizes the investigator's results and the conclusions drawn from those results. Section IV contains a listing of the computer algorithms utilized.

II. THEORY

This chapter presents the mathematical basis of the wavenumber technique.

A. THE LLOYDS MIRROR PHENOMENON

A diverging monofrequency spherical pressure wave [Ref. 5: p.112] can be written in complex form as

$$p(R,t) = \underline{p}(R) e^{-i\omega t} = \frac{A}{R} e^{i(kR - \omega t)} \quad (\text{eqn 2.1})$$

where $\underline{p}(R)$ is the spatial factor. Referring to Figure 2.1, R_1 is the range from the source to the receiver and R_2 is the range from the image to the receiver. For convenience in all that follows, we shall set A to unit magnitude. The following equations apply to the acoustic waves propagating directly out from the source \underline{p}_s and from the apparent image \underline{p}_i (which is actually the wave reflected from the surface):

$$\begin{aligned} \underline{p}_s(R,t) &= \underline{p}_s(R) e^{-i\omega t} = \frac{1}{R_1} e^{i(kR_1 - \omega t)} \\ \underline{p}_i(R,t) &= \underline{p}_i(R) e^{-i\omega t} = \frac{-1}{R_2} e^{i(kR_2 - \omega t)} \end{aligned} \quad (\text{eqn 2.2})$$

where \underline{p}_s , \underline{p}_s , and \underline{p}_i are complex functions of horizontal range r , vertical depth z and time t ; the minus sign in the equation for \underline{p}_i is derived from the surface reflection coefficient, $\psi_R = -1$, for a smooth surface. Inspection of Figure 2.1 reveals that

$$R_1 = \sqrt{(z_r - z_s)^2 + r^2}, \quad R_2 = \sqrt{(z_r + z_s)^2 + r^2},$$

$$\text{and } \Delta r = |R - R_{1,2}|$$

And so the total field can be written as

$$p_s - p_i = \underline{P}(R) e^{-i\omega t} = \frac{e^{i(kR_1 - \omega t)}}{R_1} - \frac{e^{i(kR_2 - \omega t)}}{R_2} \quad (\text{eqn 2.3})$$

Since \underline{p}_s and \underline{p}_i both have the same time factor, $\exp(-i\omega t)$, we can retain just the spatial factors and equations 2.3 reduce to

$$\underline{P}(R) = \left[\frac{e^{ikR_1}}{R_1} - \frac{e^{ikR_2}}{R_2} \right] \quad (\text{eqn 2.4})$$

Equation 2.4 is a form of the complex pressure as a function of range used in the computer algorithm shown in Appendix I.

Inspection of Figure 2.1 reveals that, for $R \gg Z_s$ and θ very small,

$$r \approx R$$

or

$$\sin \theta \approx \frac{Z_r}{R}$$

or

$$\Delta r \approx \frac{Z_r Z_s}{R} \quad (\text{eqn 2.5})$$

and the pressure amplitude can be approximated by

$$\underline{P}(R) \approx \frac{2}{R} \left| \sin \left(\frac{k Z_r Z_s}{R} \right) \right| \quad (\text{eqn 2.6})$$

Looking at just the formula for the pressure amplitude, we can see that as

$$\left(\frac{k z_r z_s}{R}\right) \rightarrow n\pi, \quad n=0,1,2,3,\dots \quad (\text{eqn 2.7})$$

the pressure amplitude goes to zero, producing the classic $|P(R)|$ vs R curve shown in Figure 2.2

B. THE RELATIONSHIP BETWEEN k , γ , AND β

In his description of the Wavenumber Technique [Ref. 1: p. 5-6], Lauer utilizes the horizontal and vertical components of the wavenumber, k . The general relationship among these three terms is illustrated in Figure 2.3 and can be written mathematically as

$$k = \text{the wavenumber} = 2\pi f/c$$

$$\gamma = \text{the horizontal component of } k = k \cos \varphi$$

$$\beta = \text{the vertical component of } k = k \sin \varphi$$

or

$$k = \sqrt{\gamma^2 + \beta^2} \quad (\text{eqn 2.8})$$

C. THE WAVENUMBER TECHNIQUE AND THE LLOYDS MIRROR

Given a point source in free space, the monofrequency pressure field at the receiver, $p(R)$, can be expressed as a spherical wave (time factor suppressed),

$$\underline{P}(R) = \frac{e^{ikR}}{R} \quad (\text{eqn 2.9})$$

where, from Figure 2.1,

$$R^2 = r^2 + z_r^2, \text{ for } z_r > z_s$$

or

$$R^2 = r^2 + z_s^2, \text{ for } z_r < z_s \quad (\text{eqn 2.10})$$

In integral form, $\underline{P}(R)$ can be written as [Ref. 7: p. 127]

$$\underline{P}(R) = \frac{e^{ikR}}{R} = \int_0^\infty \frac{J_0(\gamma r) e^{\pm i\beta|z_r - z_s|}}{i\beta} \gamma d\gamma \quad (\text{eqn 2.11})$$

which is taken from the Fourier-Bessel Transform Pair [Ref. 7: p. 126],

$$\underline{f}(r) = \int_0^\infty \underline{g}(\gamma) J_0(\gamma r) \gamma d\gamma$$

$$\underline{g}(\gamma) = \int_0^\infty \underline{f}(r) J_0(\gamma r) r dr \quad (\text{eqn 2.12})$$

where $\underline{f}(r)$ represents the acoustic pressure function in the range domain, and $\underline{g}(\gamma)$ is the acoustic pressure spectrum in the wavenumber domain. The sign of the exponential function in the integral is based on which of z_s and z_r is greater. For the case of receiver depth being greater than source depth so that waves from both image and source are traveling downward at the receiver depth, the total pressure at the receiver can be expressed as

$$\underline{P}(R) = \int_0^\infty \frac{e^{i\beta(z_r - z_s)} - e^{i\beta(z_r + z_s)}}{i\beta} J_0(\gamma r) \gamma d\gamma \quad (\text{eqn 2.13})$$

Use of Euler's Identity reduces Equation 2.13 to

$$\mathcal{L}(R) = -2 \int_0^{\infty} \frac{e^{i\beta z_r} \sin(\beta z_s)}{\beta} J_0(\gamma r) \gamma d\gamma \quad (\text{eqn 2.14})$$

Using the relationship between the Hankel functions [Ref. 5: p. 449],

$$\begin{aligned} H_0^{(1)}(\gamma r) &= J_0(\gamma r) + iY_0(\gamma r) \\ \text{and} \\ H_0^{(2)}(\gamma r) &= J_0(\gamma r) - Y_0(\gamma r) \end{aligned} \quad (\text{eqn 2.15})$$

one can re-write the Bessel function in equation 2.14 as

$$J_0(\gamma r) = \frac{1}{2} [H_0^{(1)}(\gamma r) + H_0^{(2)}(\gamma r)] \quad (\text{eqn 2.16})$$

so that

$$2\mathcal{L}(\gamma) = \int_0^{\infty} \mathcal{L}(r) H_0^{(1)}(\gamma r) r dr + \int_0^{\infty} \mathcal{L}(r) H_0^{(2)}(\gamma r) r dr \quad (\text{eqn 2.17})$$

Letting $r' = -r$ and looking at the second term on the right hand side of equation 2.17,

$$\int_0^{\infty} \mathcal{L}(-r') H_0^{(2)}(-\gamma r') r' dr' = \int_{-\infty}^0 \mathcal{L}(-r) H_0^{(1)}(\gamma r) r dr \quad (\text{eqn 2.18})$$

Now, assuming that $\mathcal{L}(r) = \mathcal{L}(-r)$, then

$$2\mathcal{L}(\gamma) = \int_{-\infty}^{\infty} \mathcal{L}(r) H_0^{(1)}(\gamma r) r dr \quad (\text{eqn 2.19})$$

Therefore,

$$P(R) = - \int_{-\infty}^{\infty} \frac{\gamma H_0^{(1)}(\gamma r)}{\beta} e^{i\beta z_r} \sin(\beta z_s) d\gamma \quad (\text{eqn 2.20})$$

For $\gamma r > 2\pi$, the asymptotic approximation of the Hankel function for large argument can be used:

$$H_0^{(1)}(\gamma r) \approx \sqrt{\frac{2}{\pi \gamma r}} e^{i(\gamma r - \frac{\pi}{4})} \quad (\text{eqn 2.21})$$

assuming $|r \underline{f}(r)|$ goes to zero faster than $(\ln r)$,

$$P(R) \approx - \sqrt{\frac{2}{\pi r}} e^{-i\frac{\pi}{4}} \int_{-\infty}^{\infty} \left[\frac{\sqrt{\gamma}}{\beta} e^{i\beta z_r} \sin(\beta z_s) \right] e^{i\gamma r} d\gamma \quad (\text{eqn 2.22})$$

Let the terms inside the brackets in equation 2.22 be defined as $\underline{g}(\gamma)$, then

$$P(R) = - \sqrt{\frac{2}{\pi r}} e^{-i\frac{\pi}{4}} \int_{-\infty}^{\infty} \underline{g}(\gamma) e^{i\gamma r} d\gamma$$

and

$$\int_{-\infty}^{\infty} \underline{g}(\gamma) e^{i\gamma r} d\gamma = - \sqrt{\frac{\pi r}{2}} \sqrt{r} P(R) \quad (\text{eqn 2.23})$$

or, using equation 2.12,

$$\underline{\xi}(\gamma) = - \left[e^{i\frac{\pi}{4}} \right] \sqrt{\frac{\pi}{2}} \frac{1}{2\pi} \int_{-\infty}^{\infty} \sqrt{r} P(R) e^{-i\gamma r} dr \quad (\text{eqn 2.24})$$

Note that equation 2.24 has the form of the Fourier transform of the pressure function if we define

$$\underline{f}(r) \equiv \sqrt{r} P(R) \quad (\text{eqn 2.25})$$

so that $\sqrt{r} \, \underline{p}(R)$ and $\underline{q}(\gamma)$ are Fourier Transform pairs.

This equation can be easily evaluated [Ref. 8],

$$\underline{q}(\gamma) = - \left[e^{i \frac{\pi}{4}} \right] \frac{1}{\sqrt{2\pi}} \left[\frac{\sqrt{\gamma}}{\beta} e^{i\beta z_r} \sin(\beta z_s) \right] \quad (\text{eqn 2.26})$$

for $z_r > z_s$. And the magnitude of $\underline{q}(\gamma)$ is

$$\left| \underline{q}(\gamma) \right| = \frac{\sqrt{\gamma}}{\beta} \sin(\beta z_s) \quad (\text{eqn 2.27})$$

For the case where $z_s > z_r$, it can be shown that

$$\underline{q}(\gamma) = - \frac{e^{i \frac{\pi}{4}}}{\sqrt{2\pi}} \left[\frac{\sqrt{\gamma}}{\beta} e^{i\beta z_s} \sin(\beta z_r) \right] \quad (\text{eqn 2.28})$$

and the magnitude of $\underline{q}(\gamma)$ is

$$\left| \underline{q}(\gamma) \right| = \frac{\sqrt{\gamma}}{\beta} \sin(\beta z_r) \quad (\text{eqn 2.29})$$

A close look at the magnitude of the pressure spectrum function in equation 2.27 reveals that nodes occur for values of

$$\beta z_s = n\pi \quad , \quad n = 0, 1, 2, 3, \dots \quad (\text{eqn 2.30})$$

If the magnitude of the pressure spectrum is plotted as a function of the vertical wavenumber then the spacing between nodes $\Delta\beta$ is uniform and the depth of the source can be derived from the relationship given by

$$z_s = \frac{\pi}{\Delta\beta} \quad (\text{eqn 2.31})$$

In the event the source is deeper than the receiver, looking at equation 2.29, we can see that nodes now occur for values of

$$8z_r = n\pi, \quad n = 0, 1, 2, 3, \dots \quad (\text{eqn 2.32})$$

Plotting equation 2.29 as a function of the vertical wavenumber, the spacing between nodes will now reveal the receiver depth based on

$$z_r = \frac{\pi}{\Delta\beta} \quad (\text{eqn 2.33})$$

Notice in equations 2.31 and 2.33 the exchange of source and receiver depths. By placing the receiver at a shallower depth than the source, no new information (namely the source depth) is to be found.

In summary, there is a way to calculate the complex pressure amplitude as a function of range using the complex pressure spectrum. Conversely, if the complex pressure $\tilde{p}(r)$ has been measured at the receiver, then the complex pressure spectrum $\tilde{p}(k)$ can be derived by making use of the relationship between the Fourier-Bessel Transform Pairs (see equation 2.12), and the depth of the source can be found from the magnitude of that spectrum (see equation 2.31).

The foregoing is the mathematics involved in deriving the theoretical pressure spectrum. One purpose of this thesis was to compare the theoretical value of the pressure spectrum as derived with the Fourier-Bessel Transform with the pressure spectrum obtained by use of the computerized Discrete Fourier Transform (DFT), otherwise known as the Fast Fourier Transform, or FFT. At this point, it will be helpful to review what happens in the FFT.

Starting with the Fourier-Bessel transform pair shown in equation 2.12, $\underline{f}(r)$ and $\underline{g}(\gamma)$ can be re-written in terms of a discrete sum as is done in the DFT:

$$FFT^{-1} \left\{ \underline{g}(\gamma) \right\} = \sum_{n=0}^{N-1} \underline{g}(n\Delta\gamma) e^{i \frac{2\pi mn}{N}} = \underline{f}(m\Delta r) \quad (\text{eqn 2.34})$$

where $N = 1, 2, 3, \dots$, up to some large positive integer, and represents the number of transform points, and

$$\gamma r = (n\Delta\gamma)(m\Delta r) = \frac{2\pi mn}{N} \quad (\text{eqn 2.35})$$

based on the relationship between Δr and $\Delta\gamma$ as described in sampling theory [Ref. 2: p. 2],

$$\Delta\gamma \Delta r = \frac{2\pi}{N}$$

or

$$\Delta r = \frac{2\pi}{N\Delta\gamma} \quad (\text{eqn 2.36})$$

By convention, the sign of the exponential function in equation 2.34 is taken as negative when performing the "forward" transform,

$$FFT \left\{ \underline{f}(m\Delta r) \right\} = \underline{g}(n\Delta\gamma) \quad (\text{eqn 2.37})$$

and is taken as positive when performing the "inverse" transform,

$$FFT^{-1} \left\{ \underline{g}(n\Delta\gamma) \right\} = \underline{f}(m\Delta r) \quad (\text{eqn 2.38})$$

$$\text{Then, } \int_{-\infty}^{\infty} \underline{g}(\gamma) e^{i\gamma r} d\gamma \approx \left[\sum_{n=1}^{N-1} \underline{g}(n\Delta\gamma) e^{i\frac{2\pi mn}{N}} \right] \Delta\gamma$$

where

$$\underline{g}(n\Delta\gamma) = \frac{\sqrt{\gamma}}{\beta} e^{i\beta z_r} \sin(\beta z_s)$$

Therefore

$$\underline{P}(m\Delta r) = - \sqrt{\frac{2}{\pi r}} e^{-i\frac{\pi}{4}} \left[\Delta\gamma FFT^{-1} \left\{ \underline{g}(n\Delta\gamma) \right\} \right]$$

and

$$\left| \underline{g}(n\Delta\gamma) \right| = \frac{\sqrt{\gamma}}{\beta} \sin(\beta z_s) \quad (\text{eqn 2.39})$$

D. THE EFFECTS OF SURFACE ROUGHNESS

Surface roughness [Ref. 5: p.409] reduces the Lloyds Mirror effect. The rougher the surface, the greater the effect for angles increasingly closer to grazing incidence. If M represents the surface roughness factor, then equation 2.3 can be re-written as

$$P(R) = \frac{e^{ikR}}{R} - e^{-M^2} \frac{e^{ikR}}{R}$$

where

$$M \equiv \frac{4H \sin\phi}{\lambda} \quad (\text{eqn 2.40})$$

ϕ is the grazing angle of incidence, H is the average height of the surface gravity waves, and λ is the wavelength of the narrowband continuous wave acoustic signal. When M is less than 1, the surface is said to be smooth; when M is greater than 1, the surface is said to be rough.

Looking at Figure 2.1, we can see that the overall effect of increasing surface roughness is to reduce the contribution of the surface reflection or "image" to the interference pattern at the receiver. In other words, as H increases, the energy detected by the receiver is increasingly only the energy coming directly from the source. When the effect of surface roughness is a maximum such that the contribution to the pressure field of the "image" is completely suppressed, then

$$\begin{aligned} g_s(\gamma) &= \int_0^\infty \frac{e^{ikR_I}}{R_I} J_0(\gamma r) r dr \\ &= \frac{e^{i\beta|z_s - z_r|}}{i\beta} \end{aligned} \quad (\text{eqn 2.41})$$

and the magnitude of the spectrum is

$$|g(\gamma)| = \frac{1}{\beta} \quad (\text{eqn 2.42})$$

E. THE EFFECT OF ADDING NOISE

In an effort to simulate a realistic ocean environment, a normally distributed narrowband noise field based on a Rician distribution [Ref. 6: p. 189] was adapted. The resulting acoustic pressure field can be expressed as

$$\underline{P}_N(R) = \underline{P}(R) + \underline{n}$$

(eqn 2.43)

where \underline{n} is a normally-distributed random function with a mean of zero, a standard deviation of one and possesses both amplitude and phase. The noise operates independently on both the amplitude and phase components of the pressure field. Since \underline{n} is independent of range and wavenumber, it is treated as a constant by the Fourier Transform.

A fourth intention of this thesis was to discover the degree to which noise degrades the wavenumber spectrum compared with the corresponding degradation of the range domain. To produce the random noise fields used in this research, the routine listed as "GGNML" in the IMSL library [Ref. 9] was called upon twice to generate independent, pseudo-random functions which interact separately and simultaneously with both the amplitude and phase components of $\underline{P}(R)$. While not an elaborate scheme, owing to time and resource constraints, it was felt that this modest simulacrum of narrowband noise would give a fairly accurate, first cut "feel" for the effects of noise on the wavenumber spectrum. The reader should be aware, however, that no direct consideration of coherency along the range path was taken into account by this method.

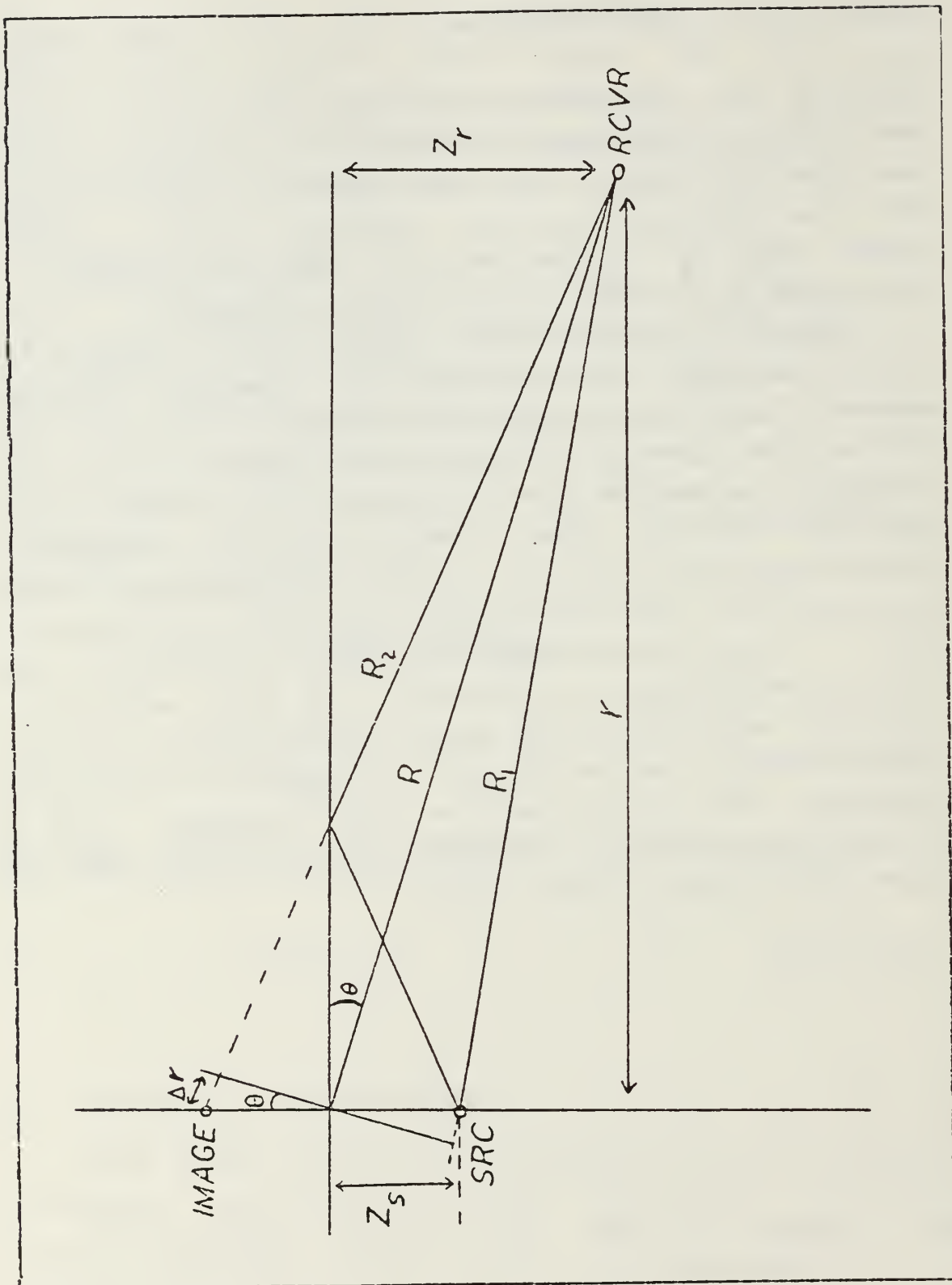


Figure 2.1 The Geometry of the Lloyd's Mirror Effect

MAGNITUDE OF PRESSURE AS A FN OF RANGE

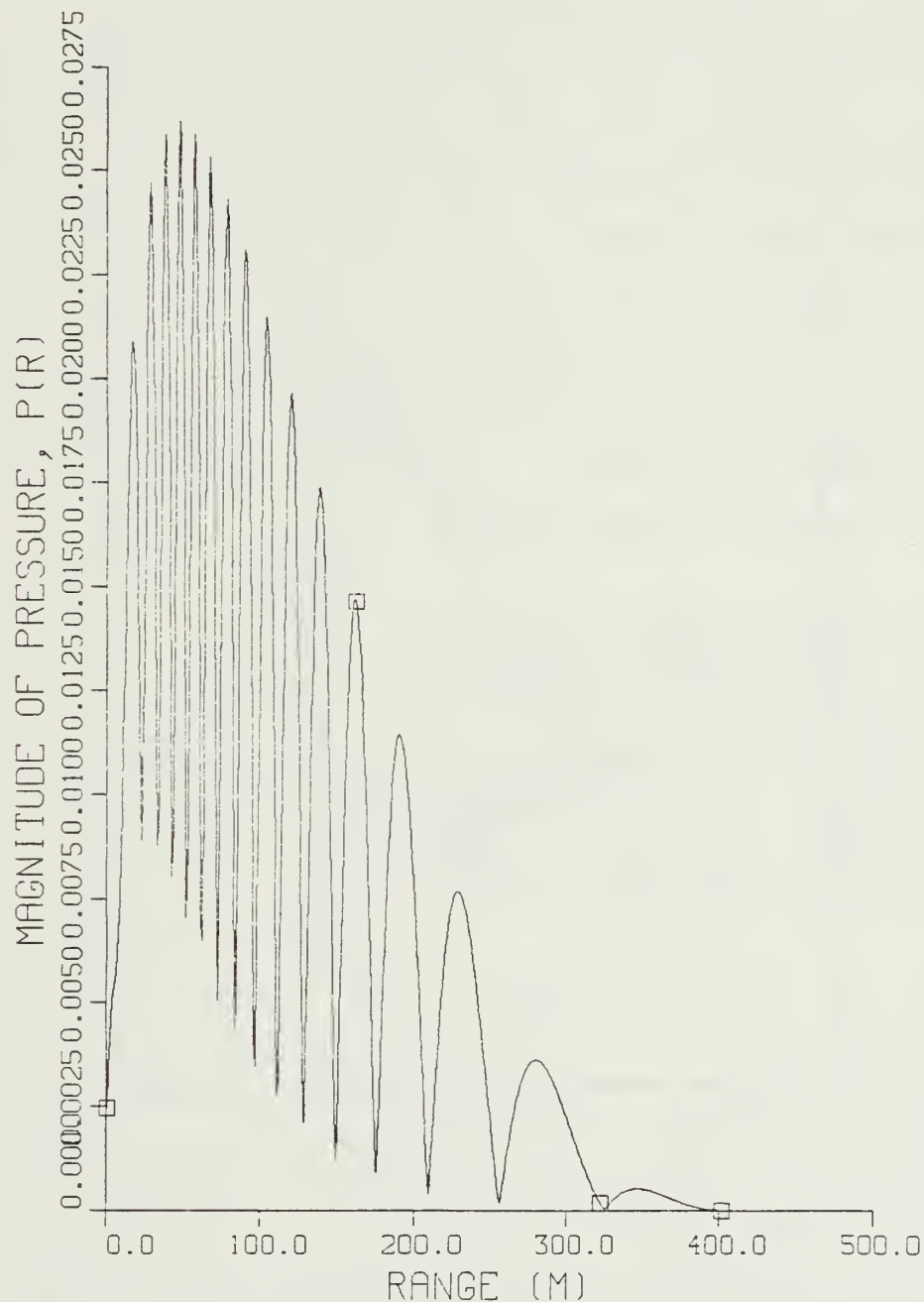


Figure 2.2 A Classic $|P(R)|$ vs. R Curve

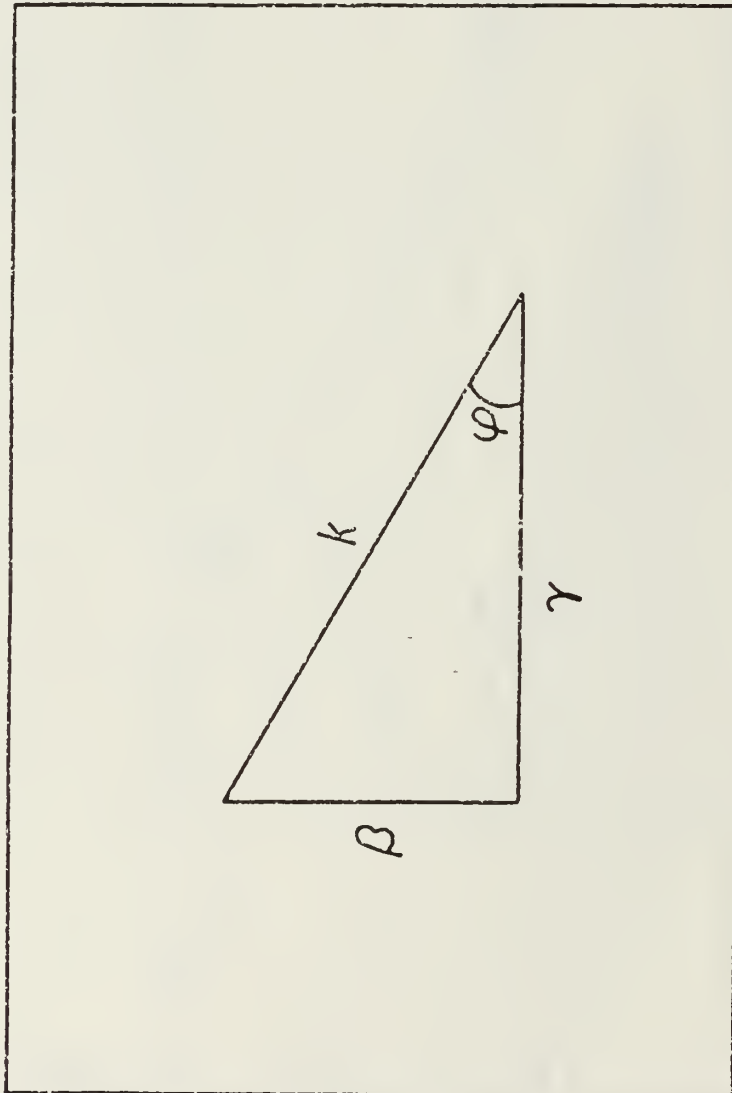


Figure 2.3 The Relationship Between k , γ and β

III. RESULTS AND CONCLUSIONS

A. THE FFT ALGORITHM

The research for this thesis was conducted entirely with computer algorithms to model the Lloyds Mirror, the Fast Fourier Transform, the range windows, waves, and the narrow-band noise. This was necessary since the Lloyds Mirror is an idealized representation of a situation that occurs only rarely in nature, and at that is limited to isospeed surface ducts. Also, time and money constraints were such that the use of computer models was an absolute necessity. For these reasons and because the FFT is the heart of the Wavenumber Technique, finding a reliable, easy-to-use computer algorithm to perform the FFT on the complex pressure function was deemed very important.

Initially, the IMSL library routines, FFT2C and FFTCC [Ref. 9: p. 232], were used to generate the pressure spectra. Although the author was unable to ascertain just how Stamey performed the FFT on his data, it is highly probable that he used an IMSL library routine. While in his thesis, Blanchard stated that he used the FFTCC routine. The magnitude of a typical spectrum generated by the routine FFT2C is shown in Figure 3.1.

The same scenario used to generate Figure 3.1 was used to produce the spectrum shown in Figure 3.2, but the routine FFTCC was utilized. As can be seen, the resulting graphs of the pressure spectrum magnitude are practically identical. Indeed, the set-up of the pressure fields for insertion into each routine differ only in that FFT2C requires a data set consisting of an integral power of two number of points, whereas FFTCC will handle any number of points. And, when

the Cooley-Tukey FFT listed in Appendix I was used to transform the same pressure field as was utilized to produce Figures 3.1 and 3.2, Figure 3.3 was the result. This algorithm differs somewhat from the IMSL routines by the manner in which the pressure field data is treated. Both FFT2C and FFTCC are designed to handle a complex array. The Cooley-Tukey FFT, on the other hand, is designed to transform real data; but the pressure field is complex. To get around this apparent conundrum, the pressure data is defined as either real or imaginary by its placement in the array. As can be seen, the resultant graph of the spectrum magnitude is almost indistinguishable from that produced by either IMSL routine. In conclusion, it does not matter which FFT routine is used to generate the pressure spectrum, as long as the pressure field in the range domain is "fitted" into the array in a manner suitable to the particular algorithm used.

TABLE I
Critical Values Used in the Research

<u>K (m^{-1})</u>	<u>N</u>	<u>r (m)</u>	<u>(m^{-1})</u>
3.0	1024	0.524	1.172×10^{-2}
2.0	1024	0.785	7.816×10^{-3}
1.0	1024	1.571	3.906×10^{-3}

It is important to note four things about the FFT at this point.

1. Since the FFT is given only a finite sample of a function while the theoretical Fourier Transform

looks at the complete function, the computer algorithm is designed to overcome this necessary shortcoming by assuming the submitted finite sample repeats its pattern an infinite number of times. This can present problems. If the right hand side of one pattern does not flow smoothly into the left hand side of the next repetition, as is shown in Figure 3.4, then high frequency oscillations known as the Gibbs Phenomenon can be introduced into the spectrum. (See Figure 3.5) This is a very real danger where acoustic pressure fields are concerned. For example: if the sample size does not include the entire pattern (i.e., the pressure magnitude has not been completely attenuated prior to the endpoints of the sample), this unwanted "jitter" in the spectrum can result. To avoid this situation, not only was a pressure field symmetric about the origin (the source) used, but also a Hanning Window was constructed to reduce both the amplitude and the phase components of the pressure field to zero at the endpoints, thus avoiding the Gibbs Phenomenon. Figure 3.6 shows the same pressure field depicted in Figure 3.4 combined with a Hanning Window. Its spectrum is shown in Figure 3.7. The Gibbs Phenomenon is absent. The form of the window is given below. The reader's attention is directed to Appendix I for a view of the manner in which it is combined with the pressure field.

The Hanning Window:

$$W = 0.5 \left[1 + \cos \left(\frac{(N-1) \pi}{NPTS} \right) \right] \quad (\text{eqn 3.1})$$

where "NPTS" is the number of data points,
and $I = 1, 2, 3, \dots, \text{NPTS}$.

The Hanning Window does not affect the acoustic pressure field in any other way; the interference pattern in the range domain characteristic of the Lloyds Mirror for an Acoustic Doublet remains the same except for its amplitude near the end points. As shall be shown later in this chapter, it is the pattern of the entire pressure field, not simply the amplitude of the pattern, on which the W.T. performs its legerdemain.

2. Because the vertical wavenumber β is real and has physical meaning for values of the horizontal wavenumber less than k , only those values of the magnitude of the acoustic pressure spectrum—corresponding to $\gamma < k$ were retained.
3. In the Wavenumber Technique, the relationship between the horizontal range step size Δr and the horizontal wavenumber step size $\Delta \gamma$ is extremely important. Recalling equation 2.36,

$$\Delta \gamma \Delta r = \frac{2\pi}{N} \quad (\text{eqn 3.2})$$

for a given "N," the term on the right hand side, $2\pi/N$, is a constant. Consequently,

$$\Delta r \propto (\Delta \gamma)^{-1} \quad (\text{eqn 3.3})$$

Simultaneously, in accordance with sampling theory, in order to prevent aliasing in the pressure spectrum, there is an upper limit on the size of Δr :

$$\Delta r \leq \frac{\lambda}{2} \quad (\text{eqn 3.4})$$

Normally, Δr is chosen such that it is much less than half a wavelength; specifically, $\Delta r < \lambda/5$ or $\lambda/6$, thus a good sample of the range domain is ensured. However, from equation 2.36, the smaller Δr becomes, the larger $\Delta \gamma$ becomes and the coarser the sample sizes of the spectrum become. Also, to ensure adequate samples in the spectrum, examination of equations 2.25 and 2.36 and [Ref. 10] reveals that

$$\Delta \gamma \leq \frac{1}{2k} \left(\frac{\pi}{z} \right)^2 \quad (\text{eqn 3.5})$$

where z is the deeper of the two depths, whether source or receiver. So there is a delicate balance to maintain between the sizes of Δr and $\Delta \gamma$. In the spirit of compromise, the investigator chose to use a range step size equal to a quarter of a wavelength where

$$\lambda \equiv \frac{2\pi}{k} \quad (\text{eqn 3.6})$$

For most cases investigated, values for k , N , Δr and $\Delta \gamma$ are summarized in Table I. As can be seen, using these values and equation 3.5, for a "Z" value of 25 wavelengths, the maximum size $\Delta \gamma$ can assume and still ensure an adequate sample size is $\Delta \gamma = 0.0004$ /m. Clearly the sizes of $\Delta \gamma$ shown in Table I are too coarse by a factor of approximately 20. Only by increasing N , the number of sample points, can this discrepancy be corrected.

However, as mentioned earlier, computer resources were limited. The effect on the research results is not significant; nevertheless, it is recommended the reader bear this limitation in mind during the succeeding pages.

4. Looking again at Figures 3.1 through 3.3, the FFT is the curve marked by the solid line, while the theoretical Fourier Transform is the curve marked by the dotted line. Notice the large discrepancy between the theoretical values and the actual values in the region corresponding to small vertical wavenumbers. This happens to correspond to a region of the spectrum characterized by more rapid fluctuations in the spectrum. However, the size of beta is constant. Consequently, fewer samples of this region of the spectrum are available as compared with that region corresponding to high beta values. Since the plotting routine utilized is interpolating between sampled points of the spectrum, the graph at this end is less smooth and results in a marked difference between the curves. Where the curves are determined by more points and are smoother, the discrepancy between theory and computerized reality is much less noticeable.

B. SOURCE DEPTH DETERMINATION

Theory predicts that, for a source shallower than the receiver, when the magnitude of the pressure spectrum is plotted as a function of the vertical wavenumber, the resultant nodal spacing can be used to determine source depth by either consulting a chart (see Figure 3.8) or by performing a simple calculation (see equation 2.31). To test this prediction, several scenarios were designed. Figures 3.9

through 3.11 are typical of the many cases run. In each, source depth is less than receiver depth. For each case, careful measurement of the $\Delta\beta$ spacing coupled with use of equation 2.31 yielded the (already known) source depth with less than a two per cent error, which can be attributed to human error in the measurement of $\Delta\beta$.

TABLE II
Results of Source Depth Determination Runs

<u>Figure Nr.</u>	<u>ZS (m)</u>	<u>ZR (M)</u>	<u>(Meas'd)</u>	<u>Z(Calc'd)</u>
3.9	21.998	47.124	0.14 m ⁻¹	22.4 m
3.10	31.416	47.124	0.10 "	31.4 "
3.11	15.708	47.124	0.20 "	15.7 "
3.12	47.124	21.998	0.14 "	22.4 "
3.13	47.124	31.416	0.10 "	31.4 "
3.14	47.124	15.708	0.20 "	15.7 "

To test what happens when the receiver depth is shallower than the source depth, the cases depicted in Figures 3.12 through 3.14 were run. The scenario is the same as for Figures 3.9 through 3.11; only the source and receiver depths have been exchanged. As can be seen, the $\Delta\beta$ spacing corresponds with the receiver depth. This is again as predicted by theory. Table II summarizes the findings of Figures 3.9 through 3.14.

The scenarios shown in Figures 3.9 through 3.14 all start with a pressure field measured horizontally from the source; i.e., the exact range to the source is known. What if the range to the source is not known, or only minimal information concerning the range is known? In this case, only a portion of the pressure field starting at some initial range P_0 can be sampled. What is the effect on the spectrum?

To answer these questions, a range window was constructed and placed at varying initial ranges from the source. As Figure 2.2 illustrates, as range from the source increases, the nodes of the Lloyds Mirror interference pattern in the range domain become more widely spaced. Given fewer nodes to sample, will the spectrum be the same? In accordance with theory, the spectrum is independent of range (see equation 2.39) and so should be the same wherever the window is placed.

Figures 3.15 through 3.17 illustrate that the spectrum is not entirely independent of range. The figures utilize the same scenario as was used above, differing only in the range from the source at which the sampling of the pressure field begins. As can be seen, beginning at the right hand side which corresponds to high vertical wavenumber values, or the low horizontal wavenumber values (see equation 2.8), a "washing out" of the spectrum occurs, increasing as the range window is moved further from the source. Again, the theoretical curve is marked by the dotted line.

When the magnitude of the pressure spectrum is plotted as a function of the vertical wavenumber, the useful portion of the resulting graph is the last two-thirds of the beta range. For $K = 2.0/m$, this is the range $0.67/m < \beta < 2.0/m$. This phenomenon is explained more fully in Section III A 4. With this caveat in mind and based upon multiple source, receiver, range window

combinations run through the model, the following criterion was established: the nodal spacing of the spectral plots was no longer determinable once the initial range R_0 was increased to approximately three times the source depth. In other words, minimum knowledge of the range from receiver to source must be available to ensure adequate sampling of the acoustic pressure field in the range domain. This, in turn, will produce a pressure spectrum of such a quality that source depth determination can be made.

What causes this not entirely unexpected result? As the range window is moved further from the source, for $Z_s \neq Z_r$, those samples of the pressure field corresponding to low gamma values are lost to the spectrum first. Low gamma values correspond to waves arriving at high angles with respect to the horizontal. At greater receiver ranges, R more closely approximates r and the arrival angles become closer to the horizontal (see Figure 2.1).

As the window is moved further from the source and fewer nodes of the interference pattern are encountered, if a wider window were used, could this "washing out" effect in the spectrum be minimized or even eliminated? In the author's opinion, it would be minimized; because of the reasoning in the preceding paragraph, it probably would not be eliminated. However, a wider window would require more sample points; because of equation 2.36, one cannot merely make Δr larger. Time and the computer resources available to this investigator were limited, and the test cases run were already using the maximum available array sizes, thus precluding a quantitative illustration of this hypothesis. Succeeding research into the W.T. might include ways to test this point.

In conclusion, the Wavenumber Technique has the potential for being a valuable operational tool in determining the depth of an acoustic source provided the receiver is at

a greater depth than the source. It is strongly recommended that further research into use of the W.T. in a realistic ocean environment be done.

C. THE EFFECT OF SURFACE ROUGHNESS

This and the succeeding section were purely qualitative portions of the research. Therefore, in the figures the spectra were plotted as functions of the horizontal wavenumber for ease of discussion except where a particular point about the vertical wavenumber was being illustrated, and the theoretical curve was omitted.

As described in Chapter II, the effect of surface roughness is to suppress the contribution of the image to the dipole interference pattern. Moreover, by increasing M , the effect is to suppress the image's contribution to the pressure field in the range domain and reduce the pressure spectrum to the contribution of the direct path wave only (see equation 2.41); the resultant magnitude of the spectrum is inversely proportional to the vertical wavenumber (see equation 2.42). As Figures 3.18 through 3.21 illustrate, this is exactly what happens in the FFT. In Figure 3.21, an inverse beta curve has been manually superimposed onto the actual curve to reflect this point.

Looking at the pressure field in the range domain $\underline{p}(R)$ the effect of surface roughness is inversely proportional to the wavelength of the signal. For longer wavelengths, the Lloyds Mirror effect is more tolerant of surface roughness than it is for shorter wavelengths. Does the same relationship hold for the pressure spectrum? Comparison of the respective sea states in Figures 3.22 and 3.23 with Figures 3.24 and 3.25 illustrate that it does.

This investigator also looked at the effect of varying the range window in the presence of waves. This is similar

to what was looked at in Section B of this chapter. Results should be similar and for the same reasons. For a given sea state, source and receiver geometry and wavelength, the range window was moved successively further from the source (see Figures 3.26 through 3.29). As can be seen, the "washing out" effect of the spectral nodes begins to effect the lower horizontal wavenumber values first.

D. THE EFFECT OF NOISE

Random noise was simulated in this research. Being independent of range and frequency, it was treated as a constant by both the Fourier Transform and the FFT. The investigator wished to compare qualitatively the effects of equal amounts of noise on the pressure field in the range domain and in the wavenumber domain. To do this, successively larger values of the "noise factor" were used in computing \tilde{p} (see equation 2.43). Values of the noise factor used in the research were limited to the maximum amplitude of the pressure field $\tilde{p}(R)$. Since dipole radiation is predicated, as range from the source increases, the maxima of the interference pattern decrease as the inverse square of the range (i.e., R^{-2}). Hence, even small noise factors can have a devastating effect on the pressure field as the receiver is stepped out in range. The destructive effect on the spectrum of successively more intense amounts of noise at varying wavelengths is illustrated in Figures 3.30 through 3.47

Several conclusions concerning the pressure spectra can be drawn from these results:

1. For equal amounts of noise, longer wavelengths are affected less than shorter wavelengths. Compare Figures 3.31 and 3.32 with Figures 3.43 and 3.44, and Figures 3.34 and 3.35 with Figures 3.46 and 3.47.

This was not a surprising result since the same principle holds for the range domain.

2. The spectrum is affected less by noise than is the range domain. Compare Figures 3.30 through 3.35 and Figures 3.36 through 3.47 for an illustration of this point at two different wavelengths and various noise levels. This was a rather welcome surprise.
3. If the magnitude of the pressure spectrum is plotted as a function of beta, the $\Delta\beta$ spacing can still be detected even after the pressure function in the range domain has been "swallowed up" by the noise field. Compare Figures 3.33 through 3.35 and Figures 3.42 through 3.44. This was not surprising in view of 2. above.

E. SUMMATION

All of the foregoing results are based specifically on the Llóyd's Mirror for an Acoustic Doublet. This is a highly idealized and artificial environment. Any thought of immediately applying conclusions reached in this paper to a real world situation is premature. However, the results are still significant if only for supporting the statement made by each preceding investigator that the Wavenumber Technique should be examined very closely for a future operational role, especially in view of the current trends in source levels and ambient noise levels.

Certain fundamental conclusions regarding the author's research into the Wavenumber Technique can now be made within the confines of the above restriction:

1. Source depth can be determined quickly and easily from the acoustic pressure spectrum provided
 - a) the receiver is deeper than the source,

- b) some knowledge of the range from receiver to source is available, and
 - c) the magnitude of the pressure spectrum is plotted as a function of the vertical wavenumber.
2. Source depth determination in even a noisy environment is possible. While the introduction of increasing amounts of narrow band noise adversely affects both the range domain and the wavenumber domain, the pressure spectrum seems able to withstand the chaotic destruction longer than does the pressure field in the range domain.
 3. The ability to determine source depth is adversely affected by the height of surface gravity waves since surface roughness reduces the Lloyds Mirror as the sea state increases.

PRESSURE SPECTRUM VS KZ

SOURCE DEPTH = 20 m, $K = 2.0/\text{m}$,
RECEIVER DEPTH = 50 m, $N = 1024$

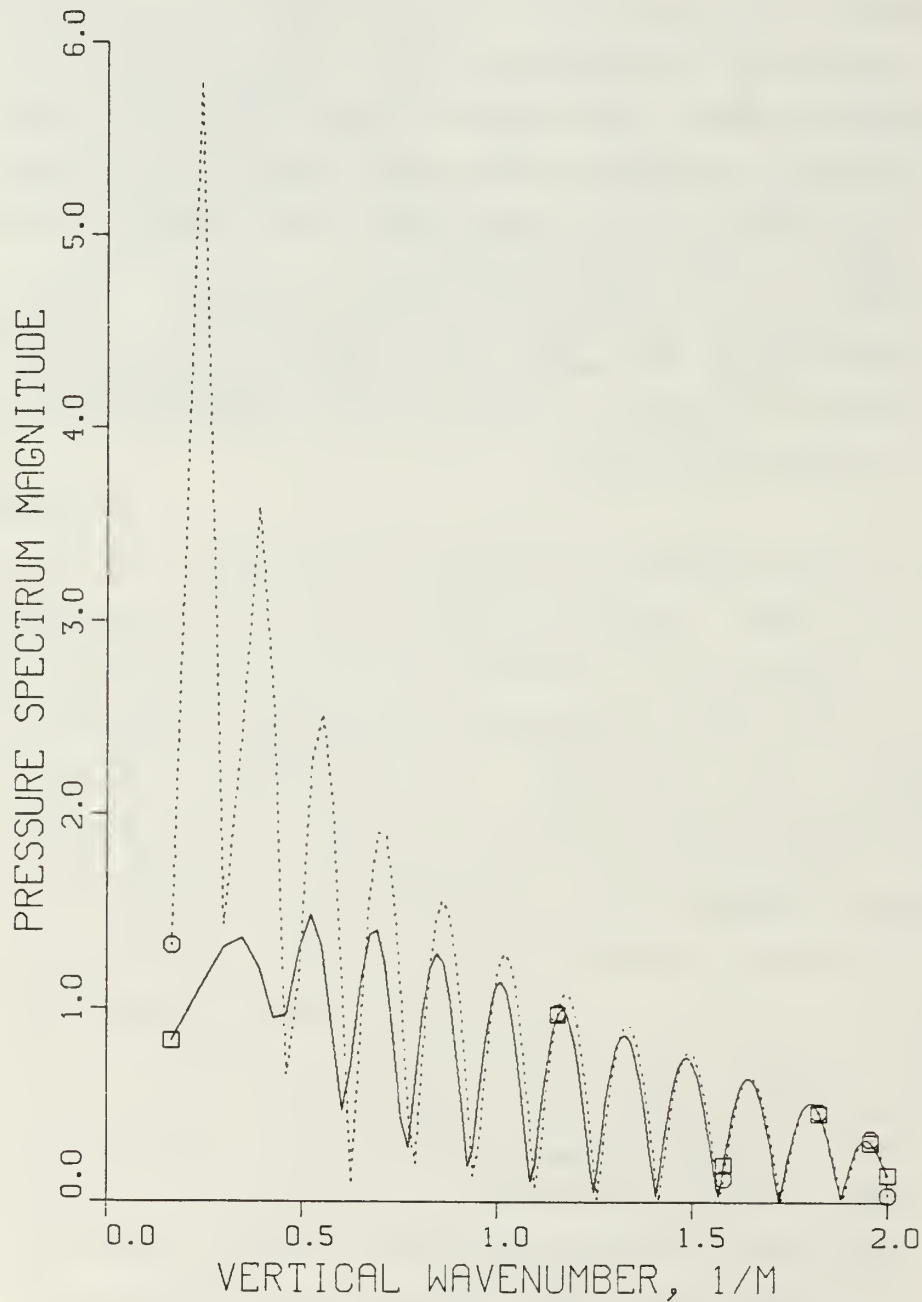


Figure 3.1 Pressure Spectrum Using FFT2C

PRESSURE SPECTRUM VS KZ

SOURCE DEPTH = 20 m, $K = 2.0/\text{m}$,
RECEIVER DEPTH = 50 m, $N = 1024$

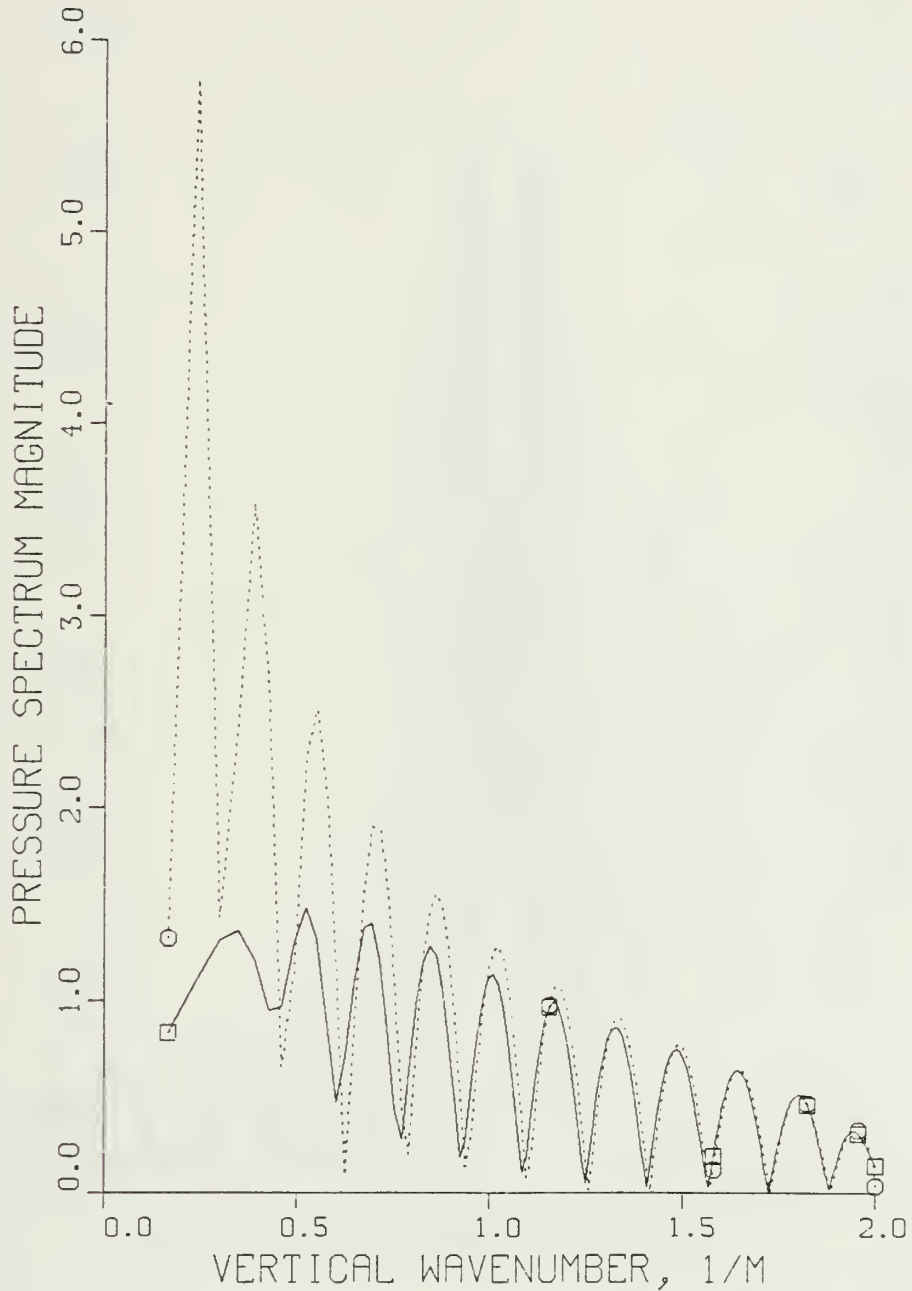


Figure 3.2 Pressure Spectrum Using FFTCC

PRESSURE SPECTRUM VS KZ

SOURCE DEPTH = 20 m, $K = 2.0/\text{m}$,
RECEIVER DEPTH = 50 m, $N = 1024$

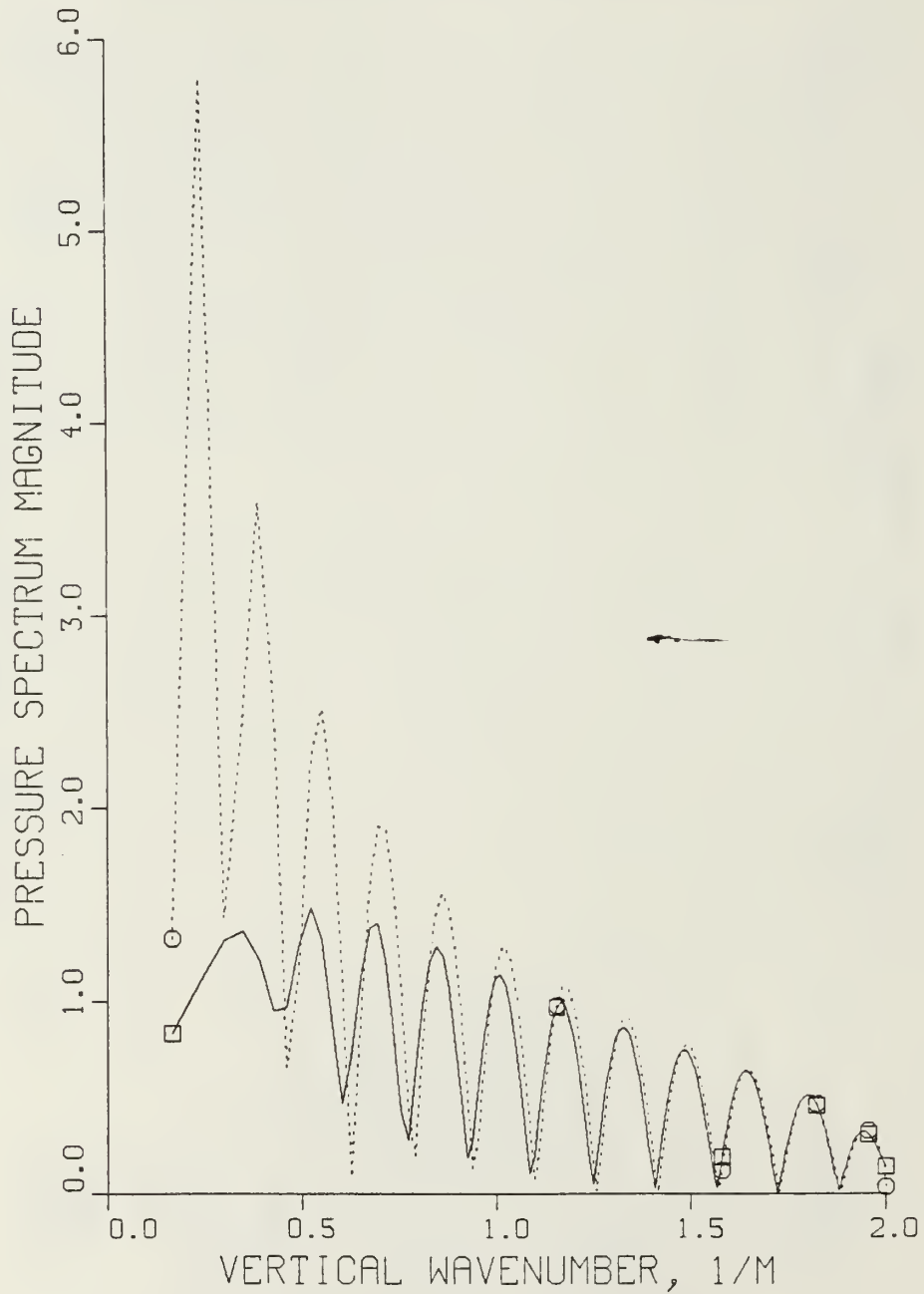


Figure 3.3 Pressure Spectrum Using Cooley-Tukey FFT

MAGNITUDE OF PRESSURE AS A FN OF RANGE

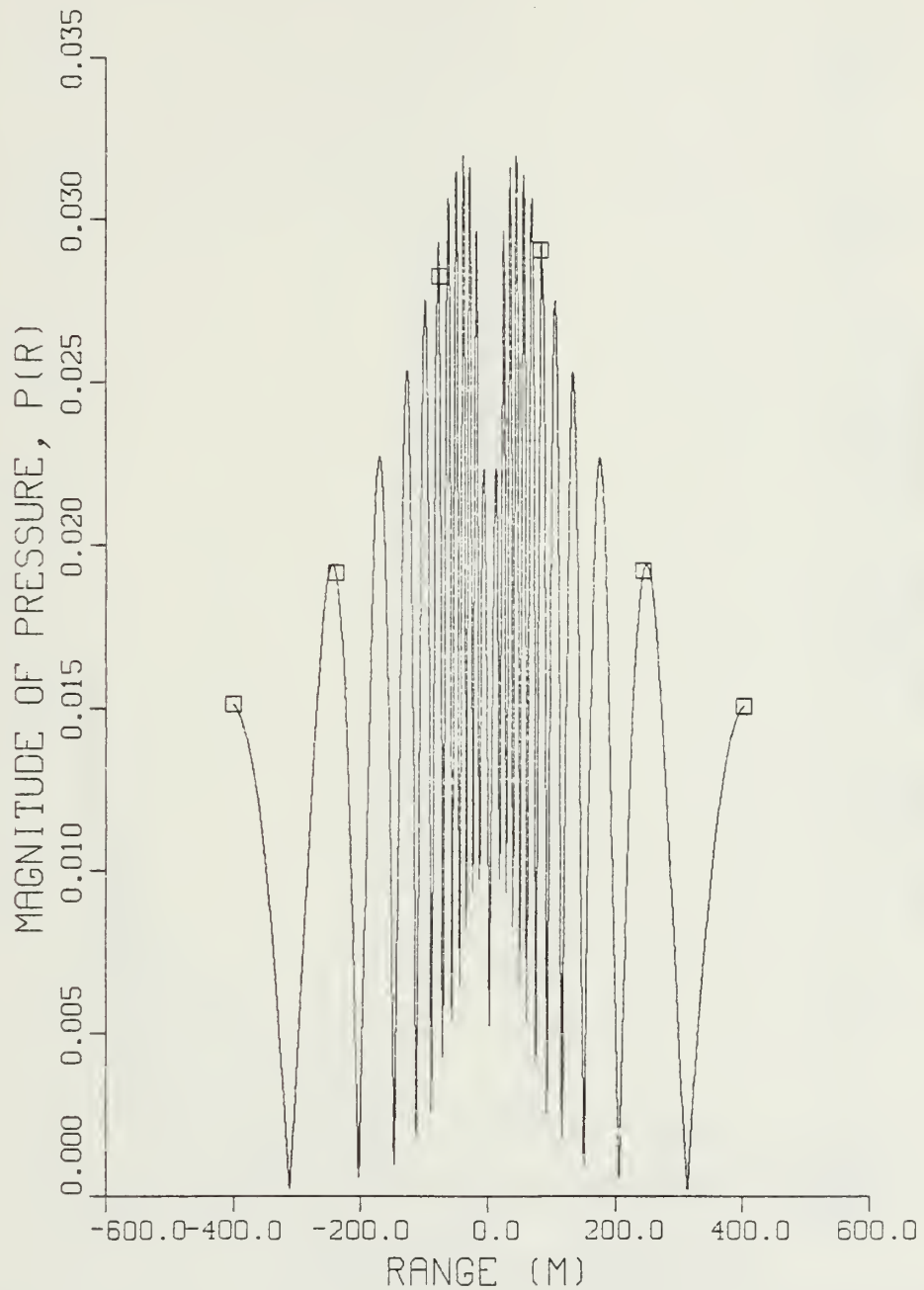


Figure 3.4 Non-smoothed Pressure Field

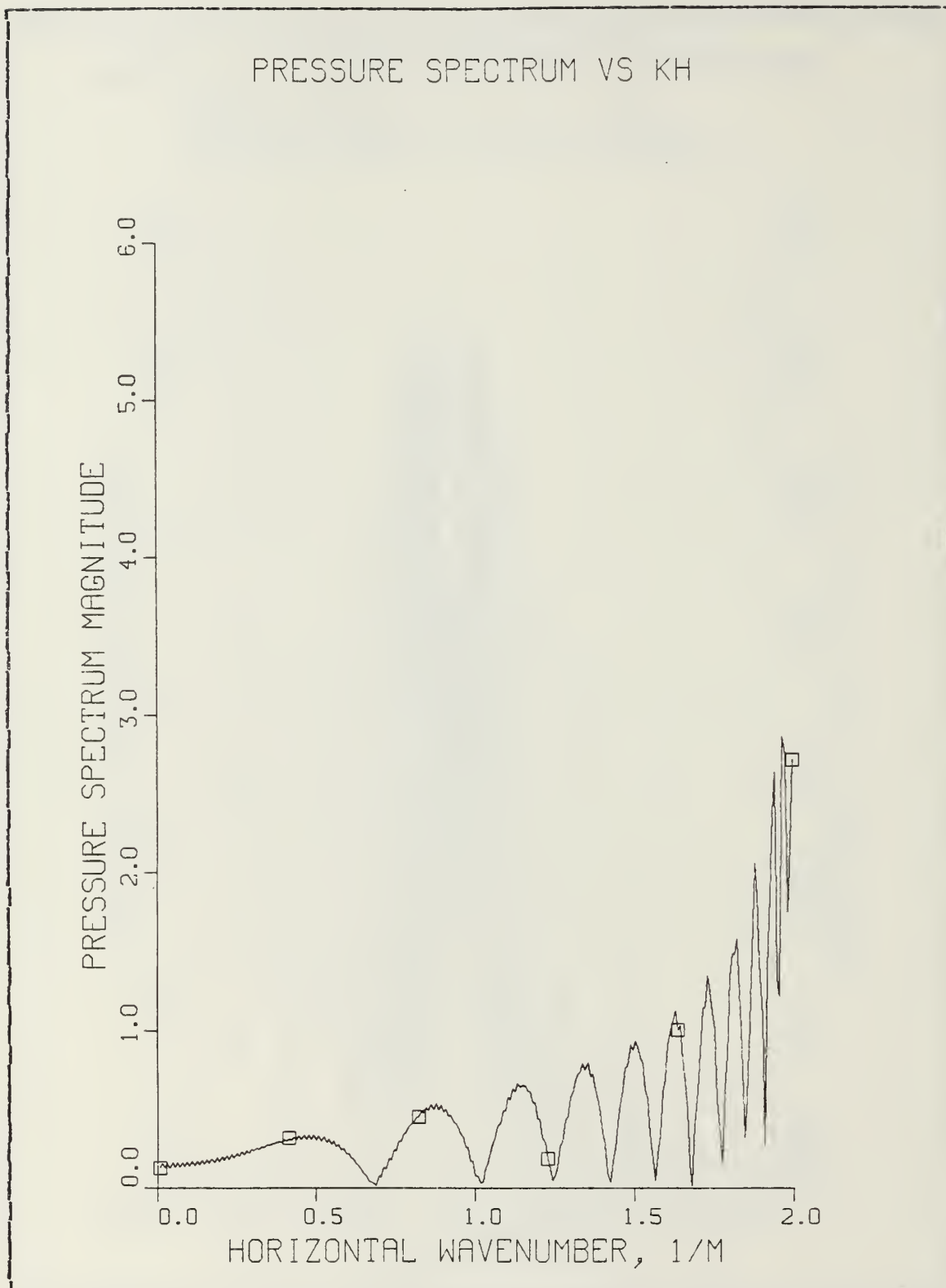


Figure 3.5 Pressure Spectrum Showing Gibbs Phenomenon

MAGNITUDE OF PRESSURE AS A FN OF RANGE



Figure 3.6 Pressure Field Combined With a Hanning Window

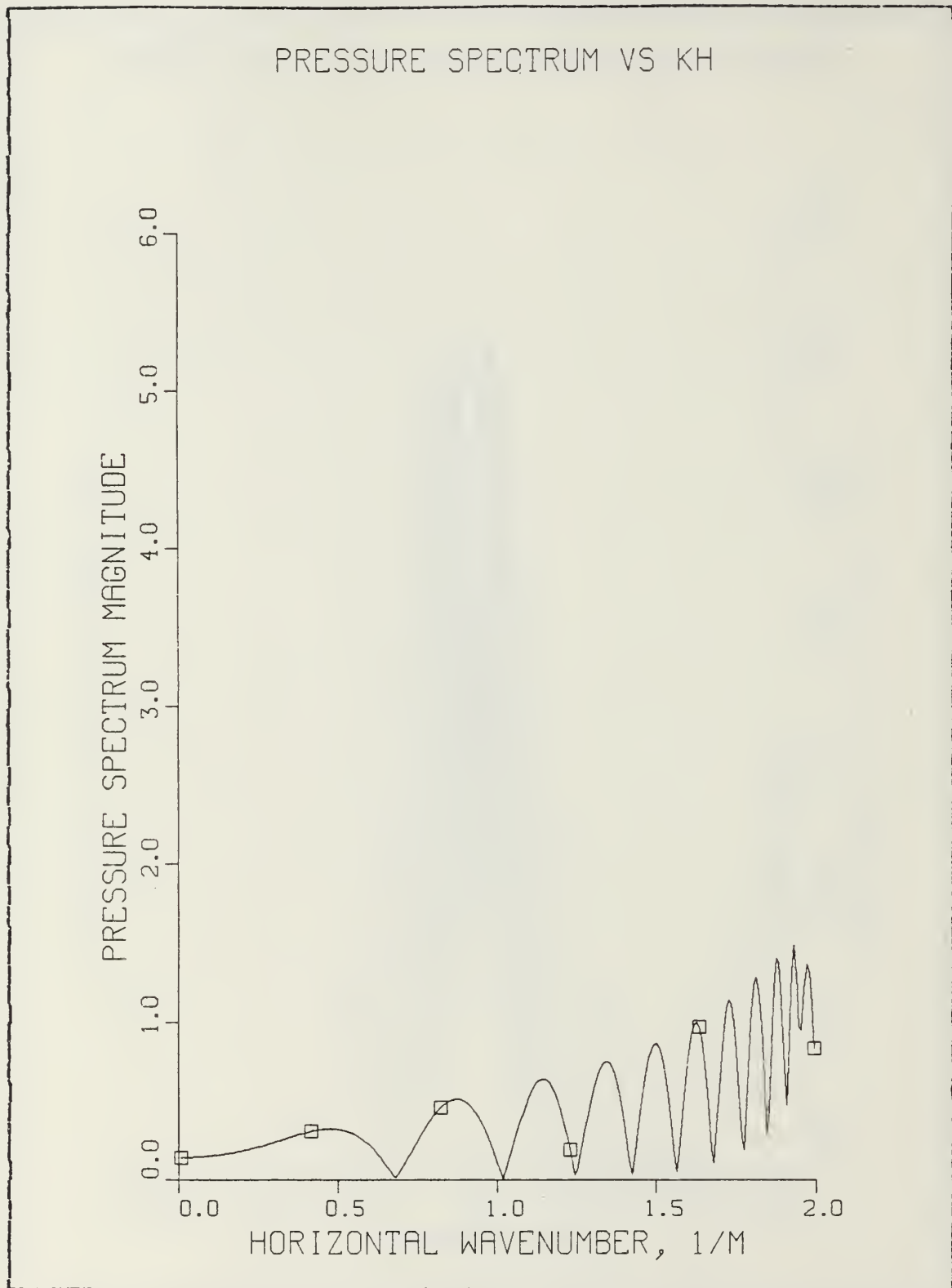


Figure 3.7 Pressure Spectrum Combined With a Hanning Window

THEORETICAL SOURCE DEPTH DETERMINATION CURVE

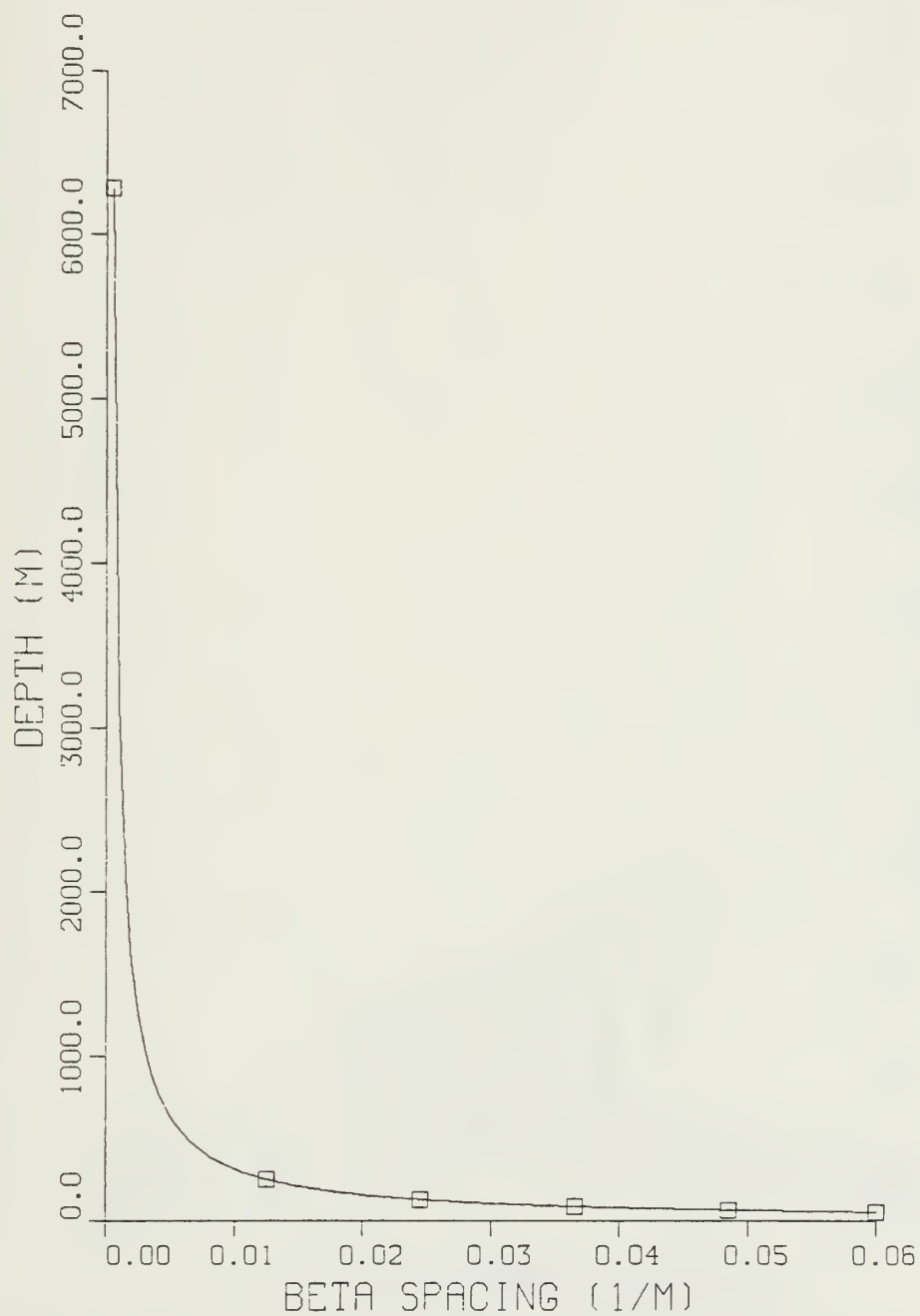


Figure 3.8 Theoretical Source Depth Determination Curve

PRESSURE SPECTRUM VS KZ

RECEIVER DEPTH = 47.124 M, $K = 2.0/\text{M}$,
 $N = 1024$

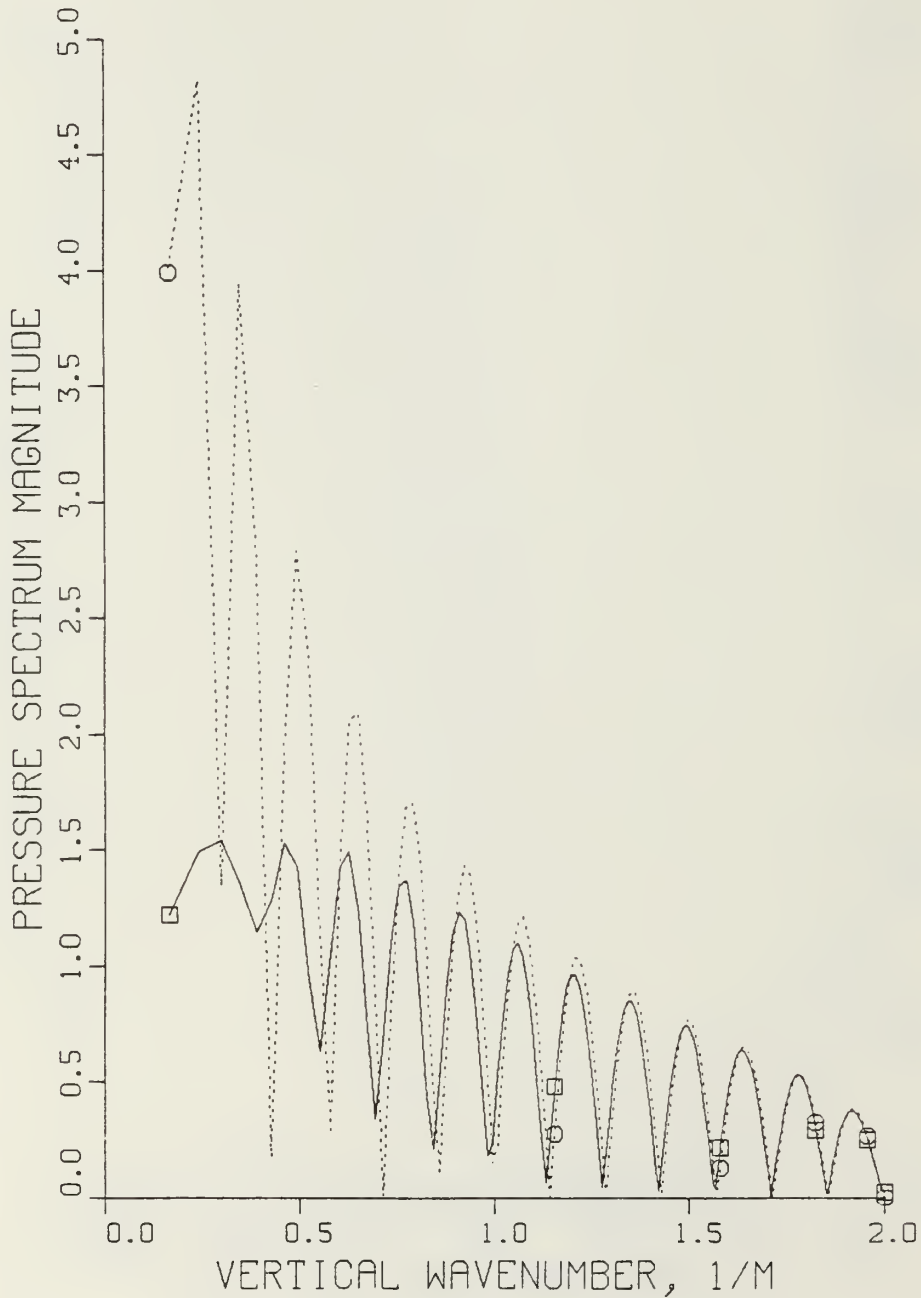


Figure 3.9 Graph of Pressure Spectrum,
Source at 22.0 Meters

PRESSURE SPECTRUM VS KZ

RECEIVER DEPTH = 47.124 M, $K = 2.0/\text{M}$,
 $N = 1024$

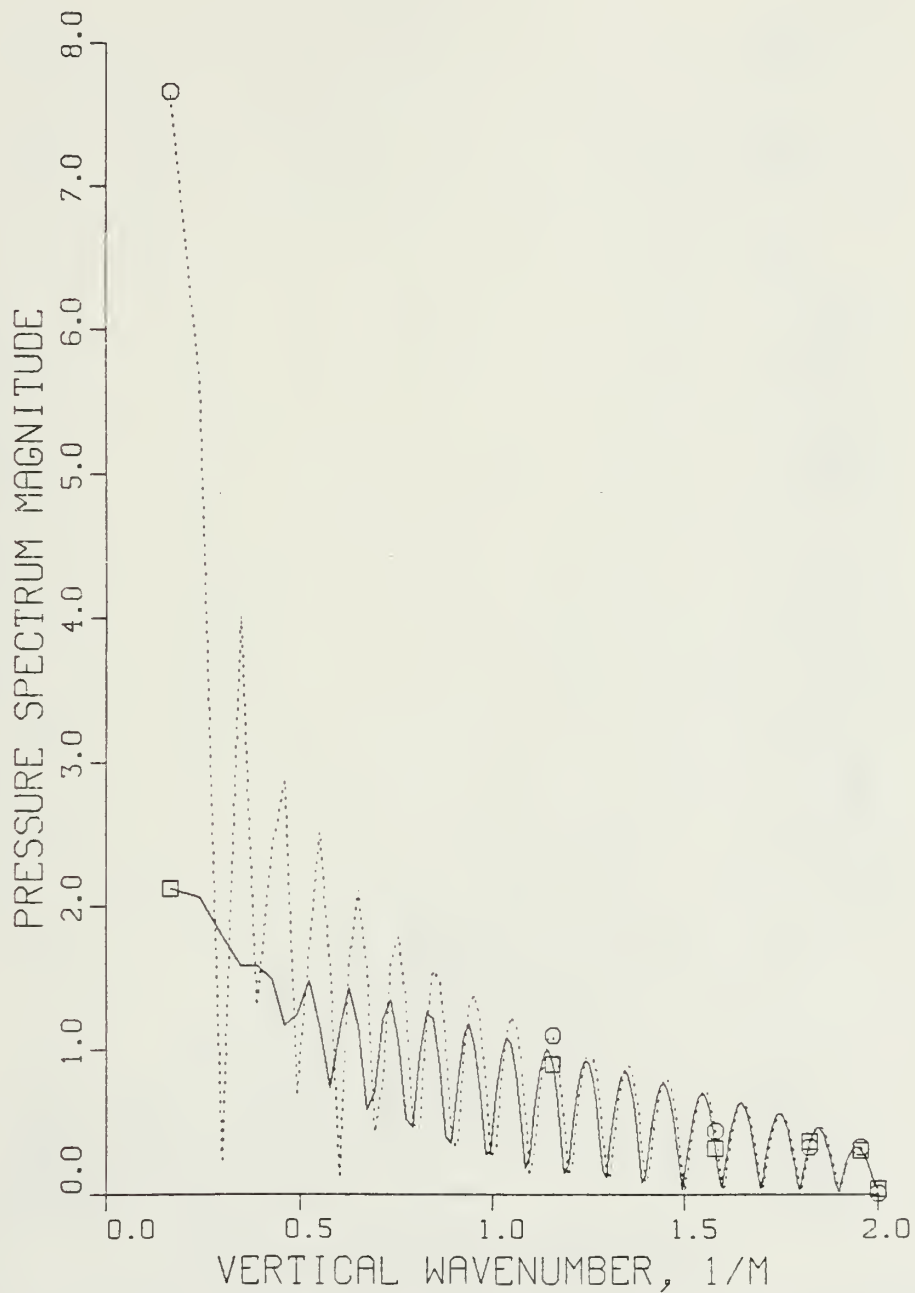


Figure 3.10 Graph of Pressure Spectrum,
Source at 31.4 Meters

PRESSURE SPECTRUM VS KZ

RECEIVER DEPTH = 47.124 M, $K = 2.0/\text{M}$,
 $N = 1024$

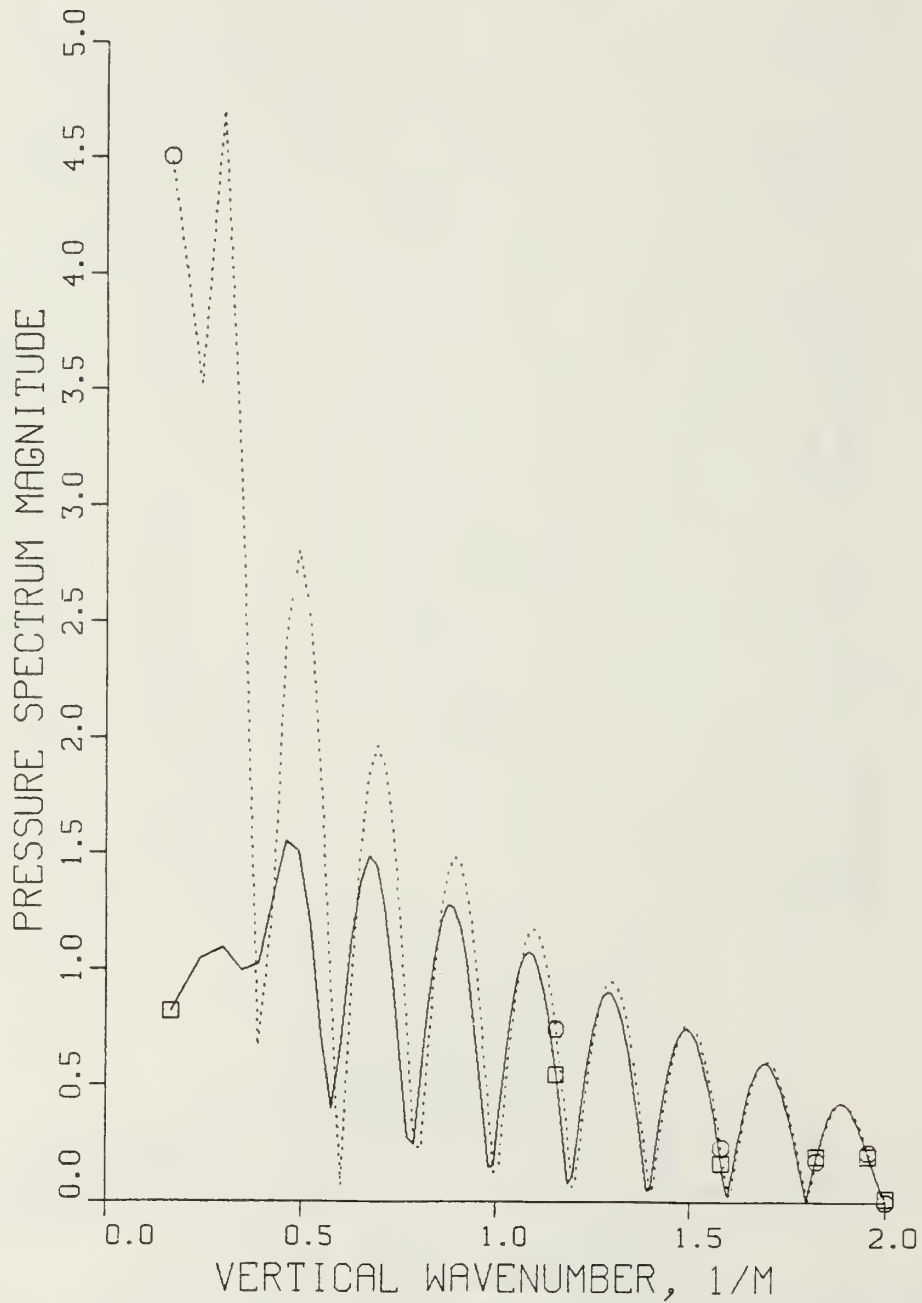


Figure 3.11 Graph of Pressure Spectrum,
Source at 15.7 Meters

PRESSURE SPECTRUM VS KZ

SOURCE DEPTH = 47.124 M, $K = 2.0/M$,

$N = 1024$

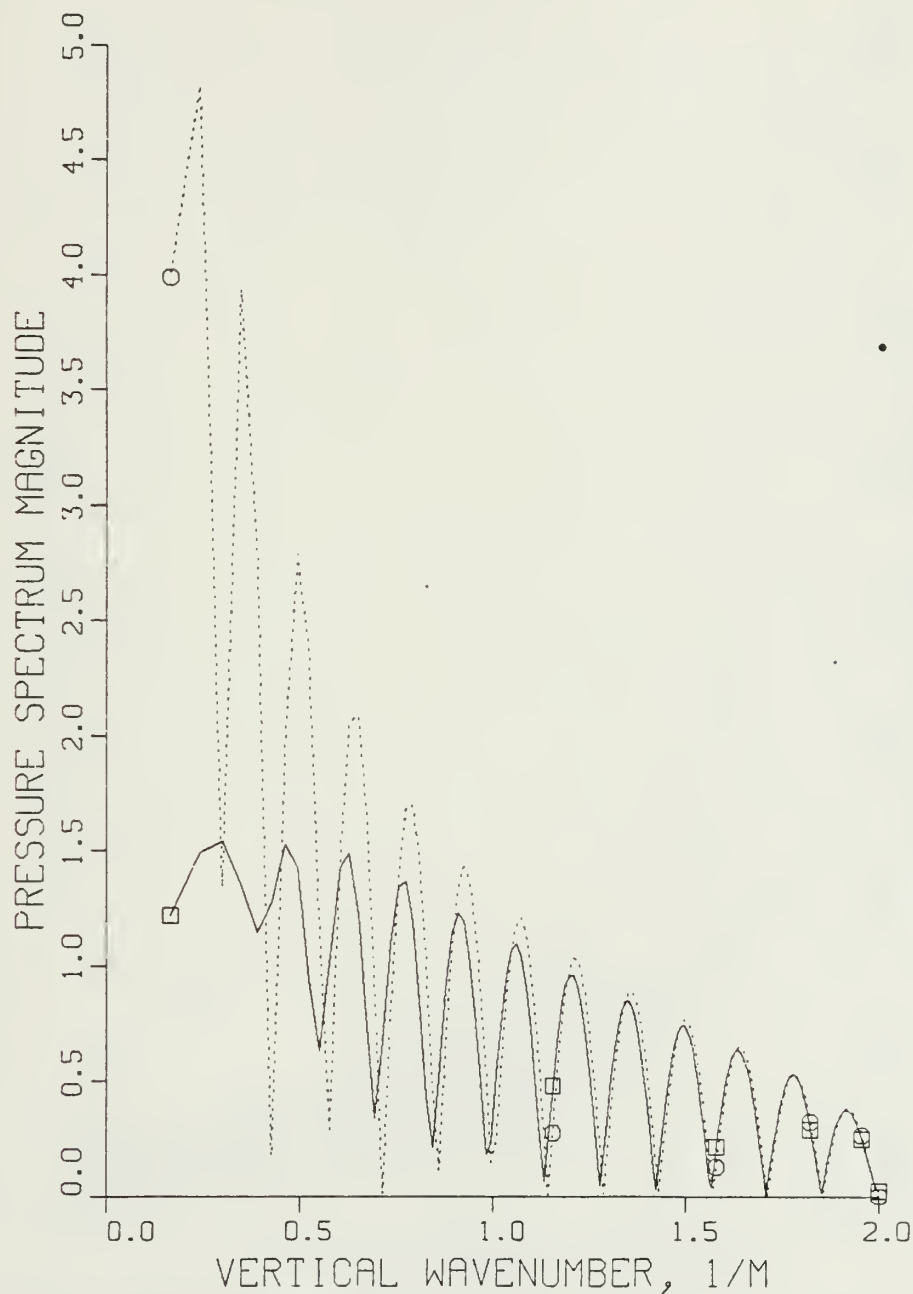


Figure 3.12 Graph of Pressure Spectrum,
Receiver at 22.0 Meters

PRESSURE SPECTRUM VS KZ

SOURCE DEPTH = 47.124 M, $K = 2.0/\text{M}$,
 $N = 1024$

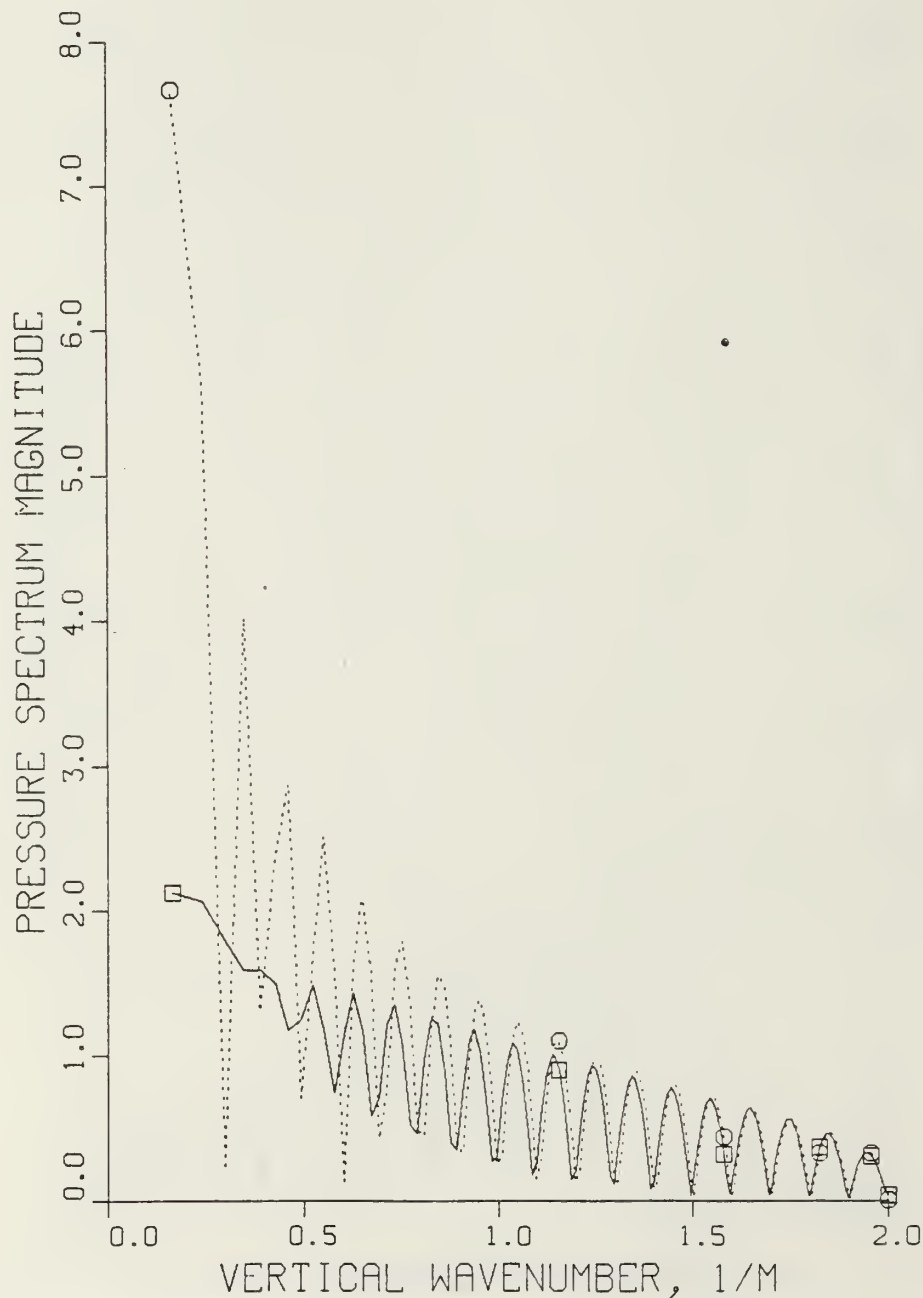


Figure 3.13 Graph of Pressure Spectrum,
Receiver at 31.4 Meters

PRESSURE SPECTRUM VS KZ

SOURCE DEPTH = 47.124 M, $K = 2.0/\text{M}$,

$N = 1024$

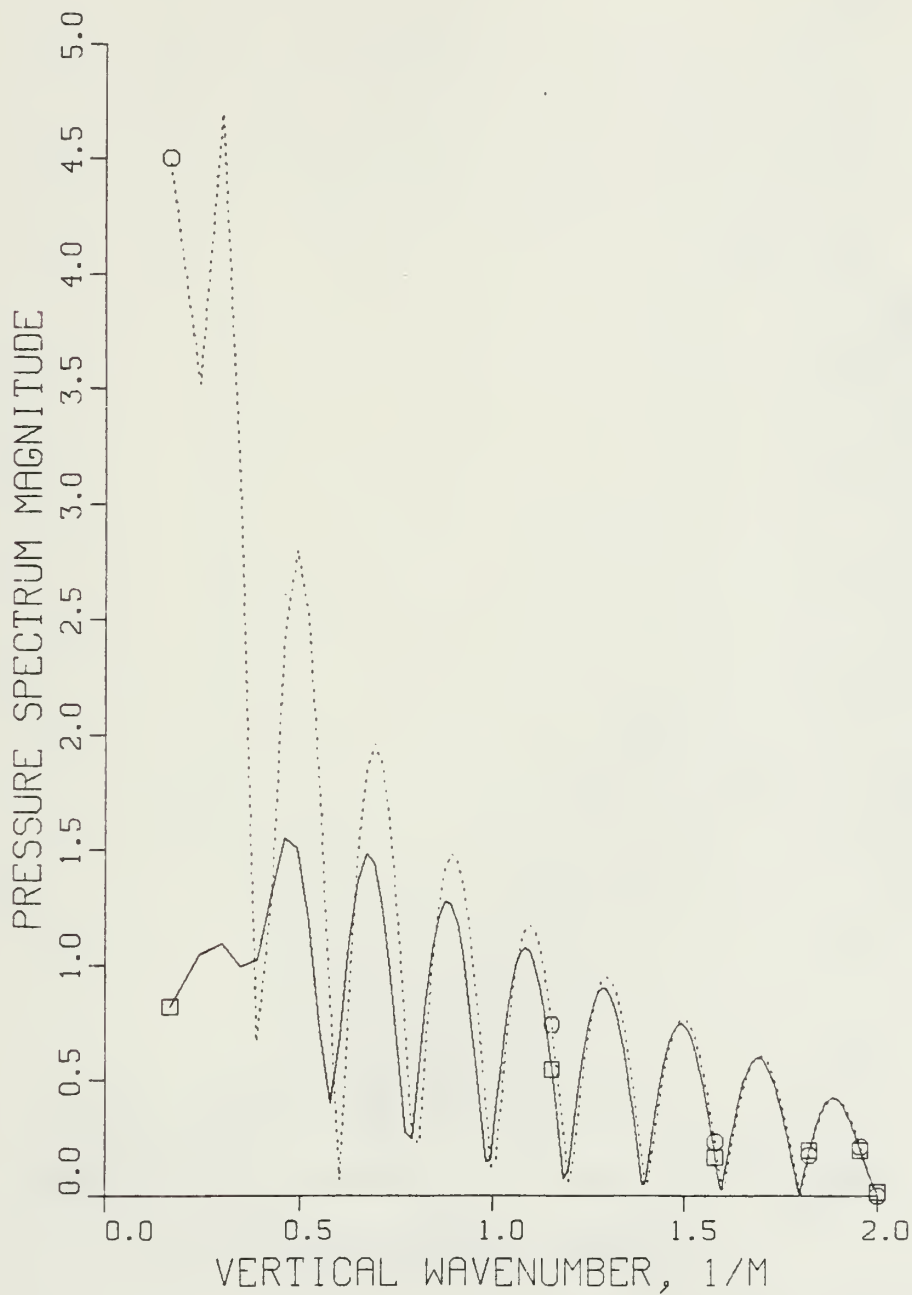


Figure 3.14 Graph of Pressure Spectrum, Receiver at 15.7 Meters

PRESSURE SPECTRUM VS KZ

SOURCE DEPTH = 21.998 M, $K = 2.0/\text{M}$

RECEIVER DEPTH = 47.124 M, $N = 1024$

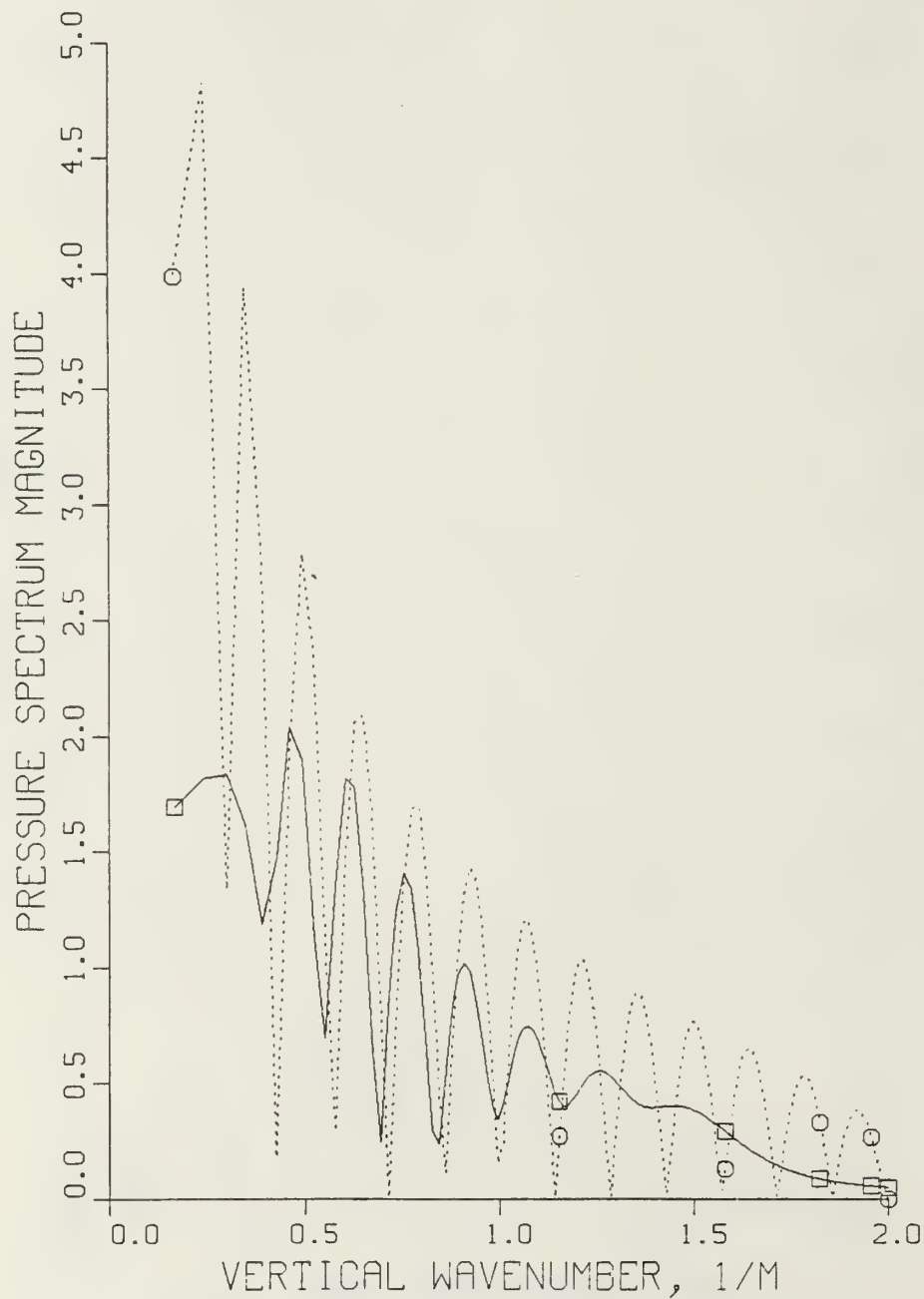


Figure 3.15 Pressure Spectrum,
Range Window Set at 47.1 Meters

PRESSURE SPECTRUM VS KZ

SOURCE DEPTH = 21.998 M, $K = 2.0/M$,

Receiver Depth = 47.124 M, $N = 1024$

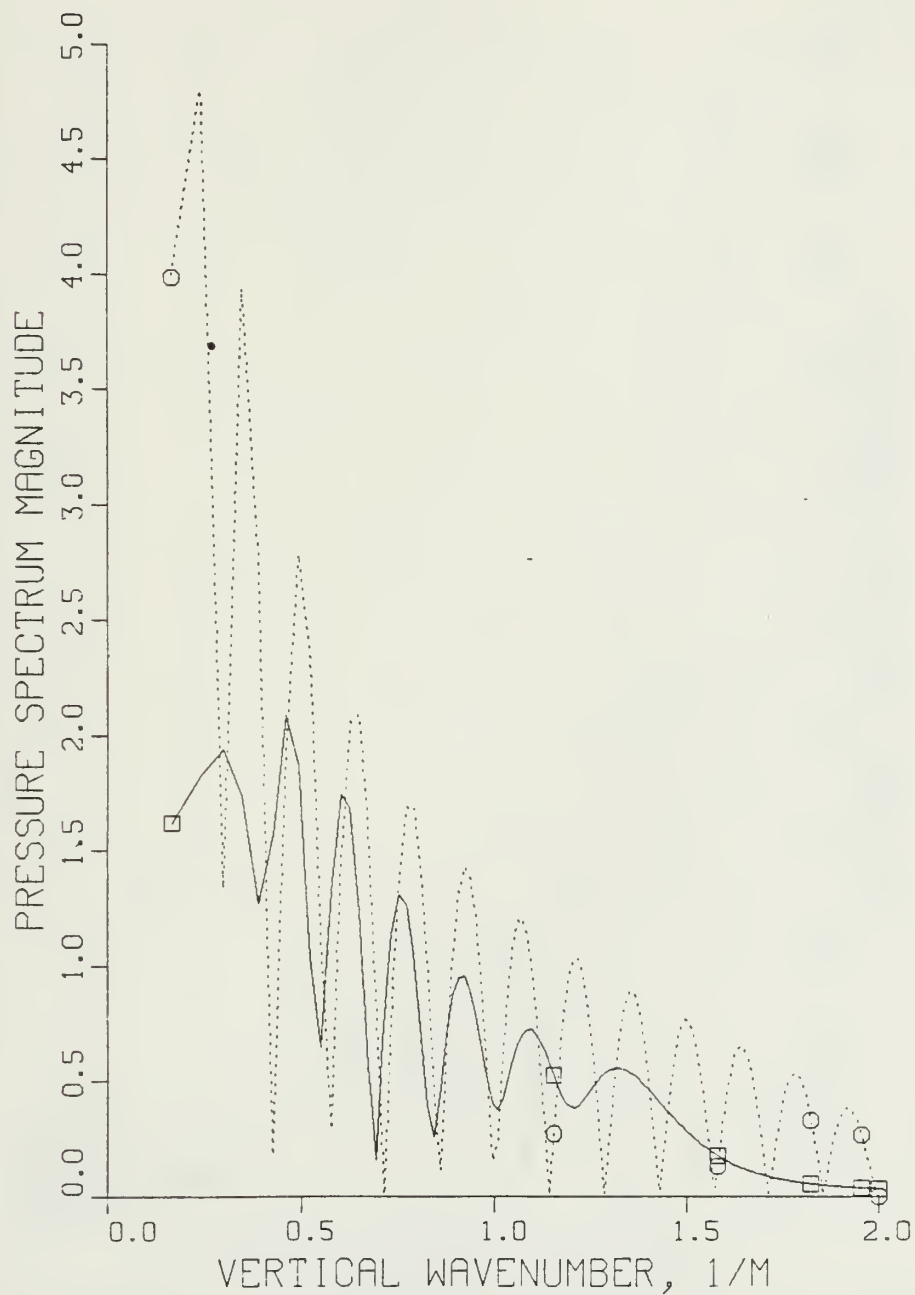


Figure 3.16 Pressure Spectrum,
Range Window Set at 50.3 Meters

PRESSURE SPECTRUM VS KZ

SOURCE DEPTH = 21.998 M, $K = 2.0/\text{M}$,

RECEIVER DEPTH = 47.124 M, $N = 1024$

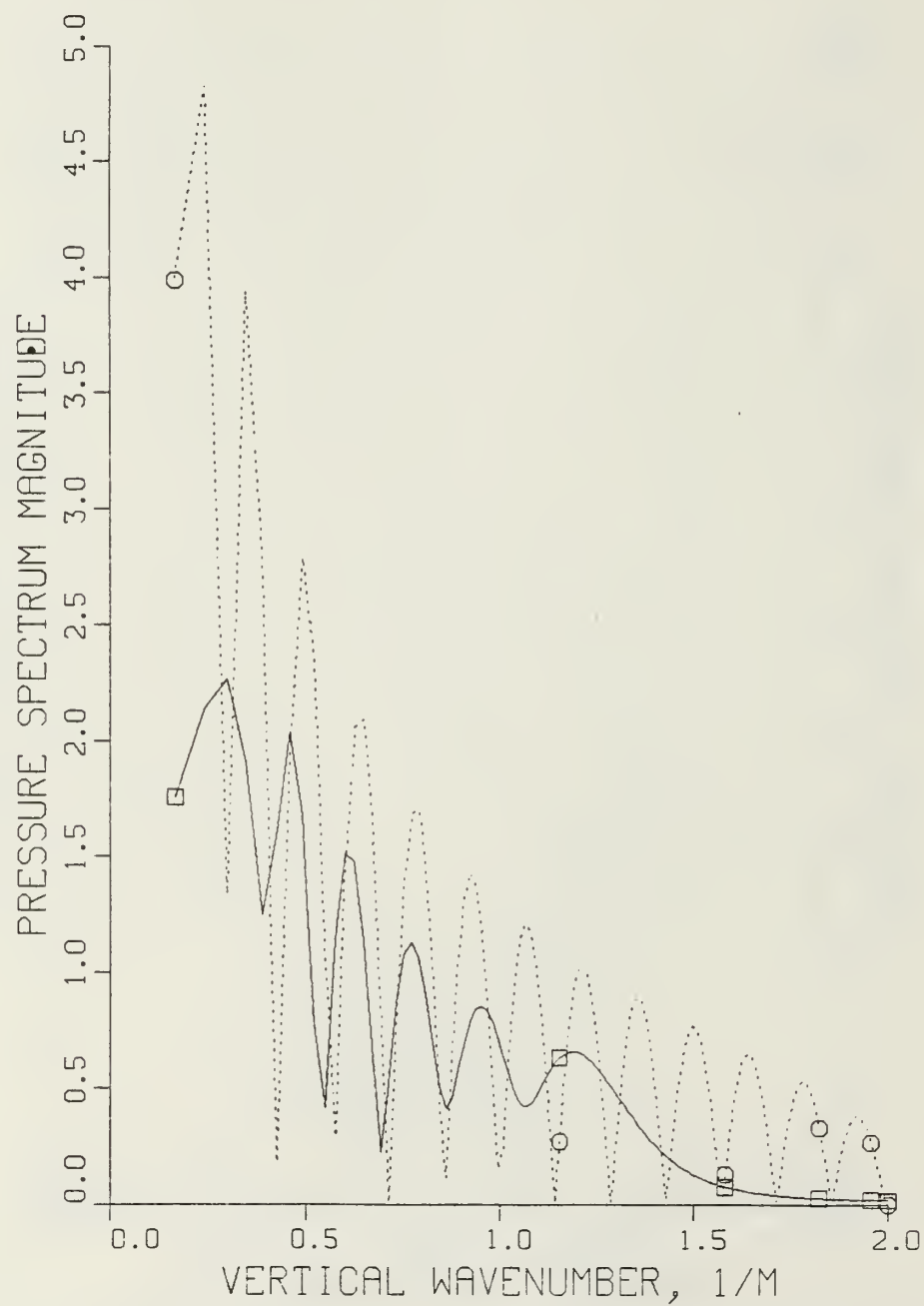


Figure 3.17 Pressure Spectrum,
Range Window Set at 62.8 Meters

PRESSURE SPECTRUM VS KZ

SOURCE DEPTH = 21.998 M, $K = 2.0/M$
RECEIVER DEPTH = 47.124 M, $H = 0.0$ M

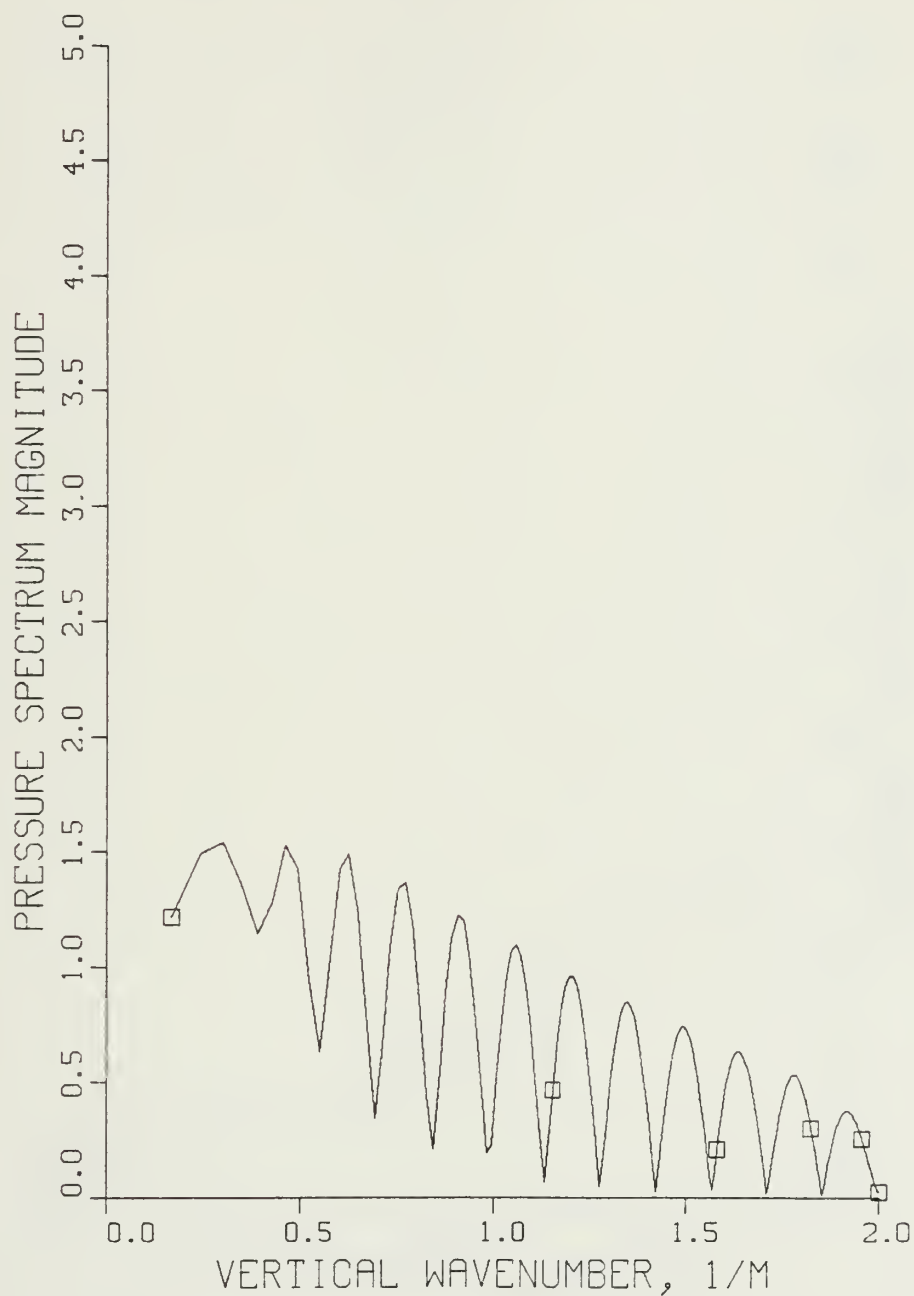


Figure 3.18 Pressure Spectrum, Sea State 0

PRESSURE SPECTRUM VS KZ

SOURCE DEPTH = 21.998 M, $K = 2.0/\text{M}$

RECEIVER DEPTH = 47.124 M, $H = 1.0 \text{ M}$

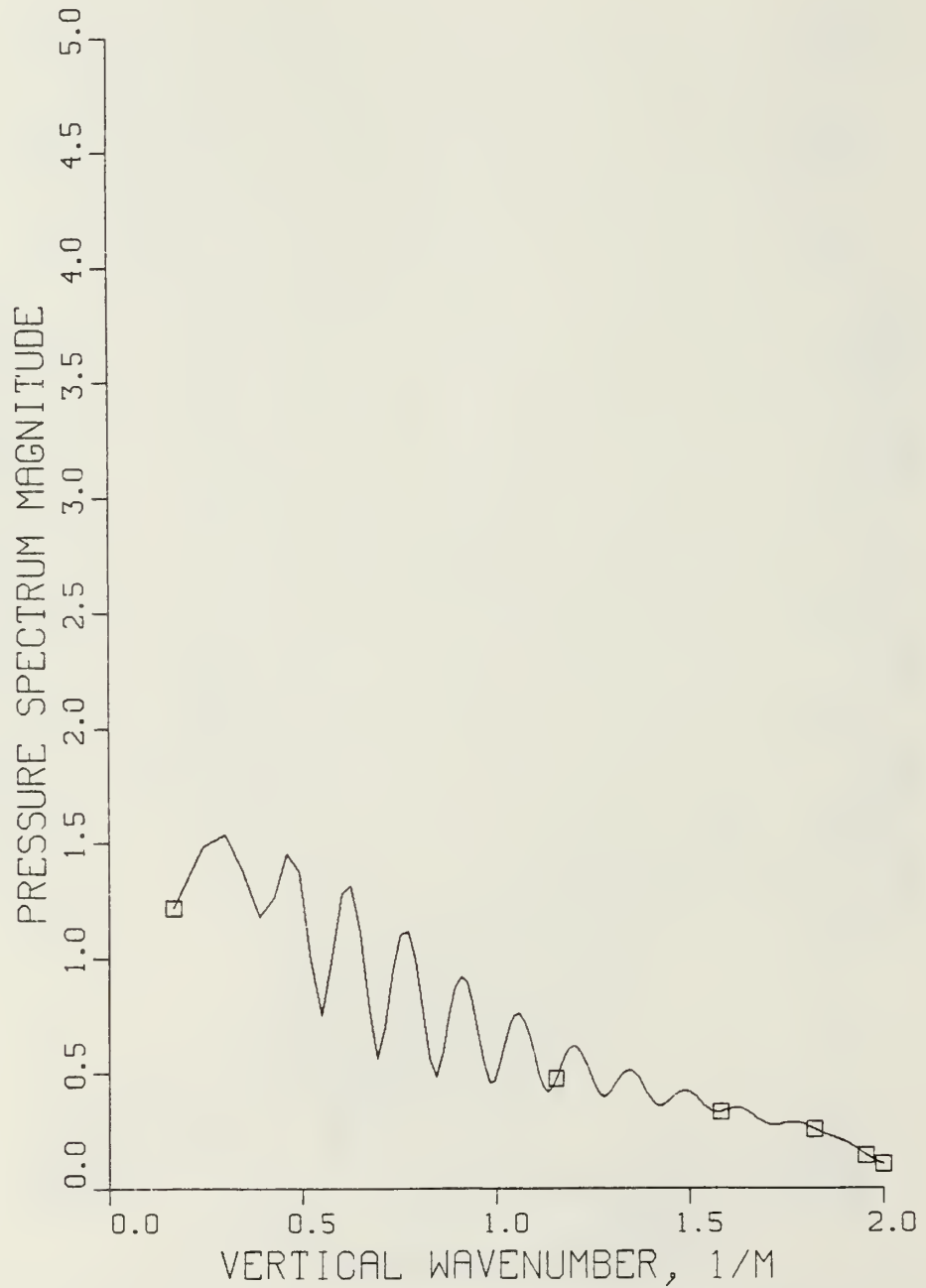


Figure 3.19 Pressure Spectrum, Sea State 2

PRESSURE SPECTRUM VS KZ

SOURCE DEPTH = 21.998 M, $K = 2.0/\text{M}$
RECEIVER DEPTH = 47.124 M, $H = 3 \text{ M}$

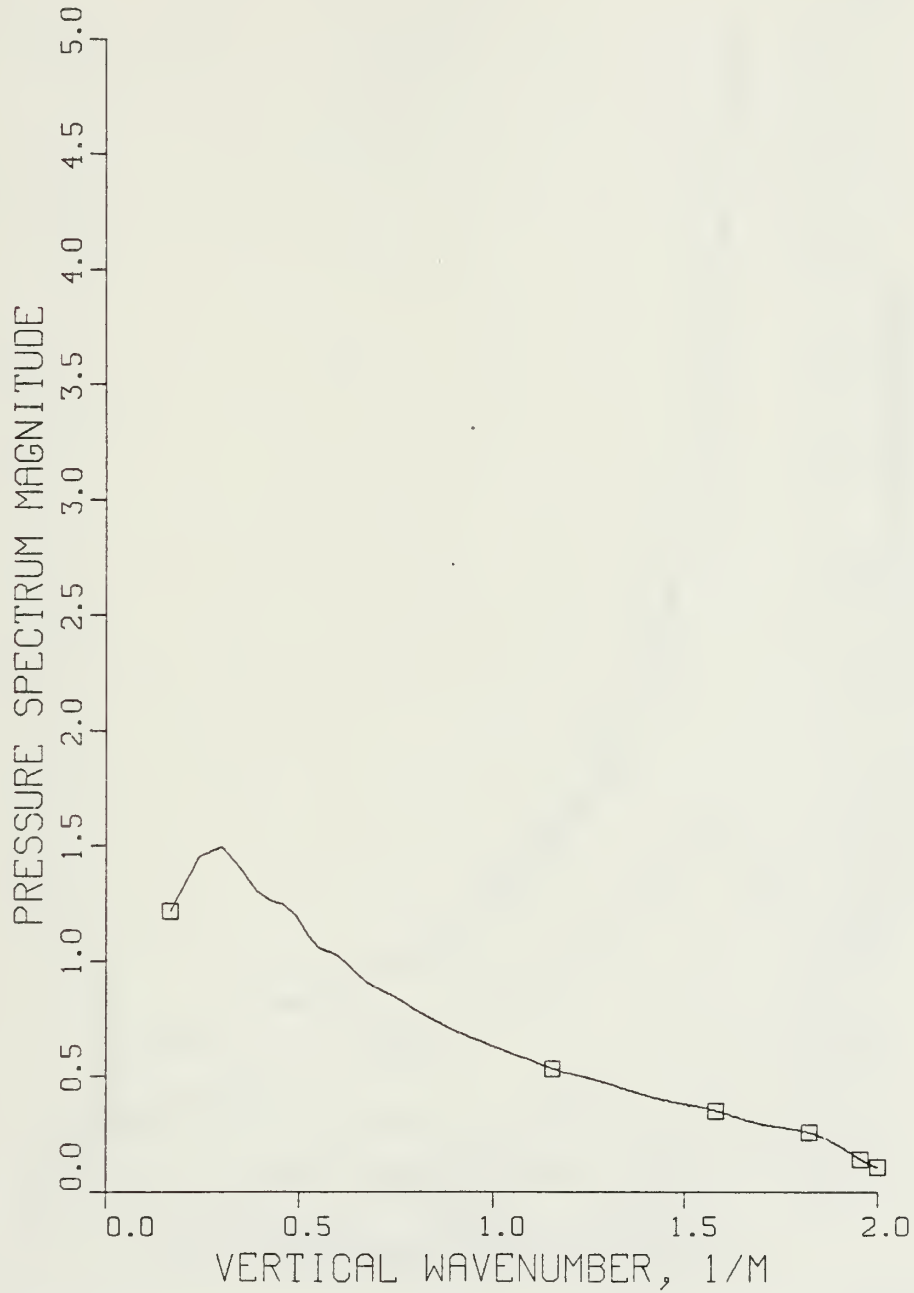


Figure 3.20 Pressure Spectrum, Sea State 3

PRESSURE SPECTRUM VS KZ

SOURCE DEPTH = 21.998 M, $K = 2.0/\text{M}$
RECEIVER DEPTH = 47.124 M, $H = 10 \text{ M}$

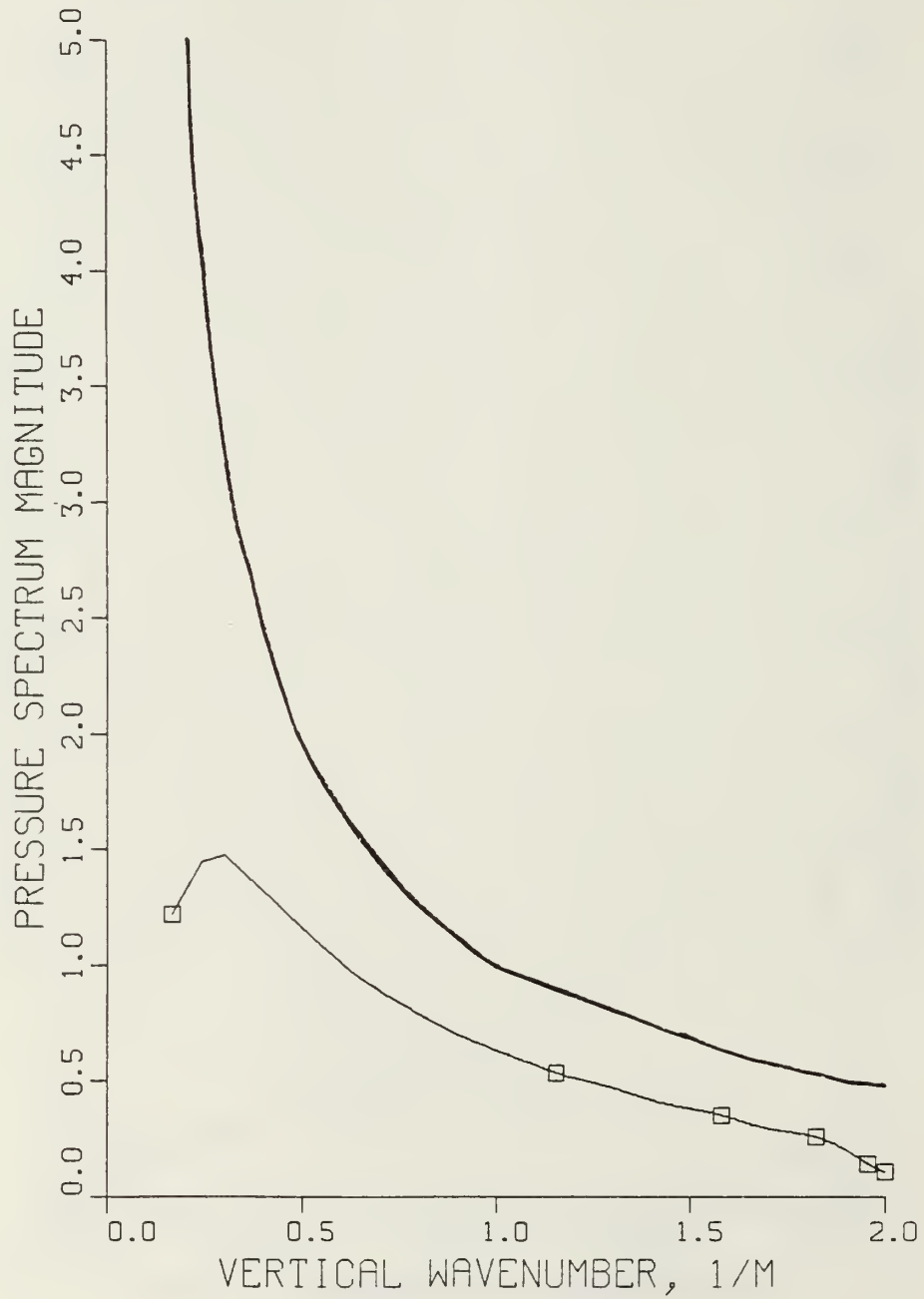


Figure 3.21 Pressure Spectrum, Sea State 5

PRESSURE SPECTRUM VS KH

SOURCE DEPTH = 21.998 M, N = 1024

RECEIVER DEPTH = 47.124 M

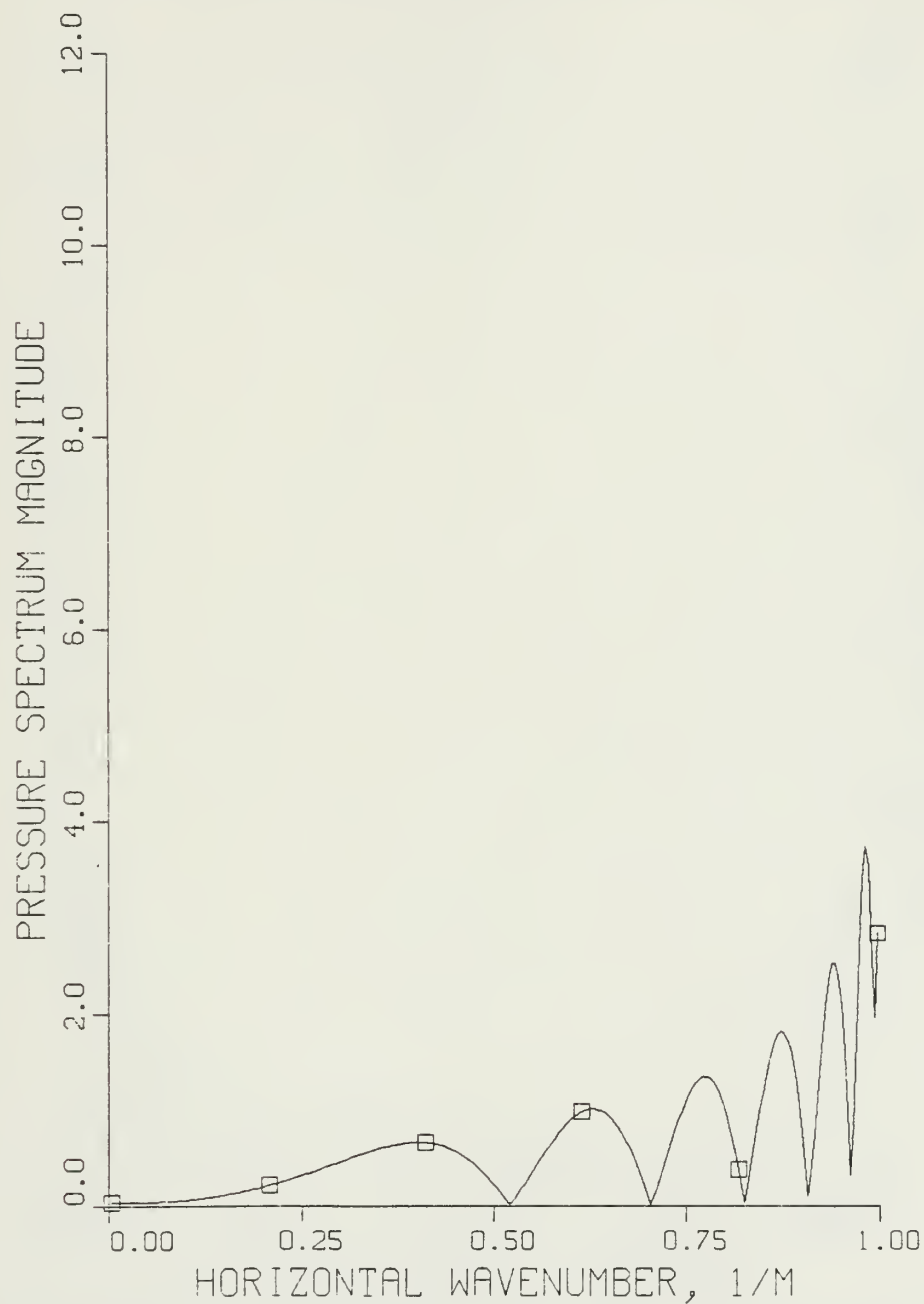


Figure 3.22 Pressure Spectrum, Sea State 0, K = 1.0

PRESSURE SPECTRUM VS KH

SOURCE DEPTH = 21.998 M, N = 1024

RECEIVER DEPTH = 47.124 M



Figure 3.23 Pressure Spectrum, Sea State 3, K = 1.0

PRESSURE SPECTRUM VS KH

SOURCE DEPTH = 21.998 M, N = 1024

RECEIVER DEPTH = 47.124 M

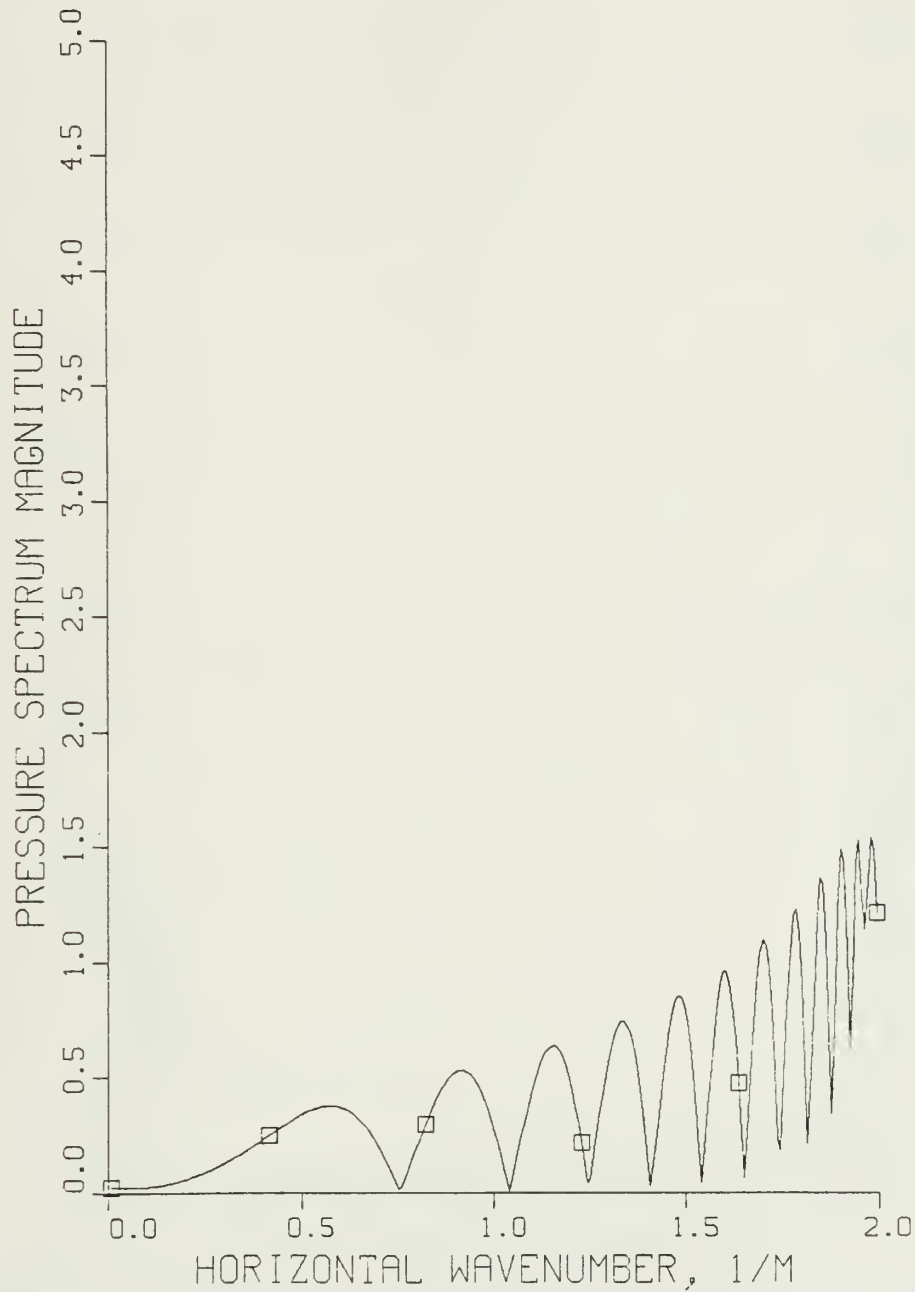


Figure 3.24 Pressure Spectrum, Sea State 0, $K = 2.0$

PRESSURE SPECTRUM VS KH

SOURCE DEPTH = 21.998 M, N = 1024

RECEIVER DEPTH = 47.124 M

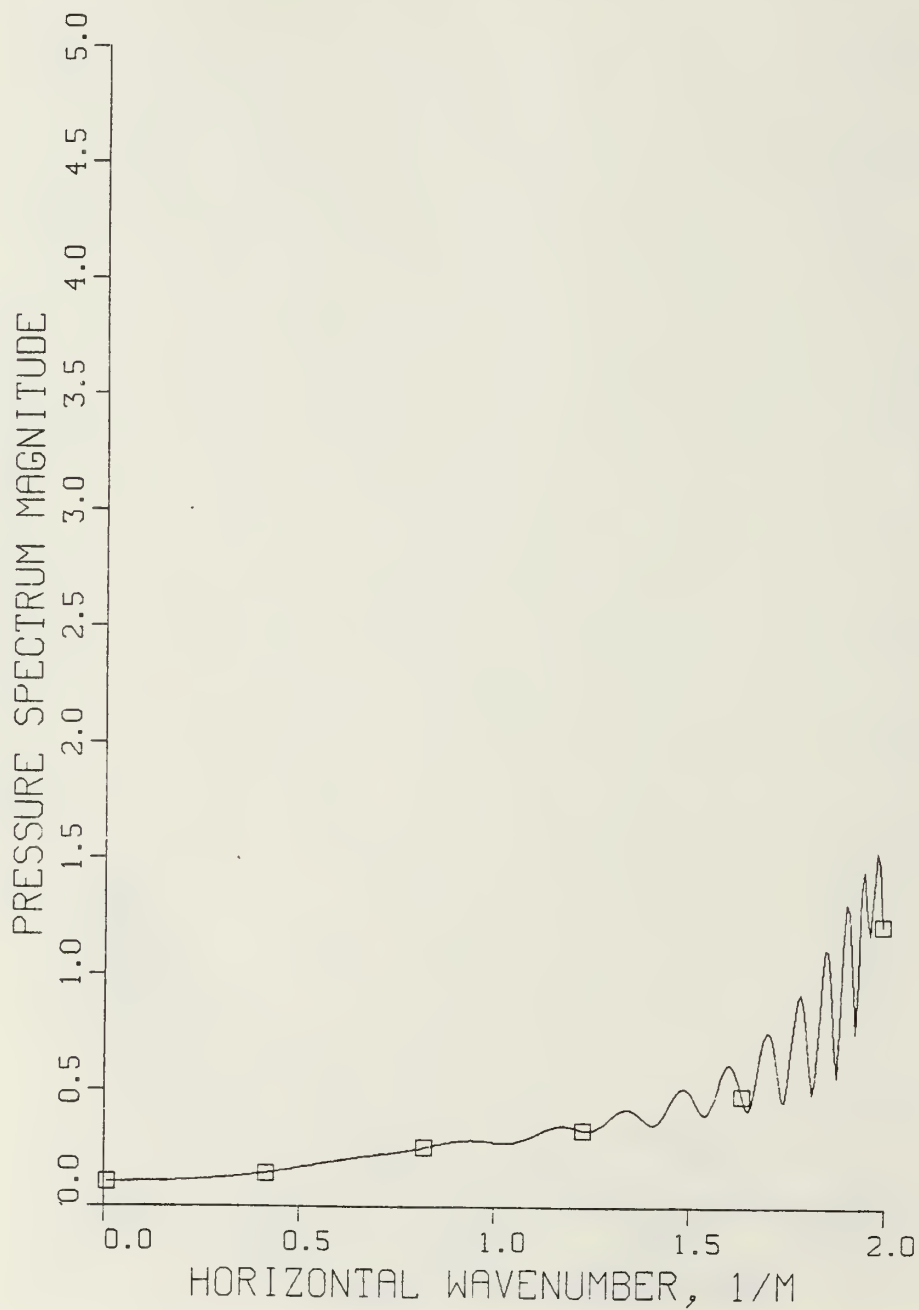


Figure 3.25 Pressure Spectrum, Sea State 3, $\kappa = 2.0$

PRESSURE SPECTRUM VS KH

SOURCE DEPTH = 21.998 M, N = 1024

RECEIVER DEPTH = 47.124 M

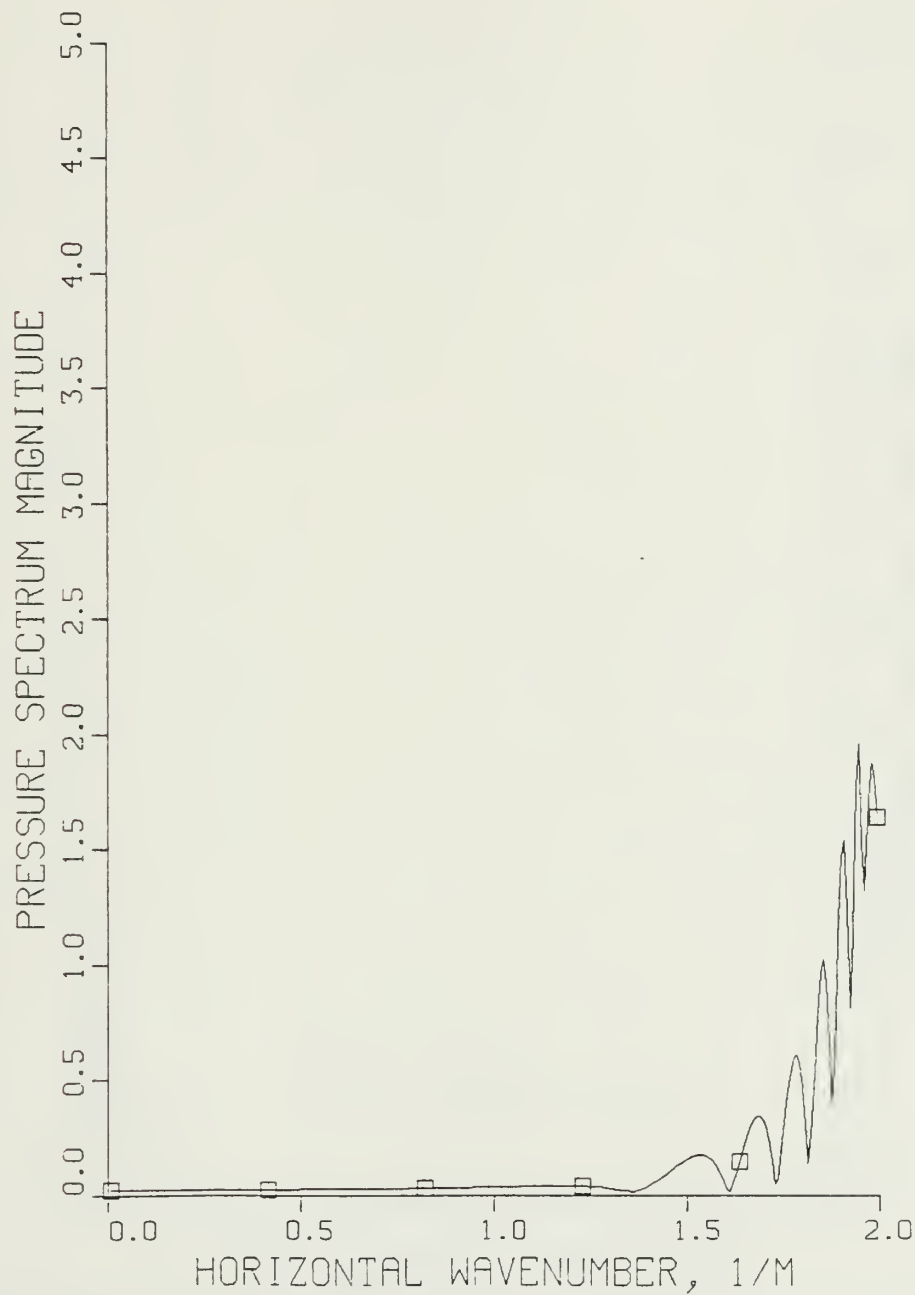


Figure 3.26 Pressure Spectrum,
SS 2, Range Window Set at 50 Meters

PRESSURE SPECTRUM VS KH

SOURCE DEPTH = 21.998 M, N = 1024

RECEIVER DEPTH = 47.124 M

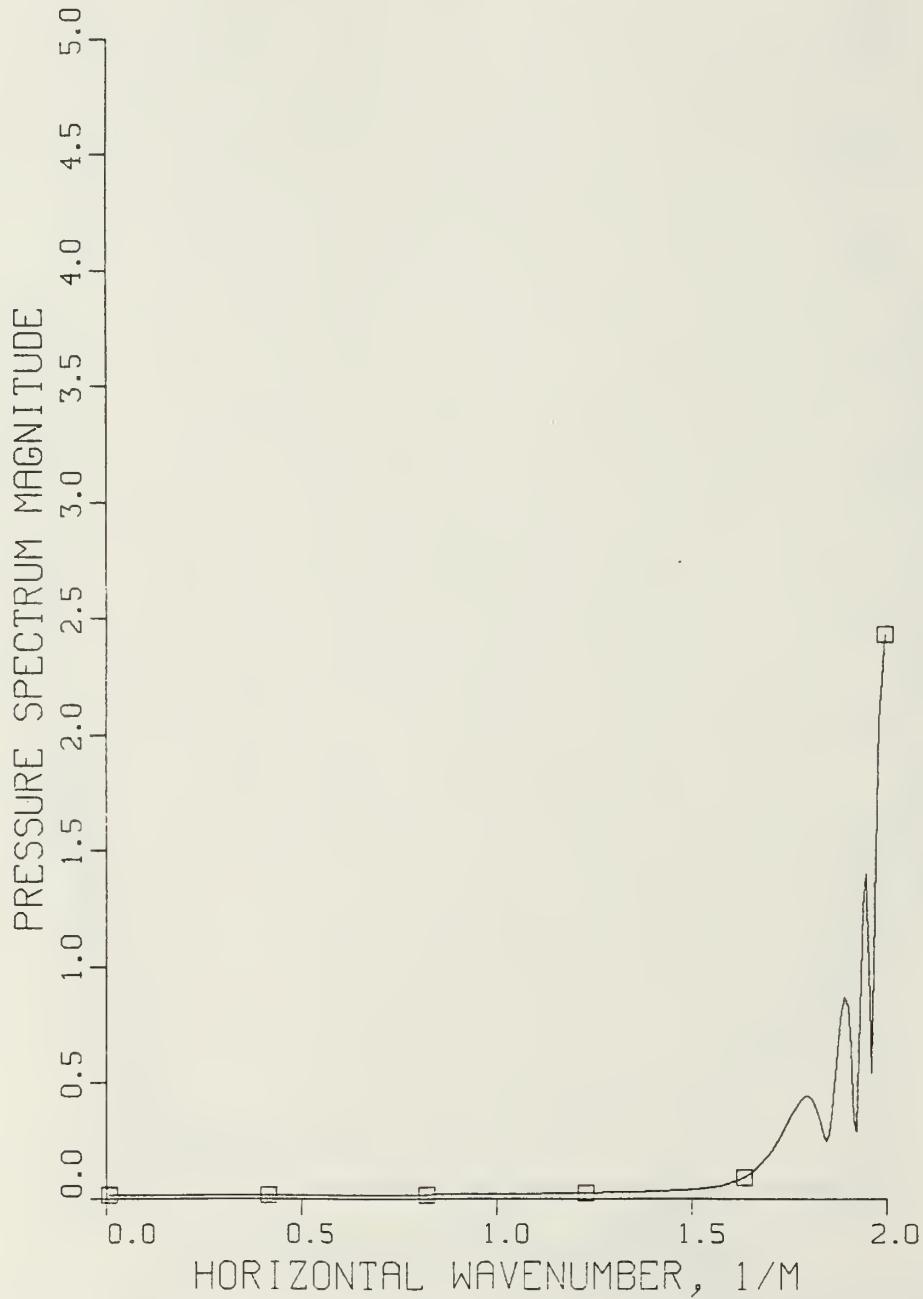


Figure 3.27 Pressure Spectrum,
SS 2, Range Window Set at 100 Meters

PRESSURE SPECTRUM VS KH

SOURCE DEPTH = 21.998 M, N = 1024

RECEIVER DEPTH = 47.124 M

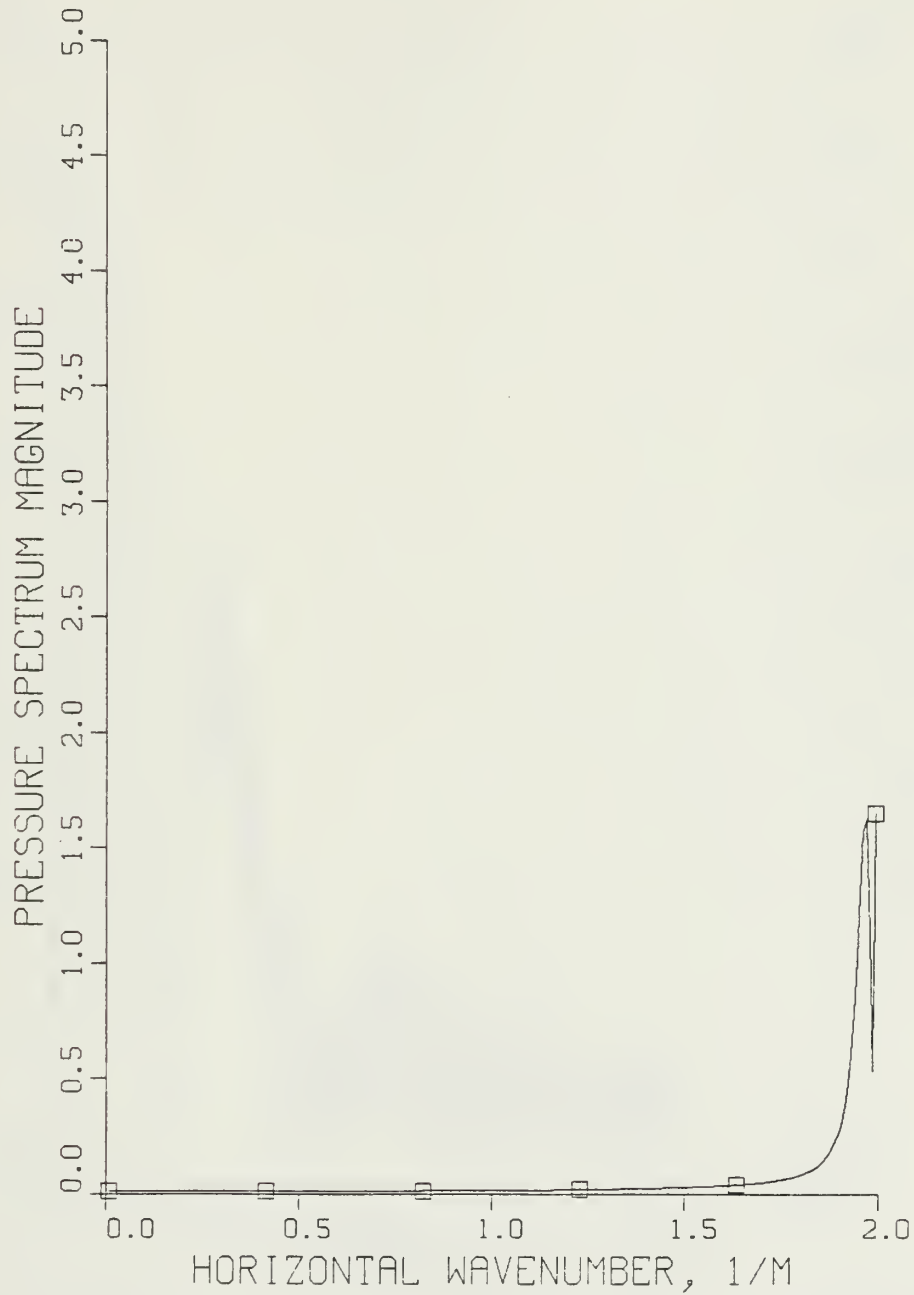


Figure 3.28 Pressure Spectrum,
SS 2, Range Window Set at 200 Meters

PRESSURE SPECTRUM VS KH

SOURCE DEPTH = 21.998 M, N = 1024

RECEIVER DEPTH = 47.124 M

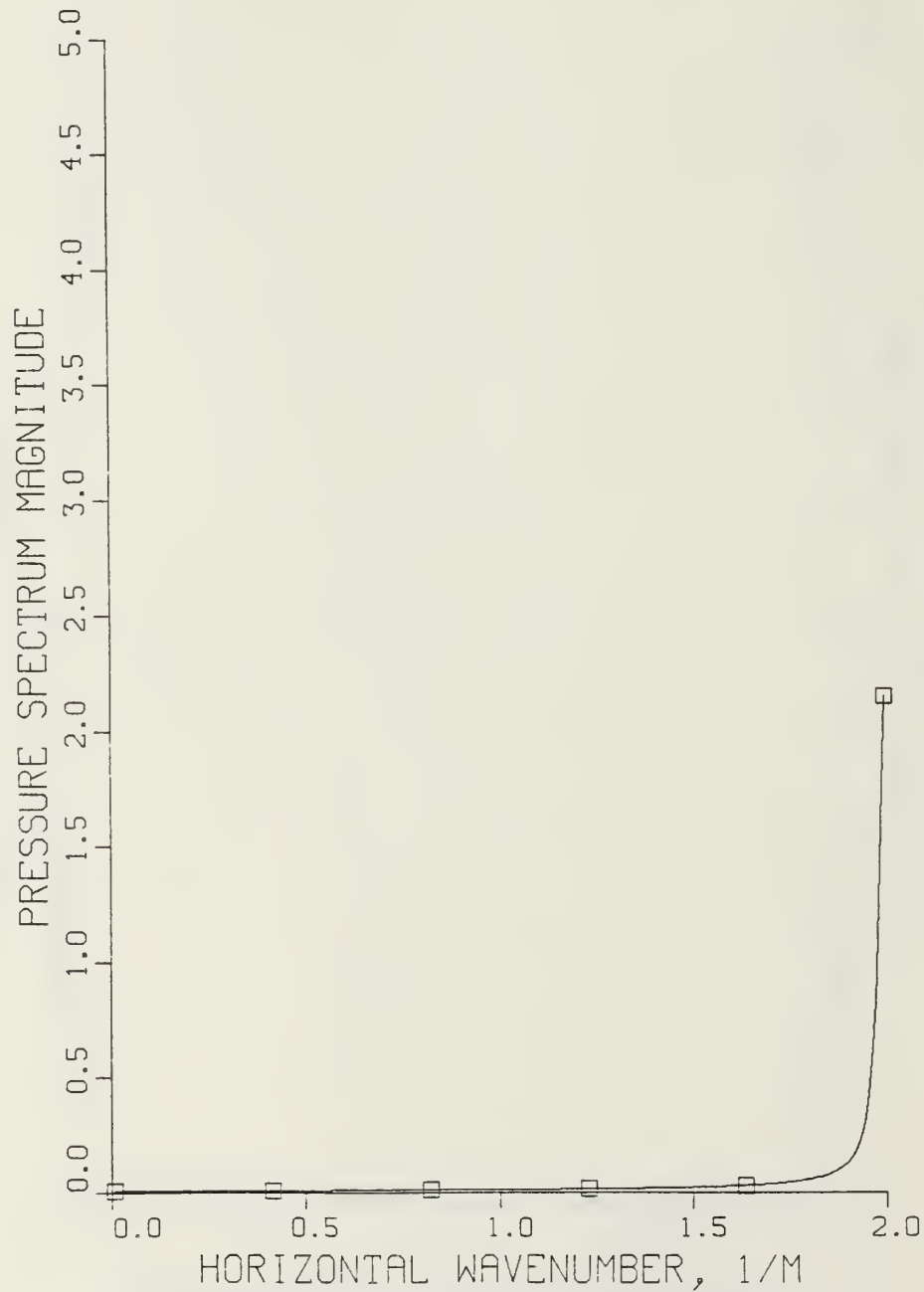


Figure 3.29 Pressure Spectrum,
SS 2, Range Window Set at 300 Meters

MAGNITUDE OF PRESSURE AS A FN OF RANGE

SOURCE DEPTH = 21.998 M, RECEIVER DEPTH = 47.124 M,
RANGE STEP SIZE = 1.57 M, N = 1024

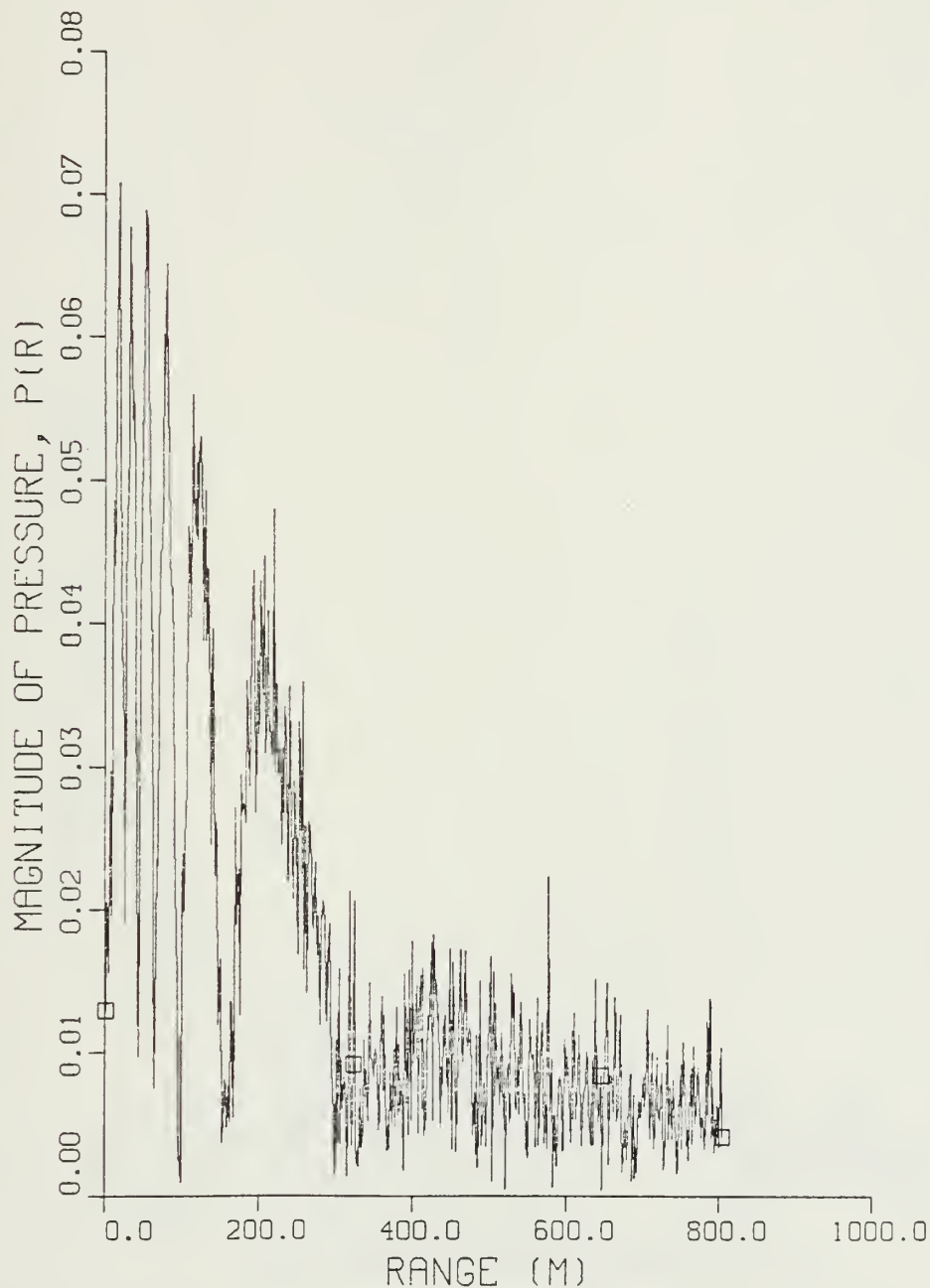


Figure 3.30 Pressure Field, $K = 1.0$, $\mu = 0.005$

PRESSURE SPECTRUM VS KH

SOURCE DEPTH = 21.998 M, $K = 1.0/\text{M}$

RECEIVER DEPTH = 47.124 M, $\mu = 0.005$



Figure 3.31 Pressure Spectrum vs. Gamma

PRESSURE SPECTRUM VS KZ

SOURCE DEPTH = 21.998 M, $K = 1.0/\text{M}$
RECEIVER DEPTH = 47.124 M, $\mu = 0.005$

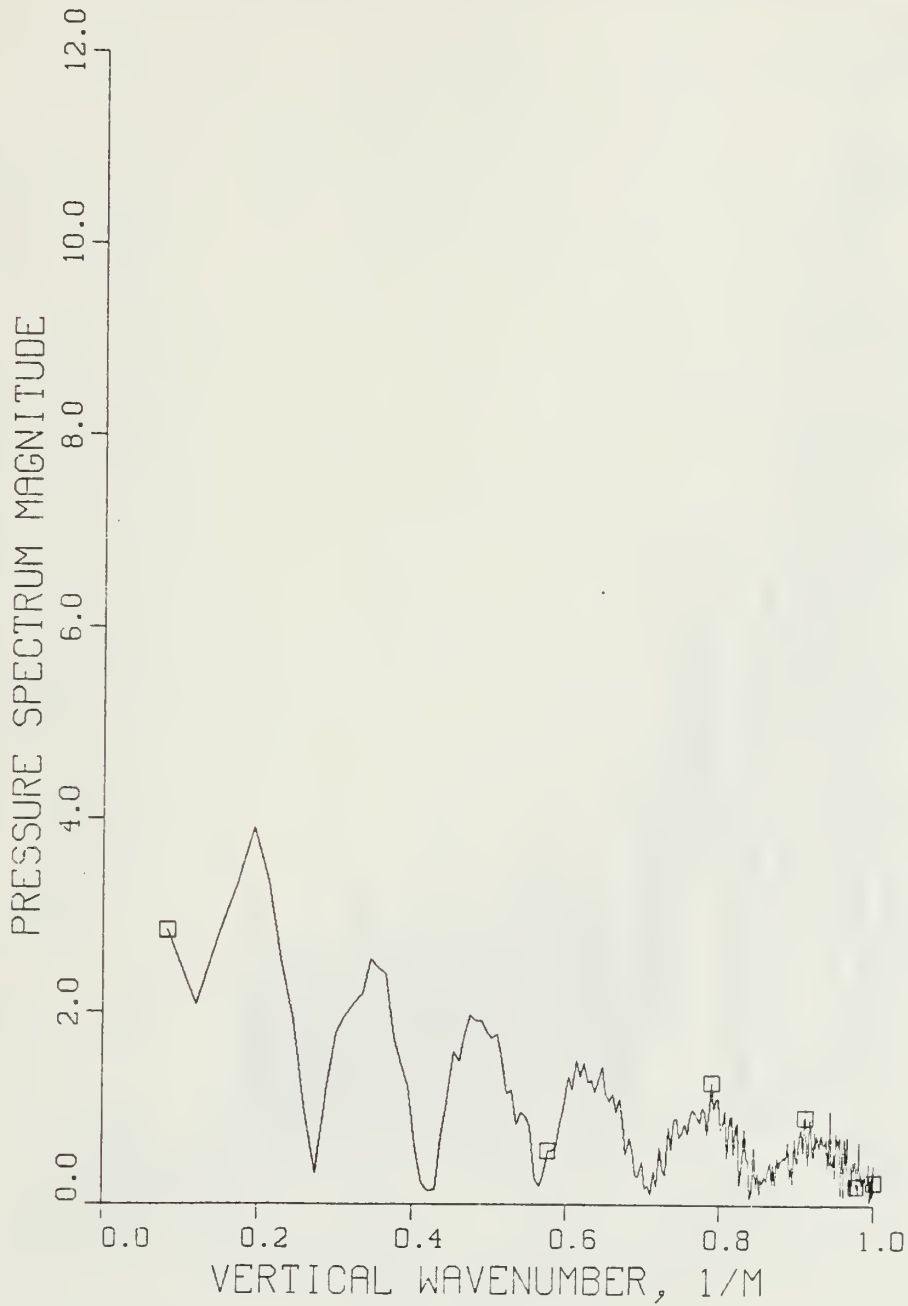


Figure 3.32 Pressure Spectrum vs. Beta

MAGNITUDE OF PRESSURE AS A FN OF RANGE

SOURCE DEPTH = 21.998 M, RECEIVER DEPTH = 47.124 M,
RANGE STEP SIZE = 1.57 M, N = 1024

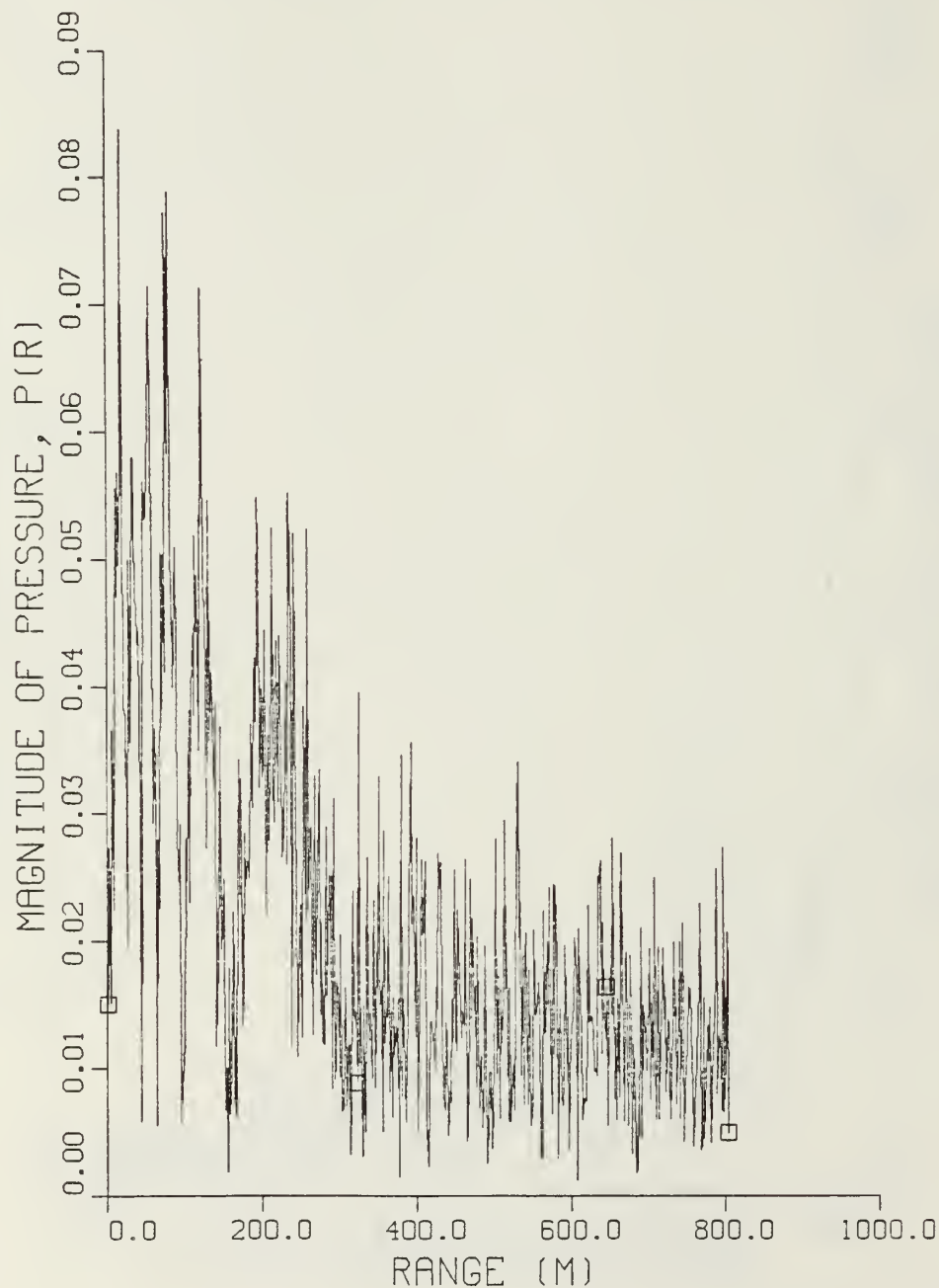


Figure 3.33 Pressure Field, $\kappa = 1.0$, $\mu = 0.01$

PRESSURE SPECTRUM VS KH

SOURCE DEPTH = 21.998 M, $K = 1.0/\text{M}$
RECEIVER DEPTH = 47.124 M, $\mu = 0.01$

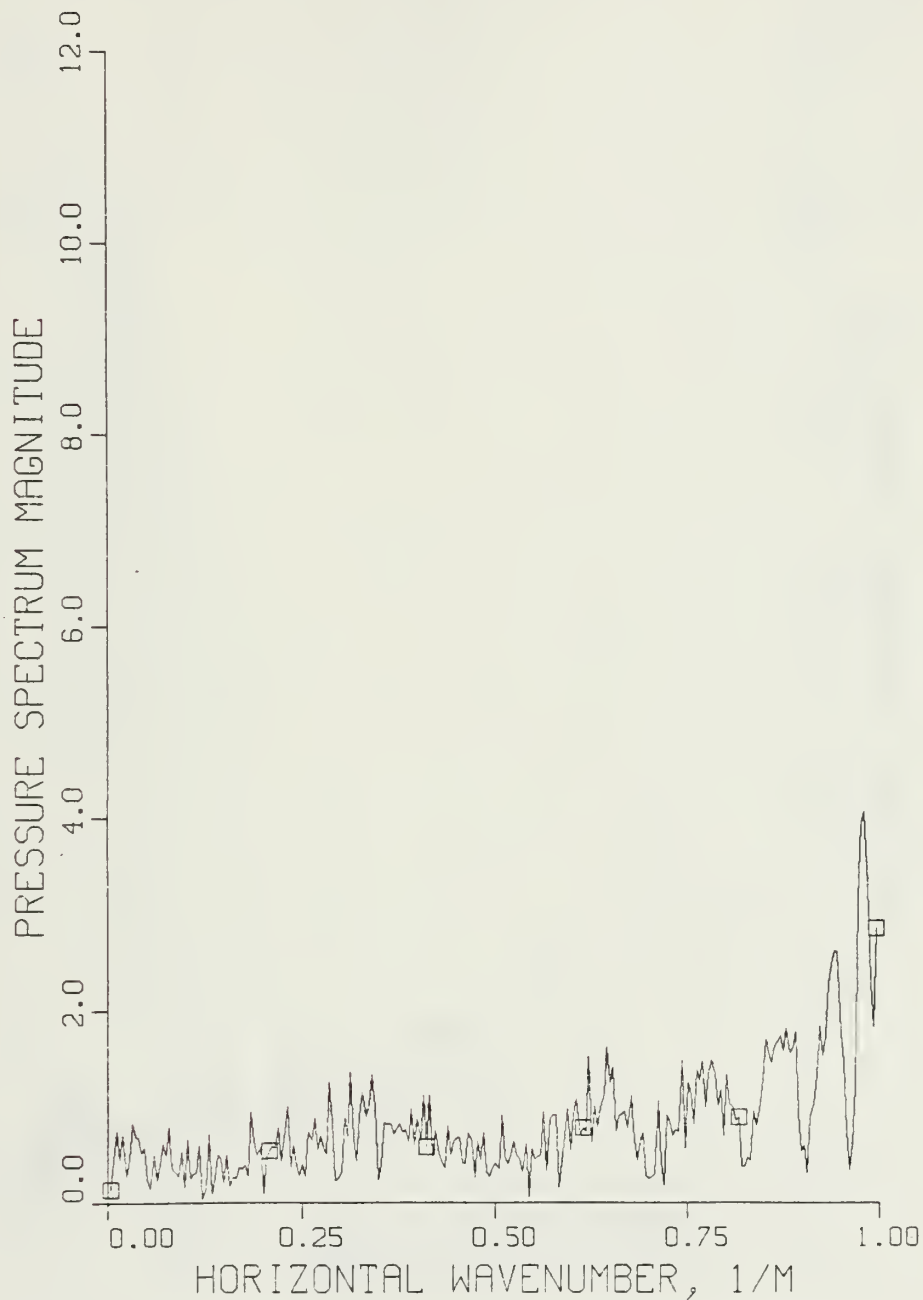


Figure 3.34 Pressure Spectrum vs. Gamma

PRESSURE SPECTRUM VS KZ

SOURCE DEPTH = 21.998 M, $K = 1.0/M$
RECEIVER DEPTH = 47.124 M, $\mu = 0.01$

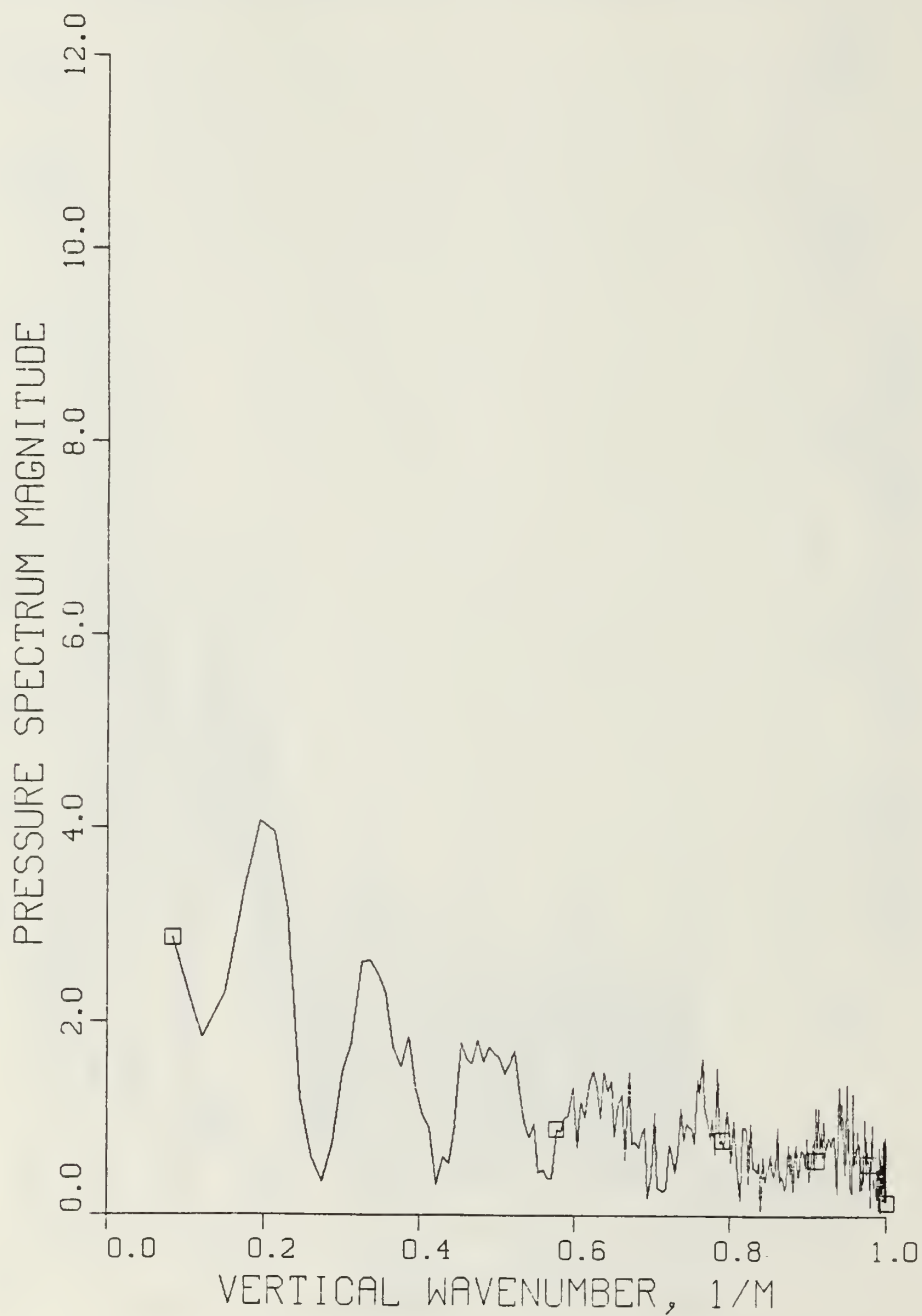


Figure 3.35 Pressure Spectrum vs. Beta

MAGNITUDE OF PRESSURE AS A FN OF RANGE

SOURCE DEPTH = 21.998 M, RECEIVER DEPTH = 47.124 M,
RANGE STEP SIZE = 0.785 M, N = 1024

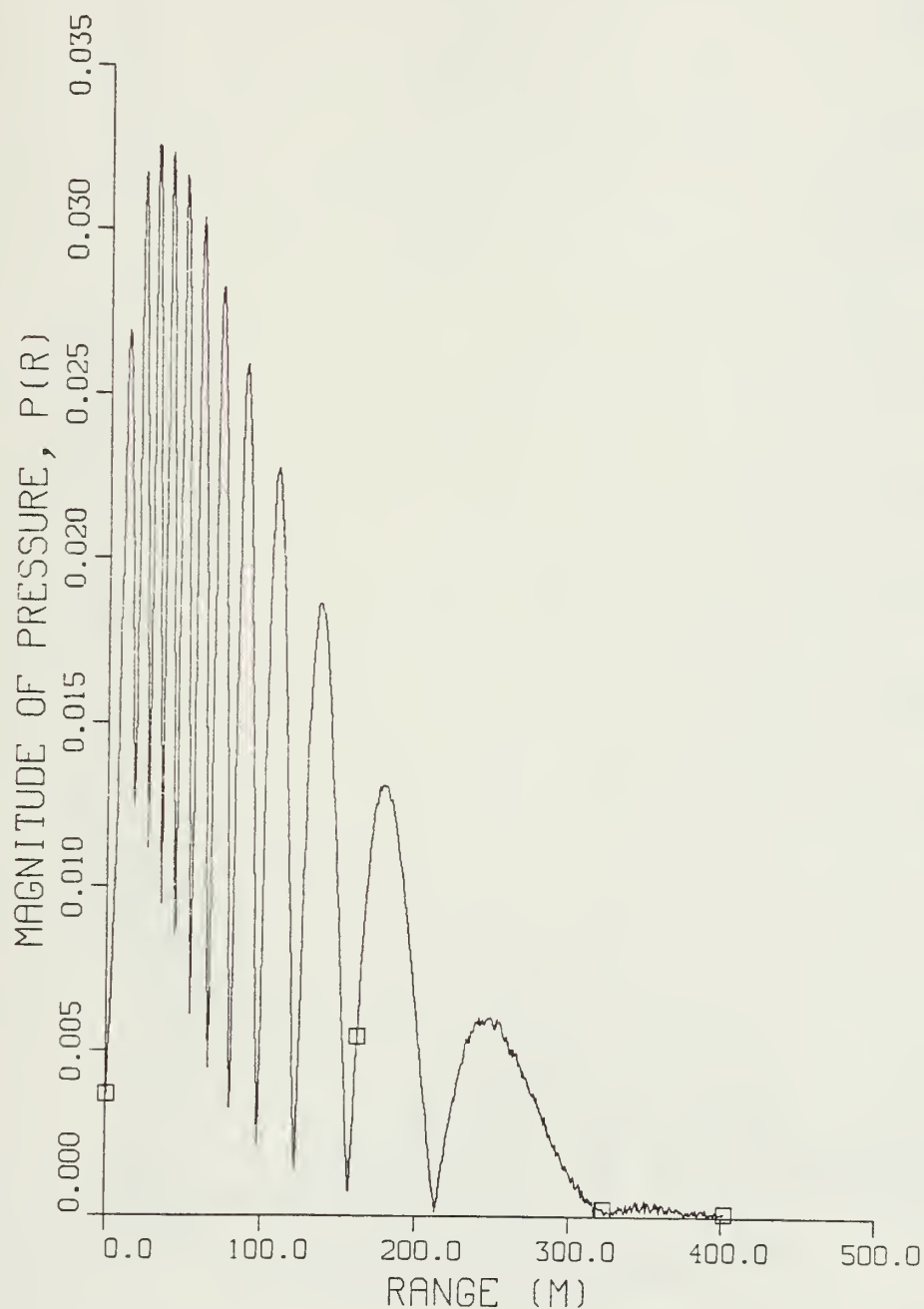


Figure 3.36 Pressure Field, $K = 2.0$, $\mu = 0.0001$

PRESSURE SPECTRUM VS KH

SOURCE DEPTH = 21.998 M, $K = 2.0/\text{M}$

RECEIVER DEPTH = 47.124 M, $\mu = 0.0001$

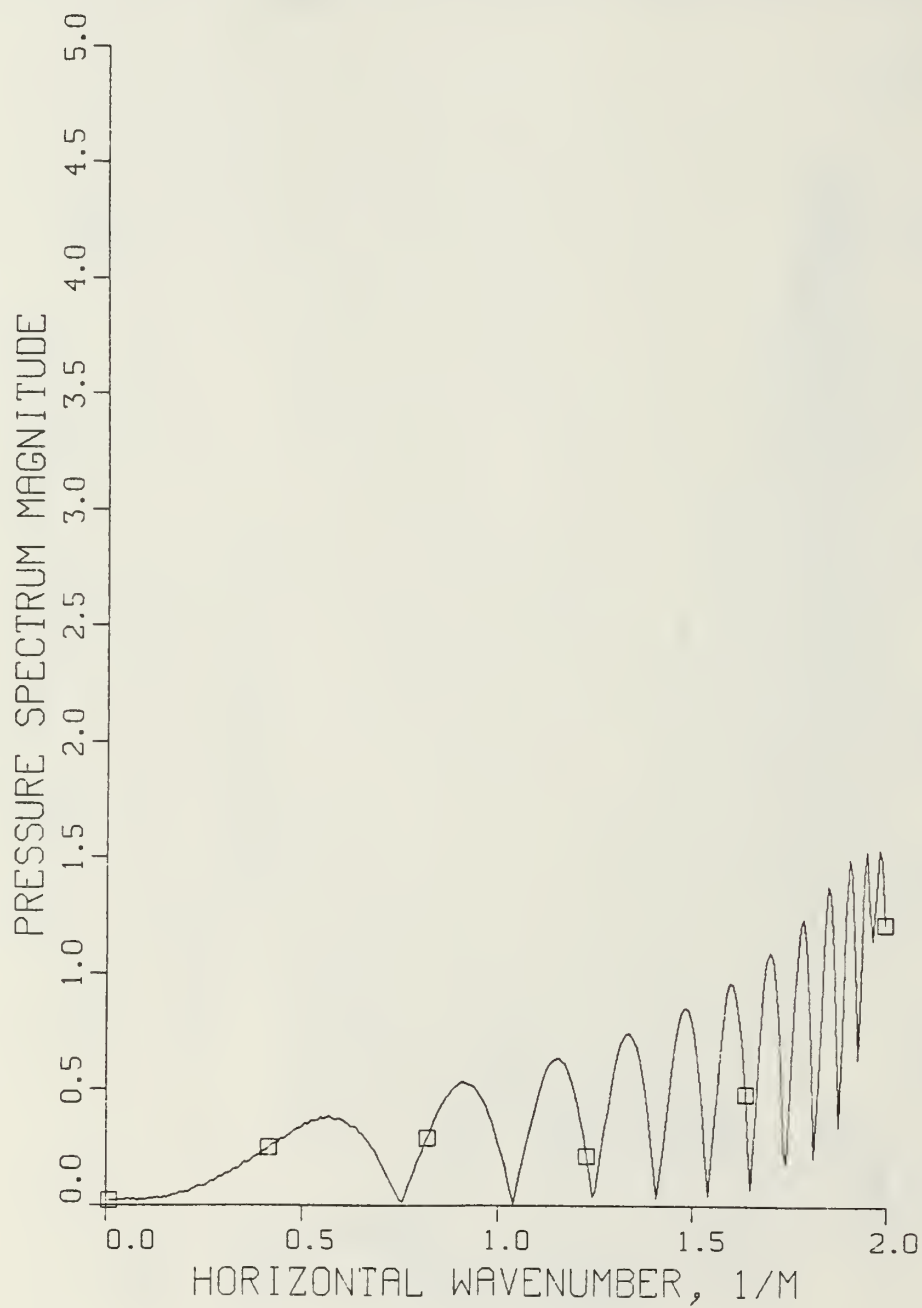


Figure 3.37 Pressure Spectrum vs. Gamma

PRESSURE SPECTRUM VS KZ

SOURCE DEPTH = 21.998 M, $K = 2.0/M$

RECEIVER DEPTH = 47.124 M, $\mu = 0.0001$

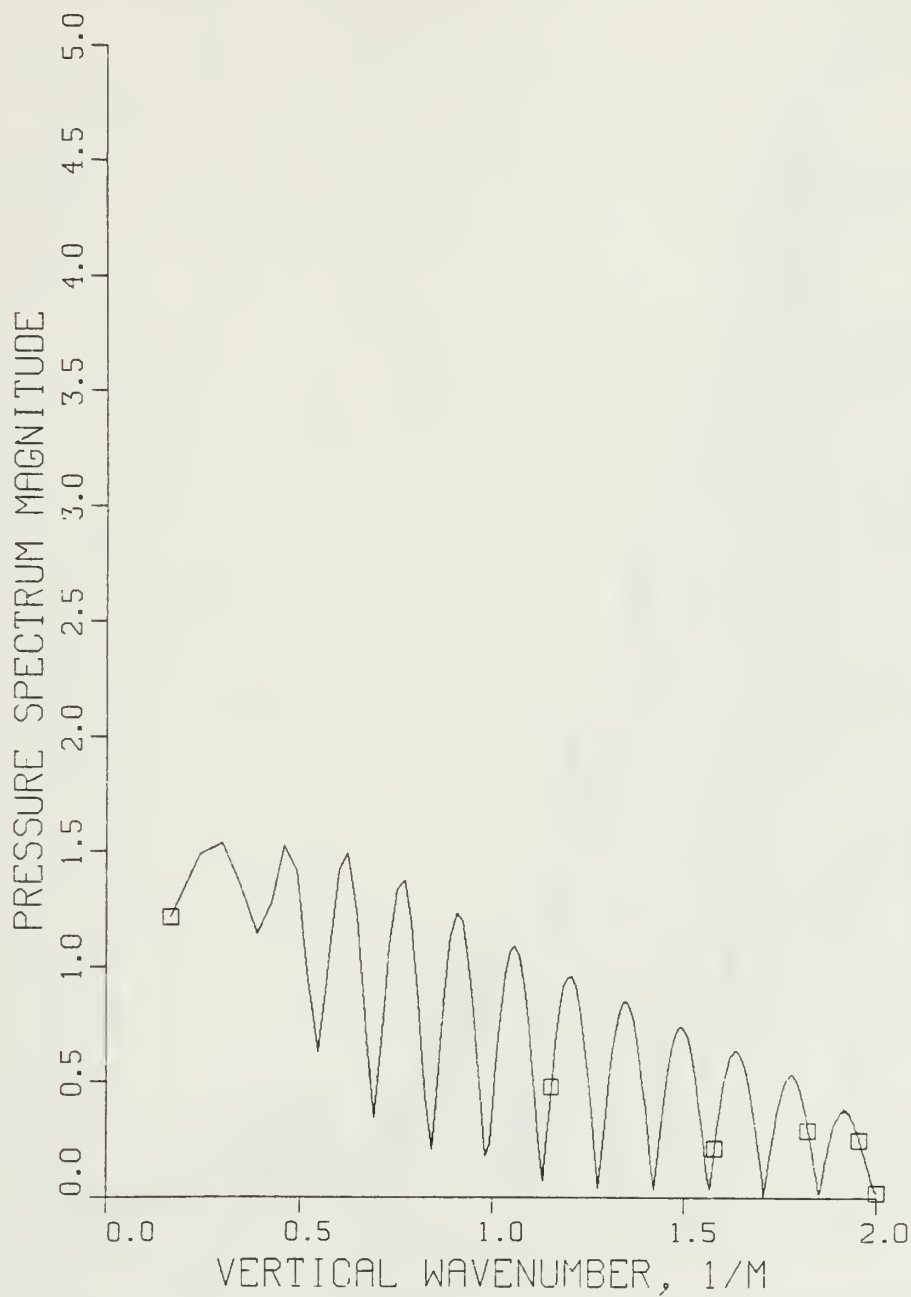


Figure 3.38 Pressure Spectrum vs. Beta

MAGNITUDE OF PRESSURE AS A FN OF RANGE

SOURCE DEPTH = 21.998 M, RECEIVER DEPTH = 47.124 M,
RANGE STEP SIZE = 0.785 M, N = 1024

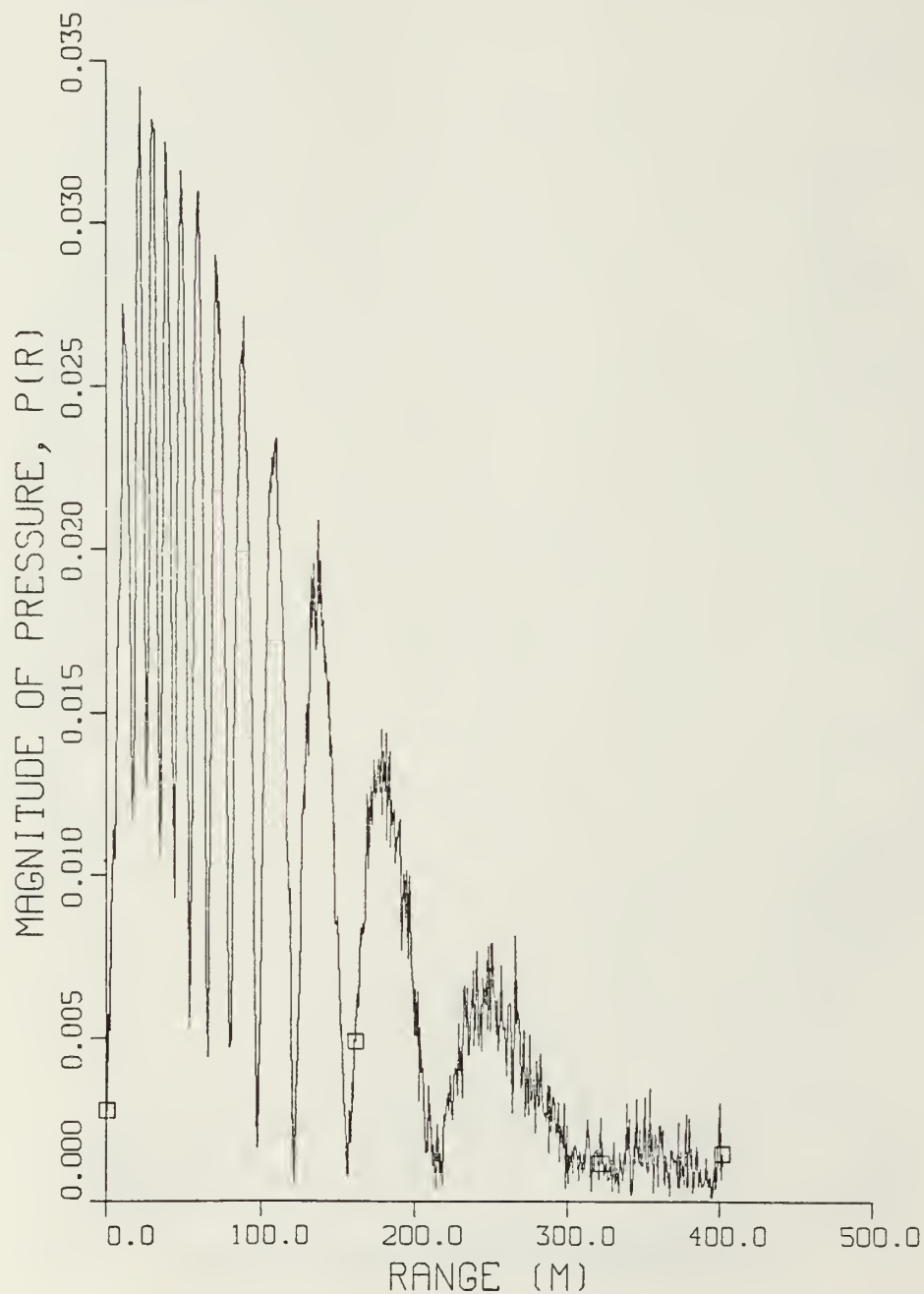


Figure 3.39 Pressure Field, $\kappa = 2.0$, $\mu = 0.001$

PRESSURE SPECTRUM VS KH

SOURCE DEPTH = 21.998 M, $K = 2.0/M$
RECEIVER DEPTH = 47.124 M, $\mu = 0.001$

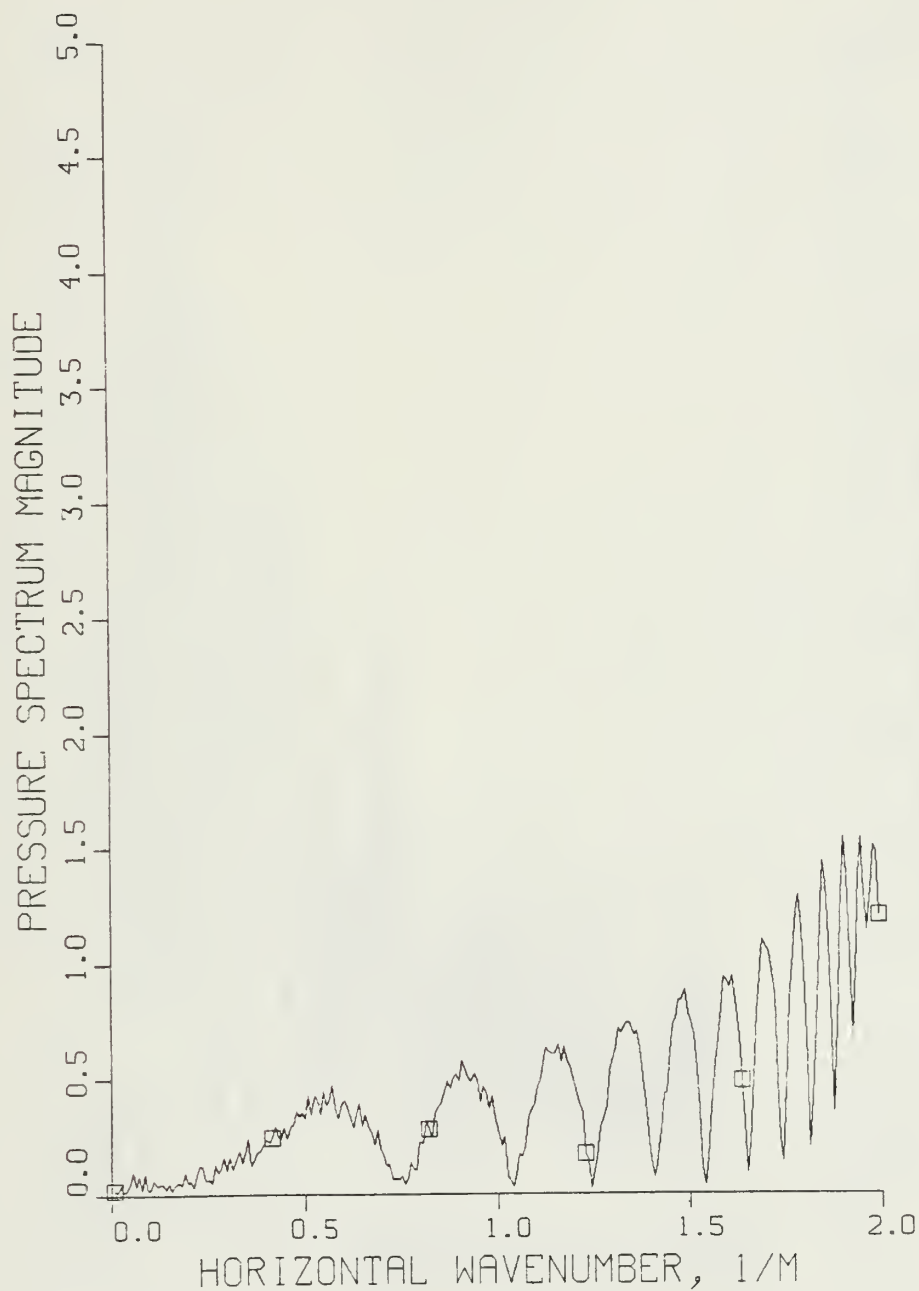


Figure 3.40 Pressure Spectrum vs. Gamma

PRESSURE SPECTRUM VS KZ

SOURCE DEPTH = 21.998 M, $K = 2.0/M$
RECEIVER DEPTH = 47.124 M, $\mu = 0.001$

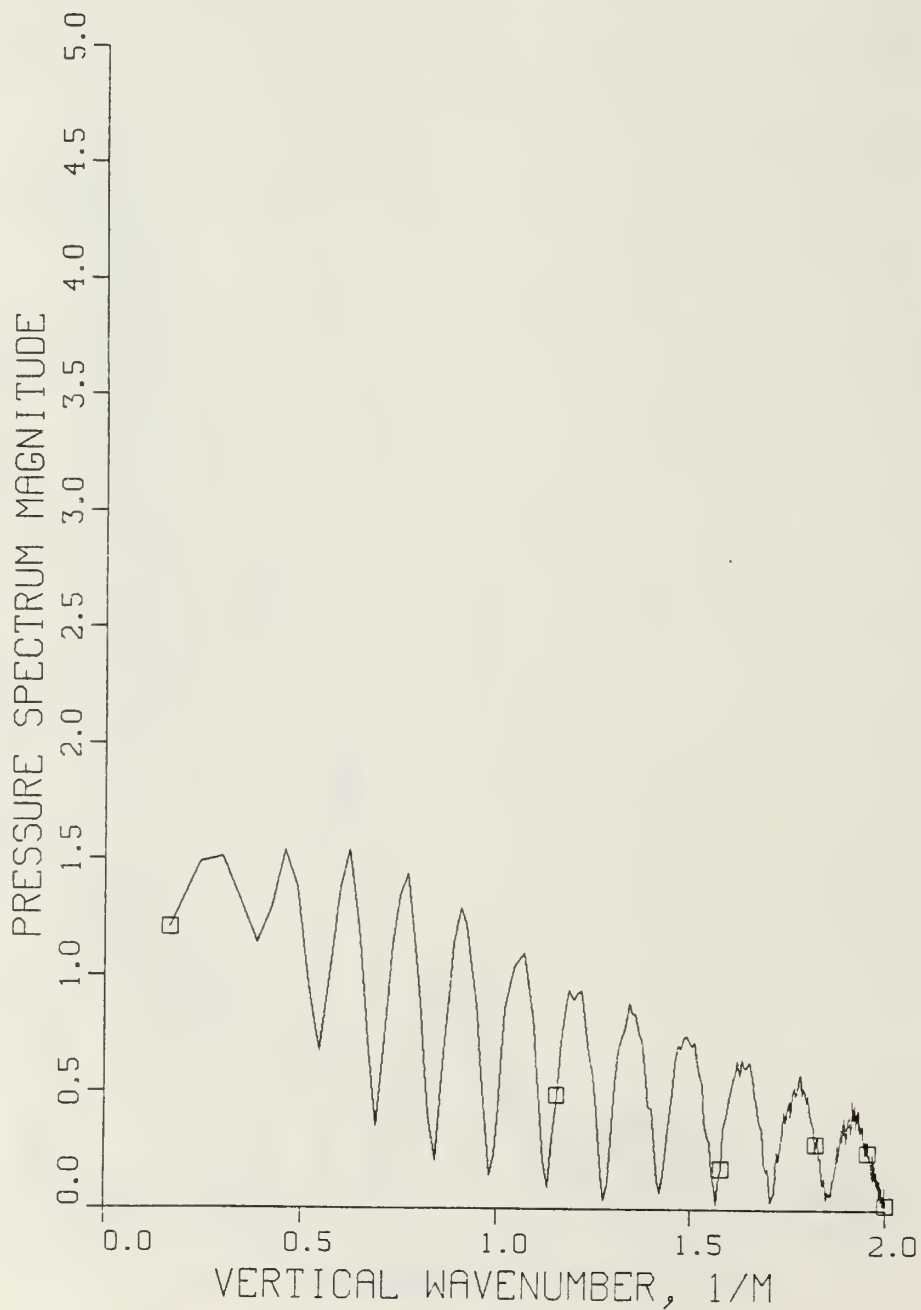


Figure 3.41 Pressure Spectrum vs. Beta

MAGNITUDE OF PRESSURE AS A FN OF RANGE

SOURCE DEPTH = 21.998 M, RECEIVER DEPTH = 47.124 M,
RANGE STEP SIZE = 0.785 M, N = 1024

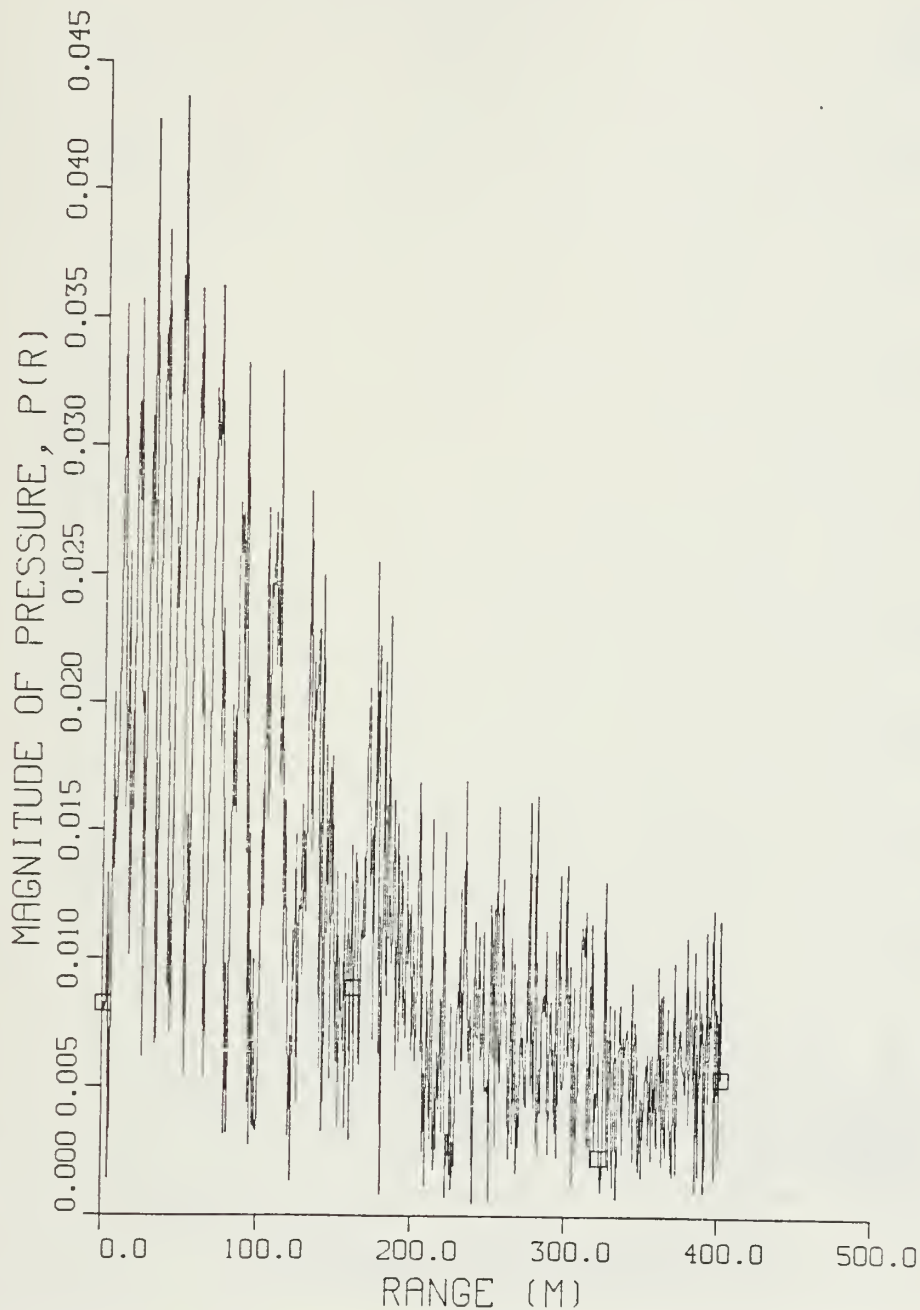


Figure 3.42 Pressure Field, $K = 2.0$, $\mu = 0.005$

PRESSURE SPECTRUM VS KH

SOURCE DEPTH = 21.998 M, $K = 2.0/M$

RECEIVER DEPTH = 47.124 M, $\mu = 0.005$

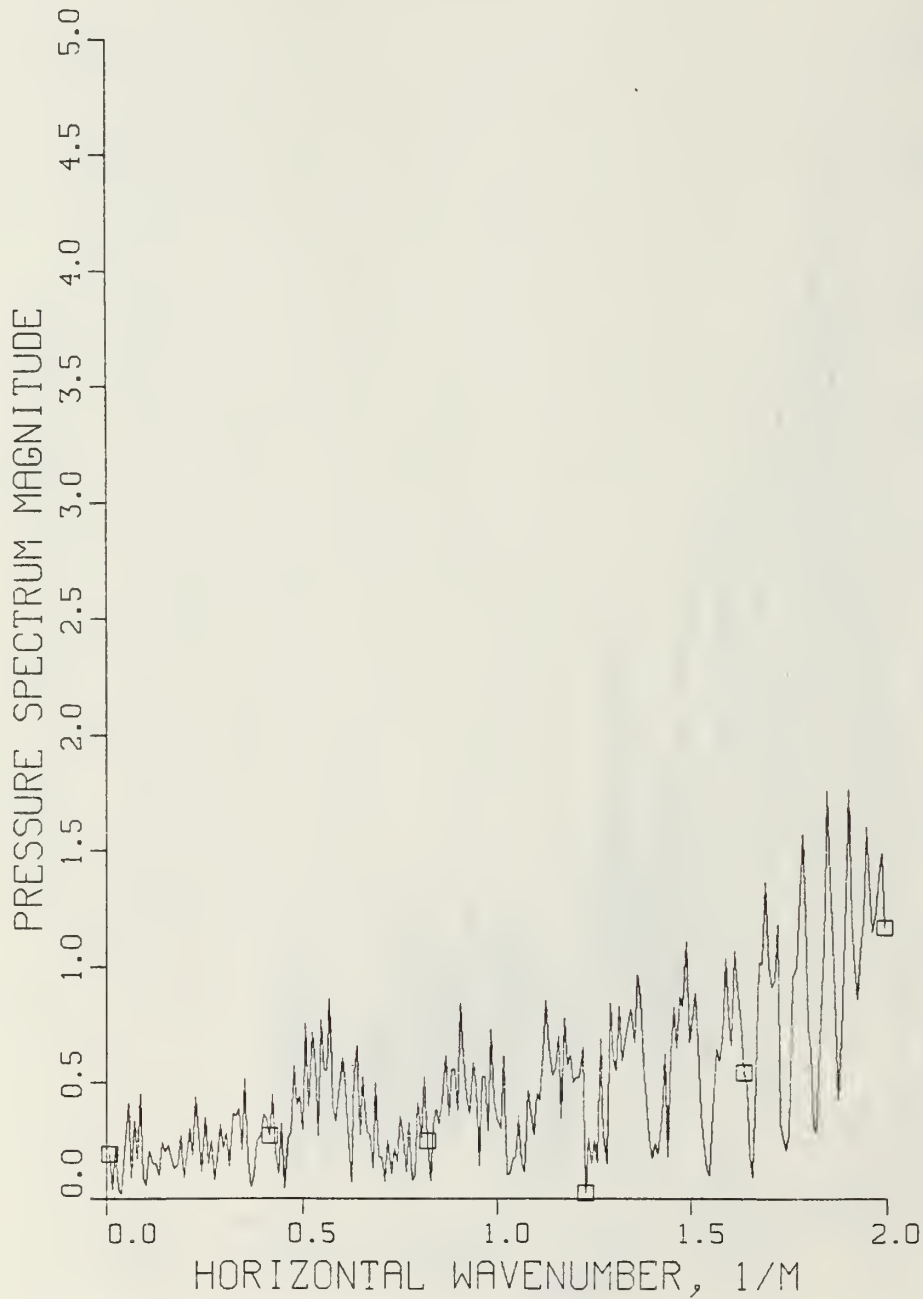


Figure 3.43 Pressure Spectrum vs. Gamma

PRESSURE SPECTRUM VS KZ

SOURCE DEPTH = 21.998 M, $K = 2.0/M$
RECEIVER DEPTH = 47.124 M, $\mu = 0.005$

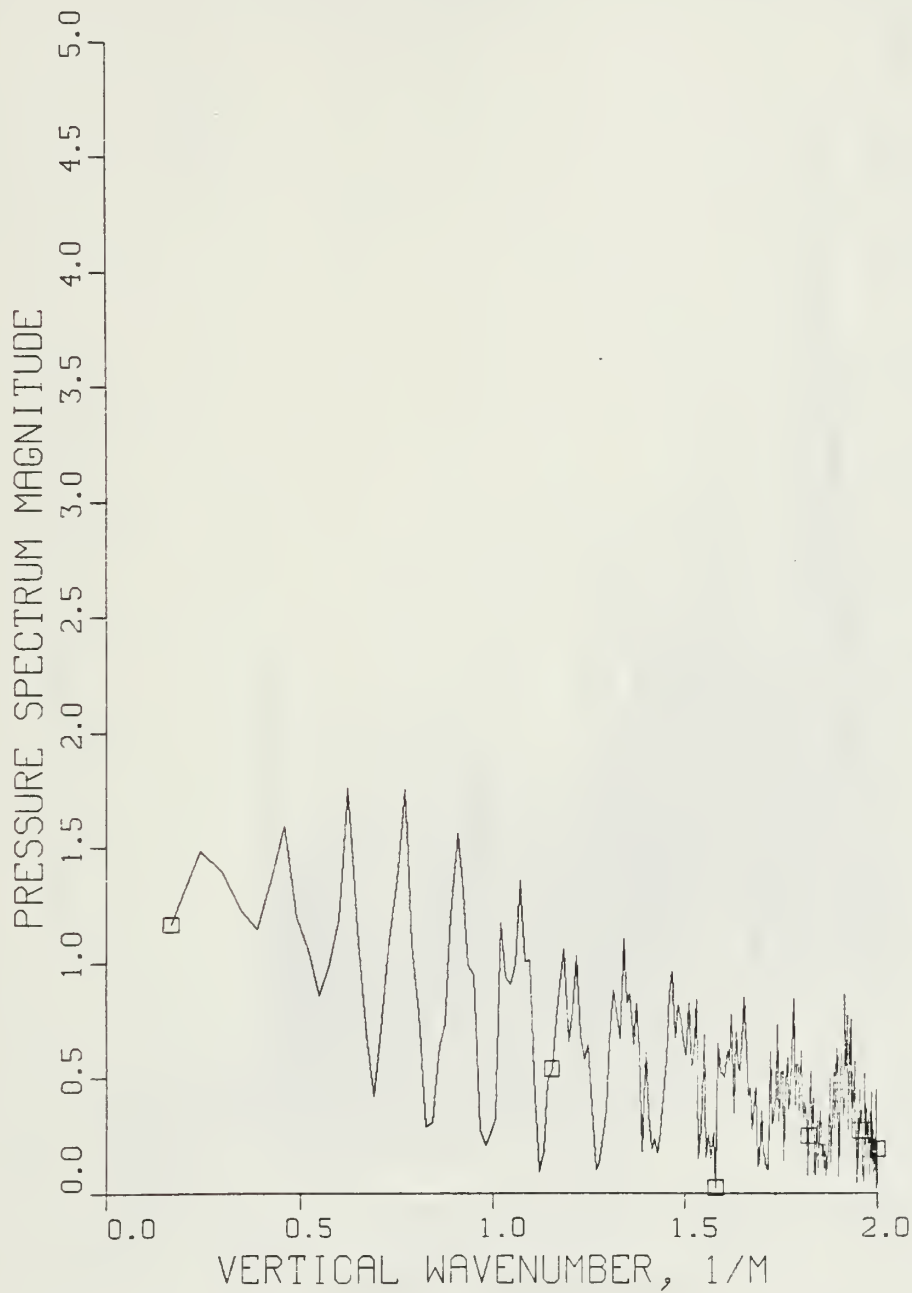


Figure 3.44 Pressure Spectrum vs. Beta

MAGNITUDE OF PRESSURE AS A FN OF RANGE

SOURCE DEPTH = 21.998 M, RECEIVER DEPTH = 47.124 M,
RANGE STEP SIZE = 0.785 M, N = 1024

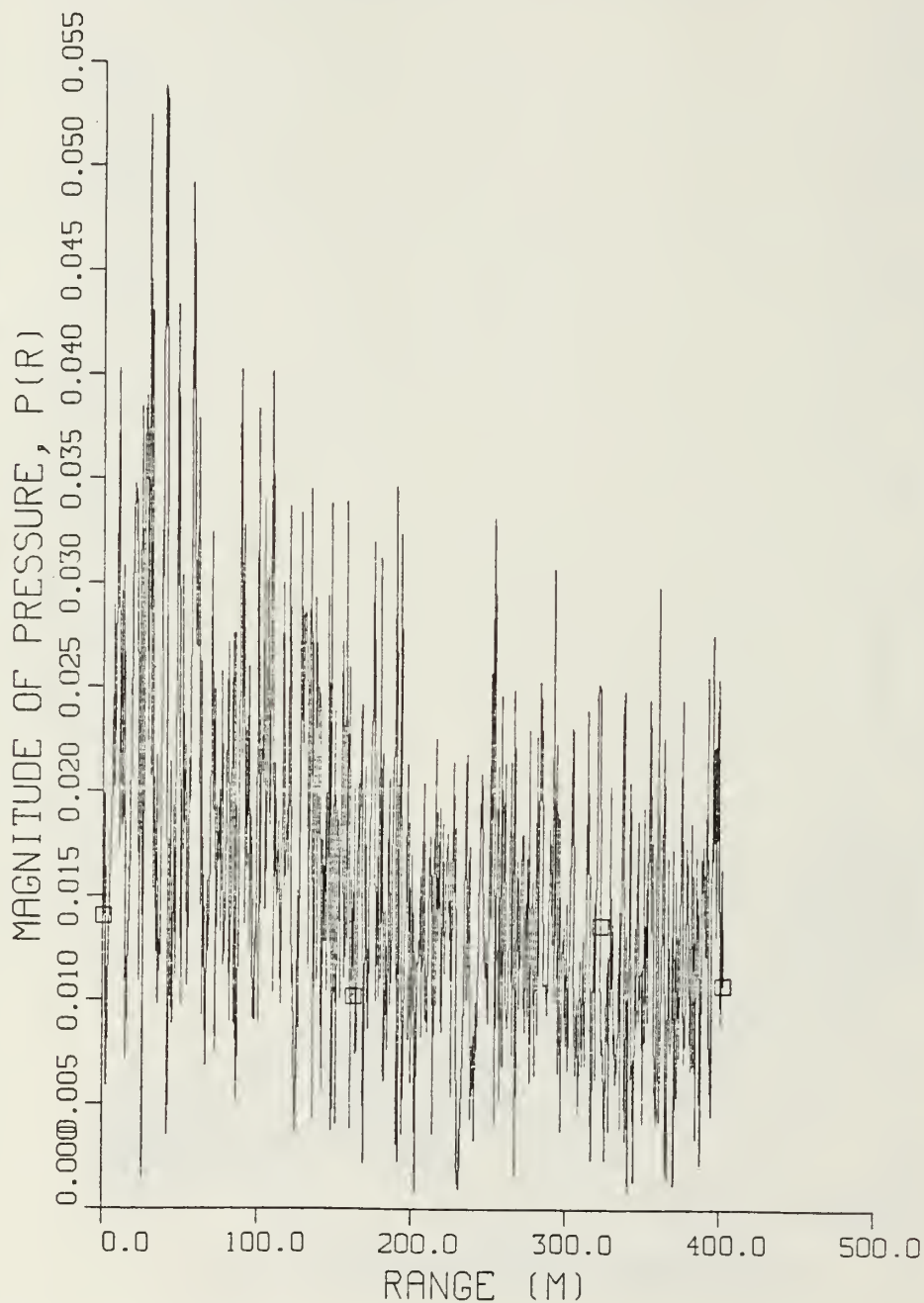


Figure 3.45 Pressure Field, $K = 2.0$, $\mu = 0.01$

PRESSURE SPECTRUM VS KH

SOURCE DEPTH = 21.998 M, $K = 2.0/\text{M}$
RECEIVER DEPTH = 47.124 M, $\mu = 0.01$

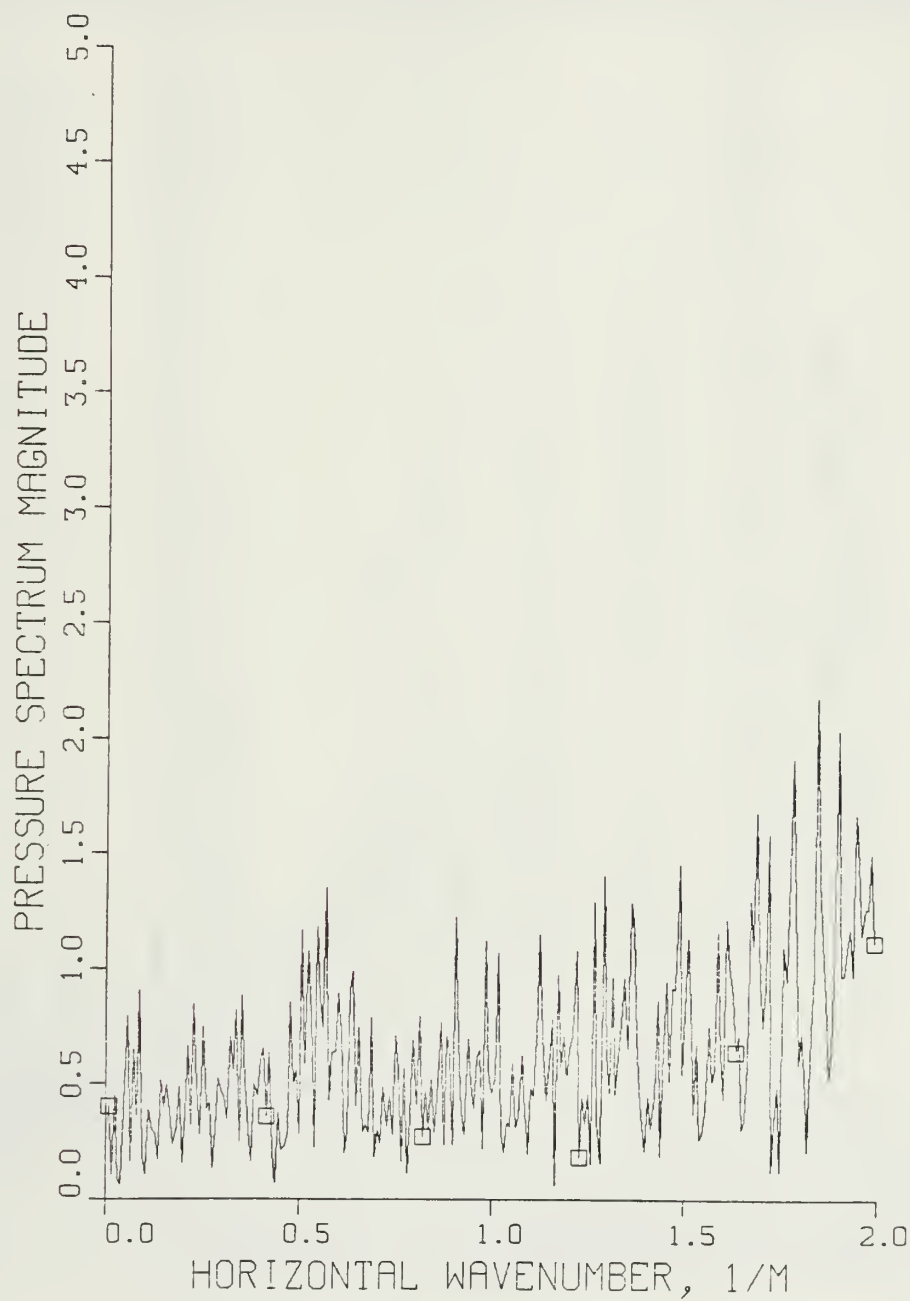


Figure 3.46 Pressure Spectrum vs. Gamma

PRESSURE SPECTRUM VS KZ

SOURCE DEPTH = 21.998 M, $K = 2.0/\text{M}$
RECEIVER DEPTH = 47.124 M, $\mu = 0.01$

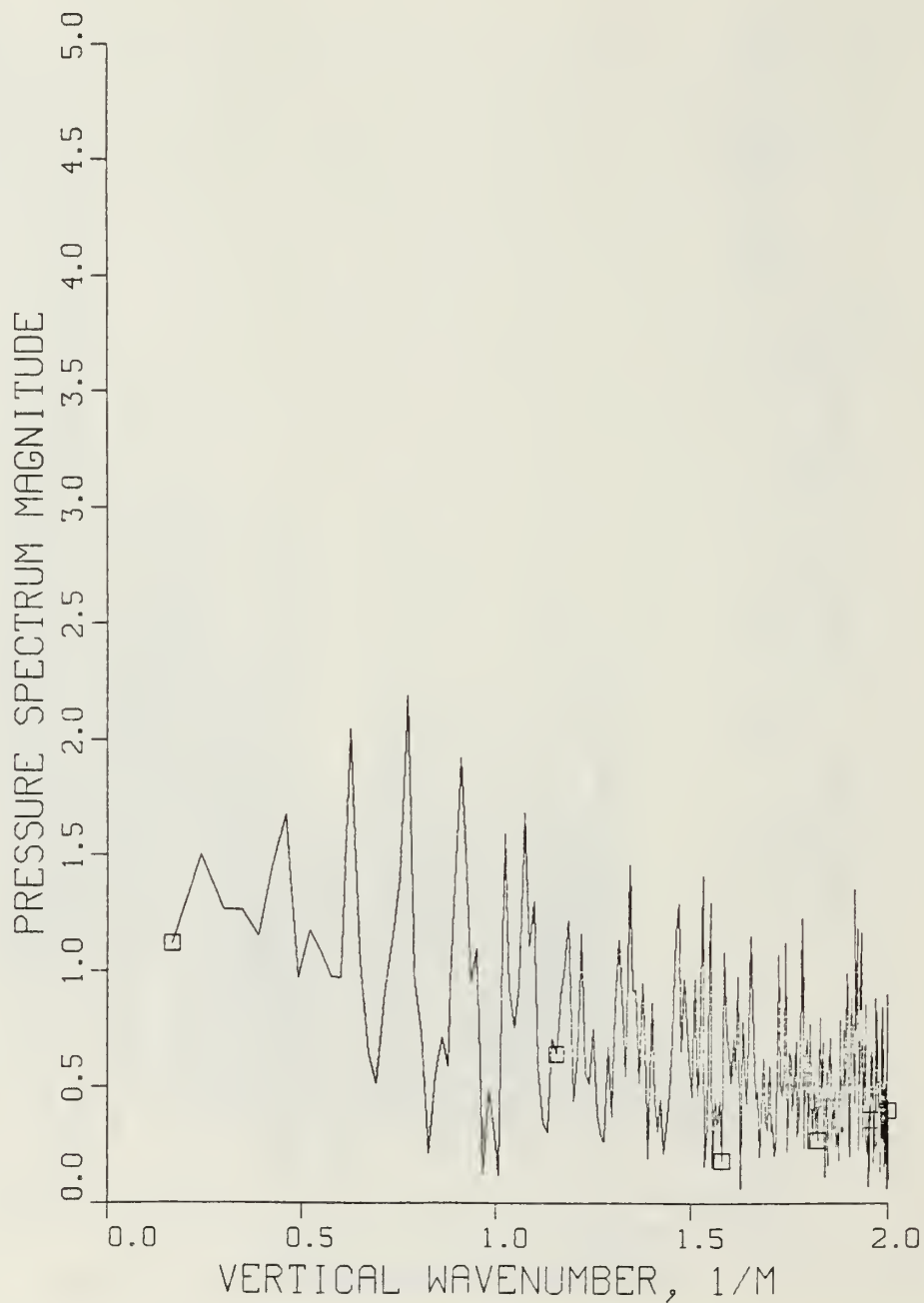


Figure 3.47 Pressure Spectrum vs. Beta

APPENDIX A: LLOYDS MIRROR PRESSURE FIELD SOURCE CODE

```

*****
THIS PROGRAM WILL PLOT THE I(P(R)) VS K CURVE STARTING AT THE ORIGIN
(I.E., THE SOURCE).
*****
THIS PROGRAM ALSO PLOTS THE SPECTRUM VS THE HORIZONTAL WAVENUMBER.
ALSO THE SPECTRUM VS THE VERTICAL WAVENUMBER.
*****
IT USES THE COOLEY-TUKEY FFT.
*****
DIMENSION DATA(8192),CKM(4096),GM(4096),T(4096),
1U(4096),RNOI2(4096),AINOI2(4096),DADA(8192)
DOUBLE PRECISION DSEED,DSEED2
REAL LAMBDA
DATA Y,Y',Y'',ON/,'.'/
PIE = 4.0 * AIAN(1.0)
EPS = 1.00E-6
*****
THE USER SELECTABLE VARIABLES ARE ENTERED
*****
WRITE(6,2),ENTER THE SOURCE DEPTH IN METERS.'')
FORMAT(1X,*)ZS
ZS = ZS
WRITE(6,4),ENTER THE RECEIVER DEPTH IN METERS.'')
FORMAT(1X,*)ZR
ZR = ZR
WRITE(6,5),ENTER THE VALUE OF K, THE WAVENUMBER.'')
FORMAT(1X,*)AK
AK = AK
WRITE(6,3),ENTER THE AVERAGE SURFACE WAVEHEIGHT, IN REAL METERS.
FORMAT(1X,*)AICH
AICH = AICH
WRITE(6,5),ENTER THE VALUE OF R (NAUGHT), RO.'')
FORMAT(1X,*)RO
RO = RO
WRITE(6,1),ENTER N, THE NUMBER OF TRANSFORM POINTS.'')
FORMAT(1X,*)NAX
NAX = NAX
*****

```



```

37      DADA(2*I) = DATA(IMAX + (2*I))
      CONTINUE
C39      CALL ERFPLOT(DADA,DE,IMAX,JMAX,RO)
C40
C41      CALL FOUR2(DATA,IMAX,-1,1)
C42
C43      WRITE(6,352)
C44      FORMAT(/,5X,'I',4X,'SPEC DATA REAL',3X,'SPEC DATA IMAG',/)
C45
C46      DO 18 I = 1,IMAX
C47      WRITE(6,353)I,DATA(2*I - 1),DATA(2*I)
C48      CONTINUE
C49      FORMAT(2X,I4,2(4X,F10.7))
C50
C51      DG = 2.0 * PI/(ELIMAX * DR)
C52      WRITE(6,300)DG
C53      FORMAT(/,2X,'DG = ',F12.8,/)
C54
C55      WRITE(6,201)
C56      FORMAT(/,5X,'I',6X,'CK',10X,'Q',10X,'KZ',/)
C57
C58      DO 50 I=1,IMAX4
C59      FLY = FLY + FLY(I)
C60      GM(I) = FLY * DG
C61      IF(GM(I).GE.AK) GO TO 400
C62      GO TO 420
C63      CONTINUE
C64
C65      IF GM(I) < AK, THEN BE(I) IS REAL, AND REDUCES TO A FORM OF
C66      THE SIN(X)/X FUNCTION, APPROXIMATELY. ACTUAL FORM IS GIVEN BELOW.
C67
C68      BE(I) = SQRT(AK**2 - GM(I)**2) + EPS
C69      Q(I) = ABS(SIN(BE(I)*ZX)*SQRT(GM(I))/BE(I))
C70      GO TO 450
C71
C72      CONTINUE
C73
C74      IF GM(I) >= AK, THEN BE(I) = SQRT OF A NEGATIVE NUMBER, AND THE
C75      HYPERBOLIC FUNCTION, REDUCES TO THE HYPERBOLIC SIN (SINH).

```

```

BER = SQRT(GM(1)**2 - AK**2)
QQ = EXP(-BER*(ZP - ZS)) - EXP(-BER*(ZR + ZS))
QQ = ABS(CQ * SQRT(GM(1)))/(2.0 * BER)
GO TO 50

CONTINUE

CKRE = DATA(2*I - 1)
CKM(I) = SQRT(CKRE**2 + CKIM**2)
CONTINUE

IMAX5 = IMAX4 - 1

CALL WHPILT(IMAX5,GM,CKM,Q,AK,BE)

CALL WTVPLT(IMAX5,CKM,Q,AK,BE)
CALL DGNPL
STOP
END

```

```

SUBROUTINE FOUR2(DATA,N,ISIGN,IFORM)
COOLEY-TUKEY FAST FOURIER TRANSFORM IN USASI BASIC FORTRAN.
MULTI-DIMENSIONAL TRANSFORM, EACH DIMENSION A POWER OF TWO,
COMPLEX OR REAL DATA.
TRANSFORM(K1,K2,...) = SUM(DATA(J1,J2,...)*EXP(ISIGN*2*PI*SQRT(-1)
*(J1-1)*(K1-1)/N(i) + (J2-1)*(K2-1)/N(2)+...)), SUMMED FOR ALL
J1 AND K1 FROM 1 TO N(1), J2 AND K2 FROM 1 TO N(2), ETC.
FOR ALL NDIM SUBSCRIPTS. NDIM MUST BE POSITIVE AND
EACH N(IDIM) MUST BE A POWER OF TWO. ISIGN IS +1 OR -1.
LET N(1) = N(1)*N(2)*...*N(NDIM). THEN A -1 TRANSFORM
FOLLOWS BY A +1 ONE (OR VICE VERSA) RETURNS NOT
TIMES THE ORIGINAL DATA. IFORM = 1, 0 OR -1, AS DATA IS
COMPLEX, REAL OR THE FIRST HALF OF A COMPLEX ARRAY. TRANSFORM
VALUES ARE RETURNED TO ARRAY DATA. THEY ARE COMPLEX, REAL OR
THE FIRST HALF OF A COMPLEX ARRAY, AS IFORM = 1, -1 OR 0.
THE TRANSFORM OF A REAL ARRAY (IFORM = 0) DIMENSIONED N(1) BY N(2)
BY COMPLEX WILL BE RETURNED IN THE SAME ARRAY, BY N(2)
IFORM = 0 OR -1, MUST BE EVEN, AND ENOUGH ROOM MUST BE
RESERVED. THE REVERSE TRANSFORMATION OF A COMPLEX CONJUGA-
TION. THE REVERSE VALUES MAY BE OBTAINED BY COMPLEX ARRAY DIMEN-
SIONED N(1)/2+1 BY N(2) BY ... MUST BE THE TRUE N(1), NOT N(1)/2+1.
TO -1. IN THE N ARRAY, N(1) MUST BE THE TRUE N(1), NOT N(1)/2+1.
THE TRANSFORM IS WILL BE RETURNED TO THE INPUT ARRAY.
RUNNING TIME IS APPROXIMATELY 10*LOG2(N(1)), RATHER THAN
THE NAIVE N(1)**2. FURTHERMORE, LESS ERROR IS BUILT UP.

```

TES02410
 TES02420
 TES02430
 TES02440
 TES02450
 TES02460
 TES02470
 TES02480
 TES02490
 TES02500
 TES02510
 TES02520
 TES02530
 TES02540
 TES02550
 TES02560
 TES02570
 TES02580
 TES02590
 TES02600
 TES02610
 TES02620
 TES02630
 TES02640
 TES02650
 TES02660
 TES02670
 TES02680
 TES02690
 TES02700
 TES02710
 TES02720
 TES02730
 TES02740
 TES02750
 TES02760
 TES02770
 TES02780
 TES02790
 TES02800
 TES02810
 TES02820
 TES02830
 TES02840
 TES02850
 TES02860
 TES02870
 TES02880

C 450
 .C

50
 C

C

C

431
 C

C C

C

C

C

C

C

C

C

C

C

C

C

C

C

C

C

```

C      WRITTEN BY NORMAN BRENNER OF MIT LINCOLN LABORATORY, JANUARY 1969.
C      JEFF AUDIO TRANSACTIONS (JUNE 1967), SPECIAL ISSUE ON FFT.
      DIMENSION DATA(1), N(1)
      NDIM = 1
      NTOI = 1
      DO 10 IDIM = 1, NDIM
        NTOI = NTOI * N(IDIM)
        IF (IFCFM) 70, 20, 20
      10  NREM = NTOI
      20  NREM = NTOI / N(IDIM) * NFE4
        NCURR = N(IDIM)
        IF (IDIM - 1 + IFOPX) 30, 30, 40
      30  NCURR = NCURR / 2
      40  CALL BITEV (DATA, NPREV, NCURR, NREM, ISIGN)
        IF (IDIM - 1 + IFOPM) 50, 50, 60
      50  CALL FIXRL (DATA, N(1), NREM, ISIGN, IFORM)
      60  NTOI = NTOI / N(1) * (N(1) / 2 + 1)
        CONTINUE
      70  RETURN
      NTOI = NTOI / N(1) * (N(1) / 2 + 1)
      NREX = 1
      DO 100 JDIM = 1, NDIM
        IDIM = NDIM + 1 - JDIM
        NCURR = N(IDIM)
        IF (IDIM - 1) 80, 80, 90
      80  NCURR = NCURR / 2
        CALL FIXPL (DATA, N(1), NREM, ISIGN, IFORM)
        NTOI = NTOI / (N(1) / 2 + 1) * N(1)
      90  NPREV = NTOI / (N(IDIM) * NREM)
        CALL BITEV (DATA, NPREV, NCURR, NREM, ISIGN)
      100 CALL COOL2 (DATA, NPREV, NCURR, NREM, ISIGN)
        NTOI = NTOI * N(IDIM)
      RETURN
      END

SUBROUTINE BITEV (DATA, NPREV, N, NREM)
  SUBROUTINE THE DATA BY BIT REVERSAL.
  DIMENSION DATA(NPREV, N, NREM)
  COMPLEX DATA
  EXCHANGE DATA (J1, J4REV, J2) WITH DATA (J1, J4, J5) FOR ALL J1 FROM 1
  TO J5, EACH J4 FROM 1 TO N (WHICH MUST BE A POWER OF TWO), AND
  ALL J5 FROM 4 TO 10 NREM. J4REV-1 IS THE BIT REVERSAL OF J4-1. E.G.
  SUPPOSE N = 32. THEN FOR J4-1 = 10, J1 = 1001, ETC.
  DIMENSION DATA(1)
  IPR = 2

```

C
C

10

20

30

40

50

60

70

80

90

100

00000000


```

C C C C C C C C C C
1 TO IFACT, J4 FROM 1 TO IKEM AND J5 FROM 1 TO NREM. THIS IS
A PHASE-SHIFTED DISCRETE FOURIER TRANSFORM OF LENGTH OVER FACTOR-
ING BY TWOS. DATA SAVES ABOUT TWENTY FIVE PERCENT INITIALLY.
IT IS NOT NECESSARY TO REWRITE THIS SUBROUTINE INTO COMPLEX
NOTATION SO LONG AS THE FORTRAN COMPILER USED STORES REAL AND
IMAGINARY PARTS IN ADJACENT STORAGE LOCATIONS. IT MUST ALSO
STORE ARRAYS WITH THE FIRST SUBSCRIPT INCREASING FASTEST.
DIMENSION DATA(1)
TWOPI=6.2831853072*FICAI(SIGN)
IP0=2
IP1=IP0*NREPV
IP4=IP1*N
IP5=IP4*NREM
IP2=IP1
IP2=IP1*IPKOD
NPAFT=N
IF (NPAFT-2) 00,30,20
NPAFT=NEART/4
GO TO 10
DO A FOURIER TRANSFORM OF LENGTH TWO
IF (IP2-IP4) 40,160,160
IP3=IP2*2
IP3=IP2*IFACT
DO 50 I1=1,IP1,IP0
I1=1+(J1-1)*IP0
DO 50 I5=I1,IP5,IP3
I5=1+(J1-1)*IP0+(J4-1)*IP3+(J5-1)*IP4
I3A=I5
I3B=I3A+IP2
I3=1+(J1-1)*IP0+(J2-1)*IP1+(J3-1)*IP2+(J4-1)*IP3+(J5-1)*IP4
TEMPK=DATA(I3B)
TEMP1=DATA(I3B+1)
DATA(I3B)=DATA(I3A)-TEMPK
DATA(I3B+1)=DATA(I3A+1)-TEMP1
DATA(I3A)=DATA(I3A)+TEMPK
DATA(I3A+1)=DATA(I3A+1)+TEMP1
IP2=IP3
DO A FOURIER TRANSFORM OF LENGTH FOUR (FROM E11 REVERSED C1DER)
IF (IP2-IP4) 70,160,160
IP3=IP2*4
IP3=IP2*IFACT
COMPUTE TWOPI/FICAI(1E3/IP1)
THETHA=PI*CD1/FICAI(2.)
SINTH= SIN (THETHA*51NTH
WSTPR=-2.*SINTH*51NTH
WSP1= SIN (THETHA)
WH=1.

```

```

TES03850
TES03860
TES03870
TES03880
TES03890
TES03900
TES03910
TES03920
TES03930
TES03940
TES03950
TES03960
TES03970
TES03980
TES03990
TES04000
TES04010
TES04020
TES04030
TES04040
TES04050
TES04060
TES04070
TES04080
TES04090
TES04100
TES04110
TES04120
TES04130
TES04140
TES04150
TES04160
TES04170
TES04180
TES04190
TES04200
TES04210
TES04220
TES04230
TES04240
TES04250
TES04260
TES04270
TES04280
TES04290
TES04300
TES04310
TES04320

```

```

WI=0
DO 150 I2=1,IP2,IP1
C      I2=1+(J2-1)*IP1
IF (I2-1) 90,90,80
W2R=WR*WR-WI*WI
W2I=2.*8*WI-K2I*WI
W3R=W2R*WI+W2I*WR
W3I=W2R*WI-W2I*WR
I1MAX=I2+IP1-IP0
DO 140 I1=I2,I1MAX,IP0
C      I1=1+(J1-1)*IP0+(J2-1)*IP1
DO 140 I5=I1,IP5,IP3
C      I5=1+(J1-1)*IP0+(J2-1)*IP1+(J4-1)*IP3+(J5-1)*IP4
I3A=I5
I3B=I3A+IP2
I3C=I3B+IP2
I3D=I3C+IP2
I3=1+(J1-1)*IP0+(J2-1)*IP1+(J3-1)*IP2+(J4-1)*IP3+(J5-1)*IP4
C      I3=1+(J1-1)*IP0+(J2-1)*IP1+(J3-1)*IP2+(J4-1)*IP3+(J5-1)*IP4
IF (I2-1) 110,110,100
APPLY THE PHASE SHIFT FACTORS
TEMPR=DATA(I3E)
DATA(I3B)=W2R*DATA(I3B)-W2I*DATA(I3E+1)
DATA(I3B+1)=W2R*DATA(I3B+1)+W2I*TEMPR
TEMPF=DATA(I3C)
DATA(I3C)=WR*DATA(I3C)-WI*DATA(I3C+1)
DATA(I3C+1)=WR*DATA(I3C+1)+WI*TEMPF
TEMPR=DATA(I3D)
DATA(I3D)=W3R*DATA(I3D)-W3I*DATA(I3D+1)
DATA(I3D+1)=W3R*DATA(I3D+1)+W3I*TEMPR
TOI=DATA(I3A)+DATA(I3B)
T1R=DATA(I3A+1)+DATA(I3B+1)
T1I=DATA(I3A)-DATA(I3B)
T2R=DATA(I3C)+DATA(I3D)
T2I=DATA(I3C+1)+DATA(I3D+1)
T3R=DATA(I3C)-DATA(I3D)
T3I=DATA(I3C+1)-DATA(I3D+1)
DATA(I3A)=TOR+T2R
DATA(I3A+1)=TOR+T2I
DATA(I3C)=TOR-T2R
DATA(I3C+1)=TOR-T2I
IF (ISIGN) 120,120,130
T3R=-T3R
T3I=-T3I
DATA(I3B)=T1R-T3I
DATA(I3B+1)=T1I+T3F
DATA(I3E)=T1R+T3I
DATA(I3D+1)=T1I-T3R

```

```

TES04330
TES04340
TES04350
TES04360
TES04370
TES04380
TES04390
TES04400
TES04410
TES04420
TES04430
TES04440
TES04450
TES04460
TES04470
TES04480
TES04490
TES04500
TES04510
TES04520
TES04530
TES04540
TES04550
TES04560
TES04570
TES04580
TES04590
TES04600
TES04610
TES04620
TES04630
TES04640
TES04650
TES04660
TES04670
TES04680
TES04690
TES04700
TES04710
TES04720
TES04730
TES04740
TES04750
TES04760
TES04770
TES04780
TES04790
TES04800

```

```

TEMPR=WF
WP=WSTRPS*TEMPR-WSTPI*WI+TEMPB
WI=WSTRPS*WI+WSTPI*TEMPR+WI
IE2=IP3
GC TO 60
RETURN
END

```

```

SUBROUTINE FIXRL (DATA, N, NREM, ISIGN, IFORM)
FOR IFORM = 0, 1 DO
  CONSIDERED COMPLEX CONJUGATE OF A DOUBLED-UP REAL ARRAY,
  FIRST HALF OF THE COMPLEX TRANSFORM, AS THE SECOND HALF HAS
  CONJUGATE SYMMETRY. FOR IFORM = -1, CONVERT THE FIRST HALF
  OF THE TABLE TRANSFORM INTO THE TRANSFORM OF A DOUBLED-UP REAL
  ARRAY. N MUST BE EVEN.
  USING COMPLEX NOTATION AND SUBSCRIPTS STARTING AT ZERO, THE
  TRANSFORM DATA IS--
  DIMENSION DATA(N, NREM)
  ZSTP = EXP(ISIGN*2*PI*I/N)
  DO 10 I2=0, NREM-1
    DATA(0, I2) = CONJ (DATA(0, I2)) * (1+I)
  DO 10 I1=1, N/4
    Z = (1+(2*I*FORM+1)*I*ZSTP**I1)/2
    I1CNJ = DATA(I1, I2) - CONJ (DATA(I1CNJ, I2))
    TEMP = Z*DATA(I1, I2) = (DATA(I1, I2) - TEMP) * (1-I*FORM)
    DATA(I1CNJ, I2) = (DATA(I1CNJ, I2) + CONJ(TEMP)) * (1-I*FORM)
  IF I1=I1CNJ, THE CALCULATION FOR THAT VALUE COLLAPSES INTO
  A SIMPLE CONJUGATION OF DATA(I1, I2).
  DIMENSION DATA(1)
  TROPI=0.283185307*FLOAT (ISIGN)
  IP0=2
  IP1=IP0*(N/2)
  IP2=IP1*NREM
  IF (IFORM) 10, 70, 70
  PACK THE REAL INPUT VALUES (TWO PER COLUMN)
  J1=IP1+1
  DATA(2)=DATA(J1)
  IF (NREM-1) 70, 70, 20
  J1=J1+IEO
  L2JIN=IP1+1
  DO 60 I2=J2MIN, IP2, IE1
  DATA(I2)=DATA(J1)
  J1=J1+160
  IF (N-2) 90, 90, 30
  L2JIN=I2+IP1
  IF MAX=I2+IP1-IEO

```

CCCCCCCCCCCCCCCCCCCCCCCCCCCCCCCCCCCC

C 10

20

30

TES04810
TES04820
TES04830
TES04840
TES04850
TES04860
TES04870
TES04880
TES04890
TES04900
TES04910
TES04920
TES04930
TES04940
TES04950
TES04960
TES04970
TES04980
TES04990
TES05000
TES05010
TES05020
TES05030
TES05040
TES05050
TES05060
TES05070
TES05080
TES05090
TES05100
TES05110
TES05120
TES05130
TES05140
TES05150
TES05160
TES05170
TES05180
TES05190
TES05200
TES05210
TES05220
TES05230
TES05240
TES05250
TES05260
TES05270
TES05280

```

40      I1=I1MIN,I1MAX,IPO
DATA(I1)=DATA(J1)
DATA(I1+1)=DATA(J1+1)
50      J1=J1+I20
DATA(I2+1)=DATA(J1)
60      J1=J1+IPO
DO 80 I2=1,I2,IPI
TEMP6=DATA(I2)
DATA(I2)=DATA(I2)+DATA(I2+1)
80      DATA(I2+1)=TEMP6-DATA(I2+1)
IF (N-2) 200,200,90
THETA=TMOP/FLOAT(N)
SINTH=SIN(THETA/2.)
ZSTPR=-2.*SINTH*SINTH
ZSTPI=SIN(THETA)
90      ZP={1.-ZSTPI}/2.
ZI={1.+ZSTPR}/2.
IF {IFORM} 100,110,110
100     ZR={1.-ZR
ZI=-ZI
I1MIN=IPO+1
I1MAX=IPO*(N/4)+1
110     DO 190 I1=I1MIN,I1MAX,IPO
DO 180 I2=I1,IPI
I2CNJ=IPO*(N/2+1)-2*I1+I2
IF {I2-I2CNJ} 150,120,120
IF {ISIGN*(2*IFORM+1)} 130,140,140
120     DATA(I2+1)=-DATA(I2+1)
130     IF (IFORM) 170,180,180
140     DIFF=DATA(I2)-DATA(I2CNJ)
150     DIFF=DATA(I2+1)+DATA(I2CNJ+1)
TEMP6=DIFF*ZR-DIFF*ZI
TEMP7=DIFF*ZI+DIFF*ZR
DATA(I2)=DATA(I2)-TEMP6
DATA(I2+1)=DATA(I2+1)-TEMP7
DATA(I2CNJ)=DATA(I2CNJ)+TEMP6
DATA(I2CNJ+1)=DATA(I2CNJ+1)-TEMP7
IF (IFORM) 160,180,180
160     DATA(I2CNJ)=DATA(I2CNJ)+DATA(I2CNJ)
DATA(I2CNJ+1)=DATA(I2CNJ+1)+DATA(I2CNJ+1)
170     DATA(I2)=DATA(I2)+DATA(I2)
DATA(I2+1)=DATA(I2+1)+DATA(I2+1)
180     CONTINUE
TEMP6=ZR-5
ZR=ZSTPR*ZI+ZSTPI*TEMP6+ZI
190     ZI=ZSTPR*ZI+ZSTPI*TEMP6+ZI
RECJESION SAVES IIDE, AT A SLIGHT LOSS IN ACCURACY. IF AVAILABLE,
C      USE DOUBLE PRECISION TO COMPUTE ZR AND ZI.
C      TES05290
C      TES05300
C      TES05310
C      TES05320
C      TES05330
C      TES05340
C      TES05350
C      TES05360
C      TES05370
C      TES05380
C      TES05390
C      TES05400
C      TES05410
C      TES05420
C      TES05430
C      TES05440
C      TES05450
C      TES05460
C      TES05470
C      TES05480
C      TES05490
C      TES05500
C      TES05510
C      TES05520
C      TES05530
C      TES05540
C      TES05550
C      TES05560
C      TES05570
C      TES05580
C      TES05590
C      TES05600
C      TES05610
C      TES05620
C      TES05630
C      TES05640
C      TES05650
C      TES05660
C      TES05670
C      TES05680
C      TES05690
C      TES05700
C      TES05710
C      TES05720
C      TES05730
C      TES05740
C      TES05750
C      TES05760

```

```

200 IF (IFORM) 270,210,210
C 210 UNPACK THE REAL TRANSFORM VALUES (TWO PER COLUMN)
      I2=IP2+1
      I1=I2
      J1=IP0*(N/2+1)*NREM+1
      GO TO 250
220 DATA(J1)=DATA(I1)
      DATA(J1+1)=DATA(I1+1)
      I1=I1-IE0
      J1=J1-IE0
230 IF (I2-I1) 220,240,240
240 DATA(J1)=DATA(I1)
      DATA(J1+1)=0.
      I2=I2-IE1
      J1=J1-IE0
250 DATA(J1)=DATA(I2+1)
      DATA(J1+1)=0.
      I1=I1-IE0
      J1=J1-IE0
260 IF (I2-I1) 260,260,230
270 DATA(2)=0.
      RETURN
      END

SUBROUTINE PRPLOT(DATA,DR,IMAX,JMAX,RO)
*****
THIS SUBROUTINE PLOTS THE IP(R) VS R CURVE, STARTING AT THE
SOURCE AND MOVING IN A POSITIVE DIRECTION OF RANGE.
*****
*****
DIMENSION DATA(4096),P40D(2048),R(2048)

IMARK = INT(IMAX/5.) + 1
KMAX = JMAX - 1
JMAX2 = JMAX - 2

DO 30 I = 1,JMAX
  FLY = FLOAT(I)
  R(I) = RO + FLY * DR
  R(JMAX-I) = -R(KMAX+I)
  CONTINUE

30 PMIN = RO
  PMAX = R(JMAX)

  WHILE(6,100)

```

```

TES05770
TES05780
TES05790
TES05800
TES05810
TES05820
TES05830
TES05840
TES05850
TES05860
TES05870
TES05880
TES05890
TES05900
TES05910
TES05920
TES05930
TES05940
TES05950
TES05960
TES05970
TES05980
TES05990
TES06000
TES06010
TES06020
TES06030
TES06040
TES06050
TES06060
TES06070
TES06080
TES06090
TES06100
TES06110
TES06120
TES06130
TES06140
TES06150
TES06160
TES06170
TES06180
TES06190
TES06200
TES06210
TES06220
TES06230
TES06240

```

```

100  FORMAT(/,3X,'I',6X,'RANGE',7X,'REALP',7X,'IMAGP',5X,'MODULUS OF P',
1,/)
C
C  DC 10 I = 1,JMAX
PMOD(I) = SQRT((DATA(2*I-1))**2 + (DATA(2*I))**2)
WRITE(6,200) I,P(I),DATA(2*I-1),DATA(2*I),PMOD(I)
C  CONTINUE
C200  FORMAT(2X,14,2X,F10.2,3(2X,F10.7))
C
PMAX = -1.0
DC 20 I = 1,JMAX
IF(PMOD(I).GT.PMAX) PMAX = PMOD(I)
C  CONTINUE
CALL COMPLES
CALL APLA2D(4.0,6.0)
CALL XNAME('RANGE(M)',$,100)
CALL YNAME('MAGNITUDE OF PRESSURE, P(R)',$,100)
CALL LINESP(0.5)
CALL HEADIN('MAGNITUDE OF PRESSURE AS A FN OF RANGE $',100,1.0,1)
CALL NOCHECK
CALL GRAF(RMIN,SCALE,RYAX,0.0,'SCALE',PMAX)
CALL CURVE(R,PMOD,JMAX,IMARK)
CALL ENDPL(1)
RETURN
END
C
SUBROUTINE WTHET(I,IMAX,G*,CKM,Q,AK,BE)
C
C *****
C THIS SUBROUTINE PLOTS THE ACOUSTIC PRESSURE SPECTRUM AS A FUNCTION
C OF THE HORIZONTAL WAVENUMBER
C *****
C DIMENSION GM(4096),CKM(4096),Q(4096),BE(4096)
C
C IMARK = INT(IMAX/5.) + 1
C GMIN = GM(1)
C GMAX = AK
C PMAX = -1.0
C QMAX = -1.0
C SMAX = 0.0
C DO 10 I = 1,IMAX
C IF(CKM(I).GT.PMAX) PMAX = CKM(I)
C CONTINUE
C DO 15 I = 1,IMAX

```

```

15      IF(Q(I).GT.QMAX)QMAX = Q(I)
C      CONTINUE
C
C      IF(PMAX.GF.QMAX)SMAX = PMAX
C      SMAX = QMAX
C
C      *****
C      GMAX IS THE MAXIMUM VALUE KH CAN TAKE ON BASED ON THE EQUATION
C      ((DELTA K) *(DELTA R)) = (2 * PI/IMAX)
C      *****
C      GMAX IS THE MAXIMUM VALUE KH CAN TAKE ON AND STILL PRODUCE "REAL"
C      THEORETICAL Q AND LFTA VALUES.  KZ < SQRI(AR**2 + KH**2) => Q REAL.
C      *****
C      SCALE THE HORIZONTAL AXIS IN KH (GM)
C      *****
C      CALL COMPRS
C      CALL AFEA2D(4.0,6.0)
C      CALL XNAME('HORIZONTAL WAVENUMBER, 1/MF',100)
C      CALL YNAME('PRESSURE SPECTRUM MAGNITUDE$',100)
C      CALL LINESP(0.5)
C      CALL HEADIN('PRESSURE SPECTRUM VS KH$',100,1.0,1)
C      CALL NCHECK
C      CALL GRAF(GMIN,'SCALE',GMAX,0.0,'SCALE',SMAX)
C      CALL CURVE(GM,CKM,IMAX,IMARK)
C      CALL DCL
C      CALL CURVE(GM,Q,INAX,IMARK)
C      CALL RFSE1('DOT')
C      CALL ENDPL(2)
C      RETURN
C      END
C
C      SUBROUTINE WTVPLI(IMAX,CKM,Q,AK,BE)
C      *****
C      THIS SUBROUTINE PLOTS THE PRESSURE SPECTRUM AS A FUNCTION OF THE
C      VERTICAL WAVENUMBER (EL).
C      *****
C      *****
C      DIMENSION CKM(4096),Q(4096),BF(4096)
C
C      IMARK = INT(IMAX/5.) + 1
C      SMAX = BE(1)
C      LMIN = BE(IMAX)
C      PMAX = -1.0
C      QMAX = -1.0

```

BIBLIOGRAPHY

- Bergland, G. D., "A Guided Tour of the Fast Fourier Transform," IEEE Spectrum, v.6, July 1969.
- Blackman, R. B. and Tukey, J. W., The Measurement of Power Spectra, Dover Publications, Inc., 1958.
- Brigham, E. O., The Fast Fourier Transform, Prentice-Hall, Inc., 1974.
- DiNapoli, F. R. and Deavenport, R. L., "Numerical Models for Underwater Acoustic Propagation," Ocean Acoustics, v. 1, Springer-Verlag, New York, NY, 1979.
- DiNapoli, F. R. and Deavenport, R. L., "Theoretical and Numerical Green's Function Field Solution in a Plane Multilayered Media," Journal of the Acoustic Society of America, v. 67(1), January 1980.
- International Series of Monographs on Electronics and Instrumentation, v.9, Pergamon Press, Inc., 1960.
- Naval Surface Weapons Center Report 75-18, A Statistical Model for the Fluctuation of Sound Transmission in the Sea, Urick, R. J., 11 February 1975.
- Naval Underwater Systems Center Technical Memorandum 781054, A Simplified Derivation of a Quadrature Subsampling Technique, Lackoff, M. R., 14 March 1978.
- Stanton, T. K. and Beyer, R. T., "The Interaction of Sound with Noise in Water," Journal of the Acoustic Society of America, v.64(6), December 1978.
- Thomas, G. B. and Finney, R. L., Calculus and Analytic Geometry, 5th ed., Addison-Wesley Publishing Company, 1979.
- Urlick, R.J., "Models for the Amplitude Fluctuations of Narrow-Band Signals and Noise in the Sea," Journal of the Acoustic Society of America, v. 64(6), December 1978.

LIST OF REFERENCES

1. Lauer, R. B., Signal Transmission in the Wavenumber Domain, Technical Memorandum, Naval Underwater Systems Center, New London Laboratory, New London, CT, 5 June 1979.
2. Naval Underwater Systems Center Report 4103, Fast Field Program for Multilayered Media, by F. R. DiNapoli, 26 August 1977.
3. Stamey, B. B., Preliminary Investigation of the Environmental Sensitivity of Acoustic Signal Transmission in the Wavenumber Domain with Respect to Source Depth Determination, Masters Thesis, Naval Postgraduate School, Monterey, CA, 1982.
4. Blanchard, J., A Comparison of Two Acoustic Parabolic Equation Transmission Loss Models for Compatibility with the Wavenumber Technique in the Determination of Source Depth, Masters Thesis, Naval Postgraduate School, Monterey, CA, 1984.
5. Kinsler, L., and others, Fundamentals of Acoustics, 3rd ed., John Wiley and Sons, 1982.
6. Urick, R. J., Principles of Underwater Sound, 3rd ed., McGraw-Hill, 1983.
7. Officer, C. B., Introduction to the Theory of Sound Transmission, McGraw-Hill, 1958.
8. Coppens, A. B., Mathematical Derivation of the Acoustic Pressure Spectrum of the Lloyds' Mirror, Naval Postgraduate School, Monterey, CA, January 1985.
9. IMSL Library Reference Manual, 9th ed., v. 2, IMSL, 1982.
10. Gabrielson, T., Mathematical Derivation of the Acoustic Pressure Spectrum for the Lloyds' Mirror, Naval Postgraduate School, Monterey, CA, February 1985.

INITIAL DISTRIBUTION LIST

	No.	Copies
1. Defense Technical Information Center Cameron Station Alexander, VA 22314	2	
2. Library, Code 0142 Naval Postgraduate School Monterey, CA 93943	2	
3. Chairman (Code 55Fo) ASW Academic Group Naval Postgraduate School Monterey, CA 93943	1	
4. Prof. A. B. Coppens (Code 61Cz) Department of Physics Naval Postgraduate School Monterey, CA 93943	4	
5. Prof. C. R. Dunlap (Code 68Du) Department of Oceanography Naval Postgraduate School Monterey, CA 93943	3	
6. Prof. Suk Wang Yoon (Code 61Yo) Department of Physics Naval Postgraduate School Monterey, CA 93943	3	
7. Prof. T. Gabrielson (Code 61Gt) Department of Physics Naval Postgraduate School Monterey, CA 93943	1	
8. LCDR P. B. King 425 Pine Shadows Drive Slidell, LA 70458	3	
9. Commanding Officer Naval Ocean Research and Development Activity NSTL, MS 39522	1	
10. Commanding Officer Naval Ocean Research and Development Activity (ATTN: Code 223) NSTL, MS 39522	1	
11. Office of Naval Research ATTN: Mr. R. B. Lauer Naval Ocean Research and Development Activity 800 N. Quincy Street Arlington, VA 22217	1	
12. Commanding Officer Naval Eastern Oceanography Center ATTN: LCDR J. Blanchard McAdie Bldg. (U-117) Naval Air Station Norfolk, VA 23511	1	

13. ICDF B. Stamey 1
5508 Buskirk Street
North Charleston, SC 29406
14. Ms Catherine Smith 2
P. O. Box 58
Carmel Valley, CA 93924

1 3 5 3 7 5

8

212099

Thesis

K4492 King

C.1

Use of the Wave-
number Technique with
the Lloyds Mirror for
an Acoustic Doublet.

212099

Thesis

K4492 King

C.1

Use of the Wave-
number Technique with
the Lloyds Mirror for
an Acoustic Doublet.

thesK4492

Use of the Wavenumber Technique with the



3 2768 001 02786 5

DUDLEY KNOX LIBRARY